Facultad de Ciencias

Departamento de Biología Molecular

Deciphering the transcriptional network of the distinct heart cell types after myocardial infarction

Wencke Walter

Madrid, 2017

Facultad de Ciencias

Departamento de Biología Molecular

Centro Nacional de Investigaciones Cardiovasculares (CNIC)

Deciphering the transcriptional network of the distinct heart cell types after myocardial infarction

Wencke Walter

Supervisor:

Mercedes Ricote Pacheco

Co-supervisor:

Fátima Sánchez - Cabo

Madrid, 2017

"I stand amid the roar

Of a surf-tormented shore,

And I hold within my hand

Grains of the golden sand-

How few! yet how they creep

Through my fingers to the deep,

While I weep- while I weep!

...

Is all that we see or seem

But a dream within a dream?"

Edgar Allan Poe

ACKNOWLEDGMENTS

ACKNOWLEDGMENTS

ACKNOWLEDGMENTS

Last, but definitely not least, I thank my family for their everlasting support, encouraging messages, chocolate packages, and frequent visits to cheer me up whenever I needed it the most. I am very lucky to have such great parents, who gave and still give me the complete freedom to follow my dreams and who never even waver in their trust in my abilities.

INDEX

INDEX

INDEX

ABBREVIATIONS

3'UTR	3'- UnTranslated Region
ARE	AU-Rich Elements
ATP	Adenosine TriPhosphate
BMDM	Bone Marrow- Derived Mφ
bp	base pair
BP	Biological Process
cAMP	cyclic Adenosine MonoPhosphate
cDNA	Complementary DNA
CC	Correlation Coefficient
CD	Cluster of Differentiation
ceRNA	competing endogenous RNA
CM	CardioMyocytes
CPM	Counts Per Million
CRM	Cardiac Resident Mφ
Ct	Cycle threshold
CVD	CardioVascular Diseases
DAMP	Damage Associated Molecular Patterns
DE	Differential Expression
DEG	Differentially Expressed Genes
EC	Endothelial Cells
ECM	ExtraCellular Matrix
FACS	Fluorescence-Activated Cell Sorting
FB	FibroBlasts
FBS	Fetal Bovine Serum
FC	Fold-change
FPKM	Fragments Per Kilobase of exon model per Million mapped reads
GEO	Gene Expression Omnibus
GFP	Green Fluorescent Protein

GM-CSF	Granulocyte Macrophage Colony-Stimulating Factor
GO	Gene Ontology
GRN	Gene Regulatory Network
GSEA	Gene Set Enrichment Analysis
IFNγ	Interferon gamma
IC	Immune Complex
IL	InterLeukin
JAK	JAnus Kinase
KEGG	Kyoto Encyclopedia of Genes and Genomes
LPS	Lipopolysaccharides
MAPK	Mitogen-Activated Protein Kinase
Mφ	Macrophages
M-CSF	Macrophage Colony-Stimulating Factor
MI	Myocardial Infarction
MP	Membrane Protein
MRE	MiRNA Response Element
mRNA	messenger RNA
miRNA	microRNA
NCBI	National Center for Biotechnology Information
ncRNA	non-coding RNAs
NES	Normalized Enrichment Score
NF-kB	Nuclear Factor kappa-light-chain-enhancer of activated B cells
NK	Natural Killer cells
NO	Nitric Oxide
nt	Nucleotide
lincRNA	Long Intergenic Non-Coding RNA
lncRNA	Long Non-Coding RNA
ODE	Ordinary Differential Equation

PBS	Phosphate Buffered Saline
PCA	Principal Component Analysis
qPCR	real-time Polymerase Chain Reaction
RNA-seq	RNA sequencing
RISC	RNA-Induced Silencing Complex
ROS	Reactive Oxygen Species
RPKM	Reads Per Kilobase of exon model per Million mapped reads
RPMI	Roswell Park Memorial Institute
RSEM	RNA-Seq by Expectation Maximization
SCC	Strongly Connected Component
SE	Standard Error
SM	Secreted Molecule
SMAD3	SMAD Family Member 3
STAT	Signal Transducer and Activator of Transcription
TGF-β	Transforming Growth Factor beta
TF	Transcription Factor
TMM	Trimmed Mean of M-values
TPM	Transcripts Per Million
TSS	Transcription Start Site
TTP	TrisTetraProlin
VEGF	Vascular Endothelial Growth Factor

SUMMARY

SUMMARY

Despite the tremendous effort undertaken so far to decipher the cellular response in cardiac repair many questions remain unanswered. The recent advances in *omics* technology have opened up the possibility to address these questions and to understand the cell type specific functional contribution. However, the massive amount of generated data requires thorough bioinformatics work by implementing a plethora of statistical analysis and mathematical methods that have to be chosen with care to understand underlying molecular mechanisms. Another integral part of the data analysis process is the visualization of the obtained results. Due to the high-dimensionality of the data this step is rather challenging and further improvement is needed to provide advanced methods that facilitate the combination of various data types to enhance graphical representation of context-dependent, relevant information.

For this purpose, we developed the R package GOplot to visually combine expression data with functional information (results chapter 1). The R package further supported the exhaustive bioinformatics analysis of ad-hoc generated transcriptomics data of murine cardiac macrophages (Mφ; results chapter 2) and distinct porcine cardiac cells (results chapter 3) in the healthy heart and after myocardial infarction (MI). The analysis revealed that murine cardiac Mφ can be distinguished from other tissue-resident Mφ by cardiac specific transcriptional programs and the expression of cardiac specific markers. The global transcriptional profile of murine post-MI Mφ could be matched to M1/M2 polarization states but systematic gene expression analysis and partial deconvolution revealed that these Mφ are a mix of described *in vitro* phenotypes. Simulated dynamics and experimental validation of identified core regulatory genes showed that the initial inflammatory response of murine Mφ is limited by hypoxia-mediated up-regulation of *Il10*. We also found that targeted mRNA degradation contributes to the resolution of inflammation and the Mφ phenotype transition. In swine, gene signatures could be identified for each cell type that were linked to distinct biological functions. *In silico* analysis of the secretome and receptome indicated a complex network of intercellular communication with numerous potential interactions between Mφ and endothelial cells (EC) and cardiomyocytes (CM) and fibroblasts (FB) post-MI.

Collectively, the gathered data provide a useful resource to improve the understanding of the regulatory network of cardiac repair and suggest potential targets for tissue and cell type specific therapeutic interventions to manipulate cardiac repair.

RESUMEN

A pesar del gran esfuerzo llevado a cabo para entender la respuesta celular durante la reparación del daño cardiaco todavía existen muchos ámbitos desconocidos. Los recientes avances en tecnologías *ómicas* han aumentado la posibilidad de entender mejor este proceso tanto a nivel global como el papel específico de cada tipo celular. Estas tecnologías, sin embargo, generan una ingente cantidad de datos que requiere del uso adecuado de herramientas bioinformáticas capaces de implementar análisis estadísticos y modelos matemáticos para entender los mecanismos moleculares subyacentes a en los datos. Otra parte fundamental del proceso es la visualización de los resultados obtenidos. Debido a la multidimensionalidad de este tipo de datos esta tarea supone un reto que requiere de nuevas aproximaciones para facilitar la combinación de datos heterogéneos de manera visual, y así ser capaces de extraer y transmitir la información relevante para cada contexto.

Esta tesis presenta los resultados obtenidos gracias al detallado análisis bioinformático de dos conjuntos de datos transcriptómicos generados *ad-hoc* en el corazón sano y en diversos tiempos tras el infarto en (*dataset 1*) macrófagos cardiacos de ratón (Mφ; capítulo 2 de resultados) y en (*dataset 2*) macrófagos, células endoteliales, fibroblastos y cardiomiocitos de cerdo (capítulo 3 de resultados). Los análisis llevados a cabo revelan que, en ratón, los Mφ cardiacos son claramente distinguibles a nivel transcripcional de los macrófagos residentes en otros tejidos. Por otra parte, el uso de técnicas de deconvolución de la expresión génica *in silico* reveló que después del infarto los Mφ cardiacos son una mezcla de los fenotipos funcionales (M1/M2) descritos *in vitro*. Adicionalmente, gracias al modelado de la red génica fundamental durante el proceso utilizando un modelo booleano, se descubrió que la respuesta inicial a la inflamación en este contexto está limitada por un incremento de Il10 en respuesta a las señales de hipoxia, resultado que fue validado experimentalmente. Del mismo modo, encontramos que la regulación post-transcripcional contribuye a la resolución de la inflamación y a la transición M1/M2.

En el modelo de infarto en cerdo se identificaron perfiles transcripcionales específicos de cada tipo de celular y de cada estado fisiológico de la célula, que a su vez fueron relacionados con funciones distintas, sugiriendo un papel propio de cada tipo celular en la respuesta al daño por infarto. Asimismo el análisis *in silico* del secretoma y del receptoma evidenció una compleja red de interacciones después del infarto, entre Mφ y células endoteliales por un lado y entre cardiomiocitos y fibroblastos

por otro. En todas las fases del análisis se utilizó el paquete de R GOplot que fue desarrollado específicamente para facilitar la interpretación de los resultados gracias a la combinación de información funcional y de expresión (capítulo de resultados 1).

En conjunto, los datos generados y analizados en esta tesis han contribuido a una mejor comprensión de la red de regulación responsable de la recuperación del daño cardiaco después del infarto de miocardio, sugiriendo dianas específicas de tejido y tipo celular y que podrán ser utilizadas para mejorar la reparación cardiaca.

INTRODUCTION

1. CARDIAC SYSTEMS BIOLOGY

Over the last decade, the cardiovascular system and its broad range of diseases have been subjected to the most intensive studies (Leal et al., 2006). Although the structure and anatomy of the mammalian heart are well known and have been described decades ago, knowledge about the complex cellular and molecular interactions and their outcomes controlling both normal and pathological cardiophysiology is limited. The mammalian heart is predominantly composed of CM, FB, EC, and hematopoietic-derived cells (Bergmann et al., 2015; Pinto et al., 2016). Each cell lineage contributes in a distinct way to maintain cardiac homeostasis or to restore homeostasis in case of tissue injury, which creates a complex and highly connected network of cell interactions. It is of prime importance to understand these fine- tuned underlying regulatory networks and the specific contribution of the distinct cardiac cell types in order to be able to develop efficient targeted treatment.

1.1. Systems biology to understand biological complexity

It has only been during the last decade that the critical developments in genome sequencing, expression profiling, proteomics, and metabolomics high-throughput data can be used to thoroughly elucidate transcriptional changes and the spatio-temporal properties of multifaceted regulatory networks (Jojic et al., 2013; Robinette et al., 2015). Furthermore, it is becoming more and more apparent that a comprehensive understanding of intricate biological processes (BP) can only be obtained through the integration of different molecular levels. The classical way of dissecting complex biological systems has been a reductionistic one, by breaking the systems down into individual, more traceable parts (Ahn et al., 2006). A reductionistic approach is very useful if the origin of a given disease can be traced back to a single factor but is challenged if multiple factors come into play. The recently established field of systems biology aims to improve the understanding of complex mechanisms by combining mathematical modeling and computational biology with experimental data, integrating different levels of regulation - a characteristic of many clinically relevant diseases such as MI (Dimmeler et al., 2005; Shay and Kang, 2013).

1.2. The bioinformatics workflow towards systems biology
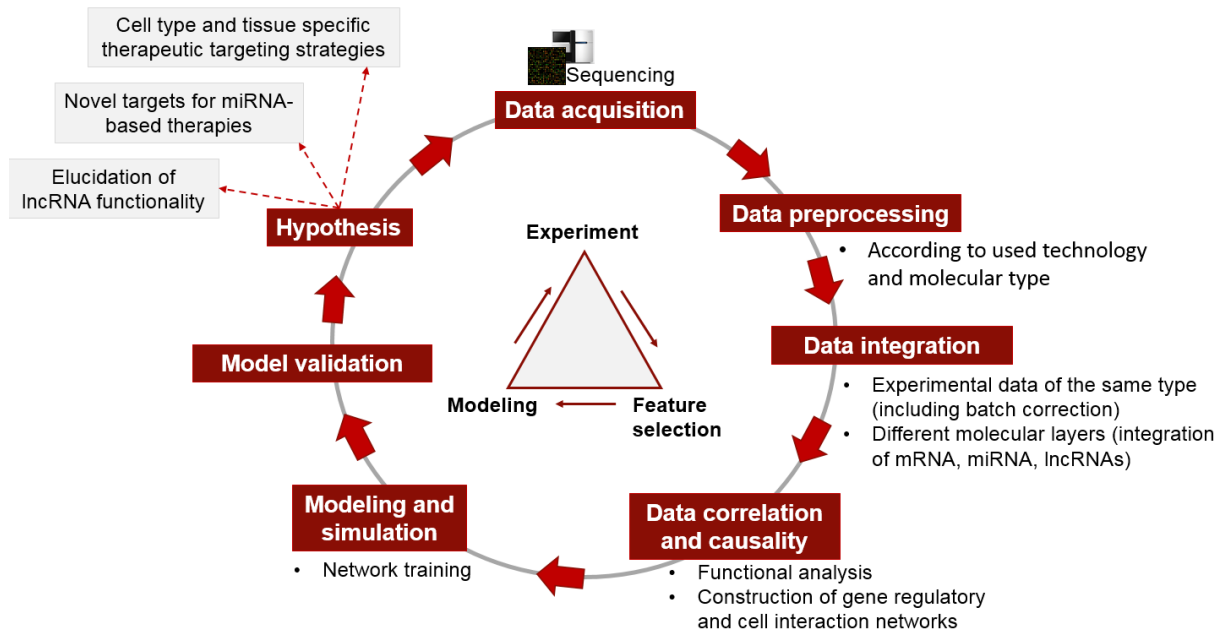
Figure 1: Flow chart for computational analysis of high-throughput experimental data.

1.2.1. Data acquisition and preprocessing

In order to answer the biological question of interest, the selection of appropriate methods and technologies is of prime importance. Due to the development of sequencing technologies such as DNA microarray and RNA- sequencing (RNA-seq), which allow to easily perform large-scale measurements, many biological questions are addressed by the analysis of genomics and transcriptomics data (Gautier et al., 2012; Miller et al., 2012).

In the case of microarray studies, fluorescently labeled target sequences are hybridized with nucleic acid probes with complementary sequence that are attached to glass slides. The slides are scanned, the obtained images are converted into signal intensities, and array specific software is used to process the data. Microarray data contain very high background noise and require a number of preprocessing steps to convert the raw data to measures with biological meaning (Silver et al., 2009). Normalization is a critical step in the data preprocessing process that differs according to the used technology and is used to remove systematic technical effects. In our study we used single channel Agilent microarrays and it has been shown that for these arrays quantile normalization performs best (Bolstad et al., 2003). The aim of this normalization technique is to make all arrays have the same distribution of probe

intensities (Irizarry et al., 2003), which allows gene expression comparisons between arrays and over various conditions. The state of the art package for gene discovery through differential expression (DE) analyses of microarray data is limma (Ritchie et al., 2015), that applies linear models to identify differentially expressed genes (DEG), which build the basis for further downstream analysis.

Hybridization-based approaches are reliable and cost effective techniques but suffer from limitations such as reliance upon existing knowledge about genome sequence, high background levels owing to cross-hybridization (Uva and De Rinaldis, 2008), and limited dynamic range of detection (Zhao et al., 2014). RNA-seq overcomes these drawbacks and has become the most popular method for transcriptome analysis (including messenger RNAs (mRNA), non-coding RNAs and small RNAs) and to quantify changing expression levels of each transcript under different conditions (Tachibana, 2015).

The general procedure of RNA-seq consists in the conversion of a population of fragmented RNA to a library of cDNA fragments with adaptors attached to one or both ends. Each molecule, with or without amplification, is then sequenced in a high-throughput manner to obtain short sequences from one end (single-end sequencing) or both ends (paired-end sequencing) of the fragment. The reads are typically 30-400 base pairs (bp), depending on the used sequencing technology. The resulting reads are then aligned to either the reference genome or reference transcriptome. In the absence of a reference genome the sequences have to be assembled *de novo*. To estimate transcript abundance from a mapping to the genome the most commonly used program is Cufflinks (Trapnell et al., 2010), whereas algorithms that quantify expression from transcriptome mappings include RSEM (RNA-Seq by Expectation Maximization) (Li and Dewey, 2011), eXpress (Roberts and Pachter, 2013), Sailfish (Patro et al., 2014), and Kallisto (Bray et al., 2016). In this dissertation reads were mapped to the transcriptome and transcript expression was estimated applying RSEM. For large transcriptomes alignment is complicated by the fact that a significant portion of sequence reads match multiple locations in the genome. This issue can be addressed in different ways of which the simplest approach involves discarding these multi-mapped reads entirely. Another way of handling these multi-mapped reads involves the partition and distribution of their expression values between all transcripts that are mapped to the reads. RSEM improves this procedure by applying an

Expectation- Maximization algorithm to estimate maximum likelihood expression levels. Raw read counts obtained from RNA-seq are affected by factors such as transcript length and total number of reads and hence have to be normalized for correctly ranking gene expression levels within a sample. Feature-length and library-size effects can be reduced through within-sample normalizations resulting in reads per kilobase of exon model per million reads (RPKM) and its subsequent derivatives fragments per kilobase of exon model per million reads (FPKM) and transcripts per million (TPM). For comparisons across samples and species, the TPM measure, as reported by RSEM, is preferred over RPKM and FPKM measures due to its independence of the mean expressed transcript length (Li and Dewey, 2011).

For DE analysis a correction for gene length is not necessary, because the gene length does not differ between different conditions. Nevertheless, normalization methods such as trimmed mean of M-values (TMM) (Robinson and Oshlack, 2010), DESeq (Anders and Huber, 2012) or PoissonSeq (Li et al., 2011) are necessary to correct for a potential heterogeneous transcript distribution. Thus, if certain transcripts are highly expressed in one experimental condition a DE analysis without normalization might be skewed towards this condition. The edgeR (Robinson et al., 2010) package can be used to perform an combined normalization and DE analysis by integration of TMM normalization factors into the statistical model used to test for DE. Methods such as edgeR and DESeq use the negative binomial distribution to compute DE genes to account for overdispersion – a characteristic feature of RNA-seq data (Trapnell et al., 2013).

1.2.2. Data integration

An essential part of systems biology approaches is the integration of different datasets to analyze and discover potential relationships and connections that otherwise would remain unnoticed. There are two levels of data integration: the combination of experimental data of the same (e.g. inter-experimental comparisons of gene expression profiles) or different molecular levels (e.g. integration of mRNA, microRNA (miRNA), long non-coding RNA (lncRNA)).

Integration of gene expression profiles that originate from different experiments requires an efficient correction for systemic errors (batch effects) that are introduced by laboratory conditions, reagents lots, as well as personnel differences and are

unrelated to biological variables in a study (Leek et al., 2010). Such a correction is necessary because batch effects can be correlated with an outcome of interest and the lack of batch correction would lead to inaccurate conclusions. Different methods have been developed or used to identify and remove batch effects from high-throughput data, but the Empirical Bayes method ComBat performs best (Chen et al., 2011a). ComBat robustly adjusts batches with small sample size by estimation of parameters for location and scale adjustment of each batch for each gene independently. The estimates are subsequently used to adjust the data for batch effects. A detailed description of the procedure can be found in (Johnson et al., 2007).

The integration of mRNA expression data with miRNA and/or lncRNA expression profiles has the potential to unravel the impact of post-transcriptional regulation on gene expression and adds an additional layer of information to reconstructed gene regulatory networks. The analysis is, however, rather challenging due to the high number of false miRNA target predictions and the limited knowledge of regulatory mechanisms of lncRNAs. The details of the computational analysis will be discussed in later sections.

1.2.3. Functional profiling of high-throughput data

The biological interpretation of high-throughput data is rather challenging due to its high-dimensional nature and the identification of DE genes is only the first step in the process of inferring knowledge from the obtained expression data. To gain further insight into altered BPs and pathways, DE genes are mapped to their biological annotation, e.g. gene ontology (GO) terms, and an enrichment analysis is performed. Alternatively, gene set enrichment analysis (GSEA) can be used to identify overrepresented processes (Subramanian et al., 2005). Obviously, such functional analysis requires the availability of sufficient functional annotation data for the species under study; otherwise, detected protein coding genes with unknown function might be functionally annotated through the identification of orthologs of better studied organisms. Once, the overrepresented processes and pathways are identified, pathway interaction and gene regulatory networks can be built as an attempt to understand the intrinsic nature of interlaced cell and/or molecular activities.

1.2.4. Network analysis

Within the context of systems biology, networks and their analysis (including both, topology and dynamics) aim to understand molecular and cellular interactions and effects of those interactions on a global scale. Networks are a collection of elements, represented as nodes or vertices, and the relationships between these elements are depicted as edges between two nodes. Intercellular biological networks, such as gene regulatory networks (GRN), are typically constructed with nodes representing molecules (genes/proteins) and edges corresponding to positive or negative interactions between them (Ma'ayan, 2011). Observation of networks over time might reveal two kinds of changes: changes in node state (e.g. activation, deactivation) and changes in network structure (e.g. rewiring of interactions).

In contrast to other molecules (e.g. cytokines) genes are less pleiotropic, i.e. one gene affects only a small number of other genes, and mainly operate within regulatory modules (Wagner and Zhang, 2011), which leads to networks that comprise only a few highly connected nodes or hubs. Network structure analysis can be used to extract meaningful subnetworks, including the identification of connected and strongly connected components (SCC), using the algorithm of Tarjan (Tarjan, 1975). A SCC is a group of genes, where every pair of genes is connected through directed paths (Albert 2007). The high interconnectivity of the SCC makes it an interesting target for network stability analysis because changes in the state of one of the genes are likely to affect the state of all remaining genes of the SCC and obtained results are often experimentally testable.

Modeling the dynamics of GRNs can be broadly categorized into continuous and discrete modeling approaches (Garg et al., 2009). The continuous modeling approach uses coupled ordinary differential equations (ODEs) to model evolution of gene expression over time and requires knowledge of kinetic rate constants. Although high-throughput technologies significantly improved our knowledge of molecular interactions, stoichiometry and kinetics are still largely unknown for gene regulatory processes, limiting the application of ODEs. Discrete modeling approaches on the other hand, such as Boolean networks, are mostly independent of quantitative data. In Boolean networks each node, or gene, has a discrete value of 1 (activated/present) or 0 (deactivated/absent) and the interaction between the genes are modeled applying

INTRODUCTION

Boolean functions (e.g. AND, OR). In a Boolean network the state of a gene i at time t is represented by a variable $x_i(t)$. In order to model the dynamics of each gene the state of each gene at time $t+1$ is described as a function of the state of those genes that influence the state of the gene in question. The overall state of the network at time t is described as the activation state of all genes in the network and its dynamics can be modeled by combining the dynamics of the individual genes. For that purpose a transition function $T(x_t, x_{t+1})$ is defined that represents the transition from the present state x_t to the next state x_{t+1}.

Transition functions can be either synchronous or asynchronous. In a synchronous dynamic model, all genes change their expression levels simultaneously in consecutive time points, whereas in asynchronous updating schemes all genes take different time for making a transition (Garg et al., 2008). Asynchronous updating schemes capture biological processes more accurately but they are also more complex to model and are computationally intense, even when modeling moderately sized networks. Synchronous models on the other hand can be computed within a few minutes (Garg et al., 2008). Nevertheless, due to the fact that in real biological systems not all genes undergo changes in expression at the same time the synchronous models are less precise.

It is well known that gene expression and its regulation are stochastic processes (Chalancon et al., 2012). In Boolean networks stochastic effects are included by flipping node states from 0 to 1 or vice versa with some predefined flip probability (Liang and Han, 2012). The integration of stochastic effects is required in order to simulate the differentiation of a Boolean model into multiple stable states (Garg et al., 2009). However, biological functions are characterized by different levels of complexity and show varying levels of stochasticity. Hence, it has been proposed to model stochastic effects on the level of biological functions rather than at the level of gene expression and the functionality of this approach has been demonstrated by modeling the T-helper network (Garg et al., 2009).

The simulated network evolves over time and reaches finally a stable state (or attractor), which represents the long-term behavior of the genes that build the network. It has been shown that these attractors can be associated with cellular steady states or phenotypes (Huang et al., 2005; Maamar et al., 2007). Here it is interesting to note,

that some cells seem to reach a robust stable state whereas other cells, such as Mφ, exhibit high plasticity and continuously shift their functional phenotype, i.e. transit from one attractor to another (Mantovani et al., 2013; Martinez and Gordon, 2014). Hypothesis and predictions derived from GRN modeling can then be tested and validated by *in vitro* or *in vivo* experiments.

2. MYOCARDIAL INFARCTION AND THE TEMPORAL CHANGES DURING INFARCT HEALING

With worldwide over 17 million deaths cardiovascular diseases (CVD), including diseases of the heart and vasculature such as MI, cardiac arrhythmias and stroke, are the leading cause of death as reported in World Health Statistics 2014 (Organization, 2015). In the case of MI, coronary artery occlusion results in an insufficient oxygen supply to the downstream myocardium. Sudden induction of ischemia, if left untreated for a prolonged period of time, leads to massive necrotic cell death within the infarcted tissue, initiating sterile inflammation and immune cell infiltration (Frangogiannis et al., 2002). The infiltrating cells clear the site of inflammation of cellular debris and the emerging gap is filled with granulation tissue, which subsequently develops into a dense scar (Boudoulas and Hatzopoulos, 2009). The temporal phases of the cardiac repair process are explained in detail in the subsequent section.

After coronary artery occlusion the sudden induction of ischemia triggers necrotic CM death within the affected myocardium, accompanied by impaired vascular EC integrity that facilitates leukocyte infiltration (Eltzschig and Eckle, 2011)(Figure 2). Danger associated molecule patterns (DAMP) released from necrotic cells lead to the onset of an intense sterile inflammation which is further amplified by infiltrating immune cells (Figure 2). Neutrophils are the first cells to enter the damaged heart and start to clear necrotic cellular debris from the tissue (Sun, 2008). The initial beneficial effect of neutrophil activity results later into further tissue damage and recruitment of pro-inflammatory monocytes to the infarcted area (Horckmans et al., 2016), which replenish the cardiac Mφ pool (Heidt et al., 2014; Lavine et al., 2014). These Mφ resemble an M1-like phenotype (Figure 2) and contribute to the inflammatory response by the release of cytokines, growth factors, and the generation of reactive oxygen species (ROS), which may activate the complement system and nuclear factor kappa-light-chain-enhancer of activated B cells (NF-kB) (Wang et al., 2007). NF-kB activation

in turn leads to the upregulation of cytokine and chemokine production, which effect cardiac repair in an autocrine or paracrine fashion (Masters and Riley, 2014). ECs and mononuclear phagocytes produce a variety of chemokines and cytokines in response to the same stimulus, amplifying and extending the inflammatory reaction. Cytokines are characterized by functional pleiotropy and redundancy: different cell types can be affected by the same cytokine, providing that they express the adequate receptor, and structurally related cytokines can activate similar pathways and trigger overlapping functions on the same cell type. The robust up-regulation of pro-inflammatory cytokines has to be timely confined in order to prevent chronic inflammation and to start the reparative phase with resolution of inflammation, FB proliferation, scar formation, and neovascularization over the next several days (Frangogiannis et al., 2002; Sedlyarov et al., 2016).
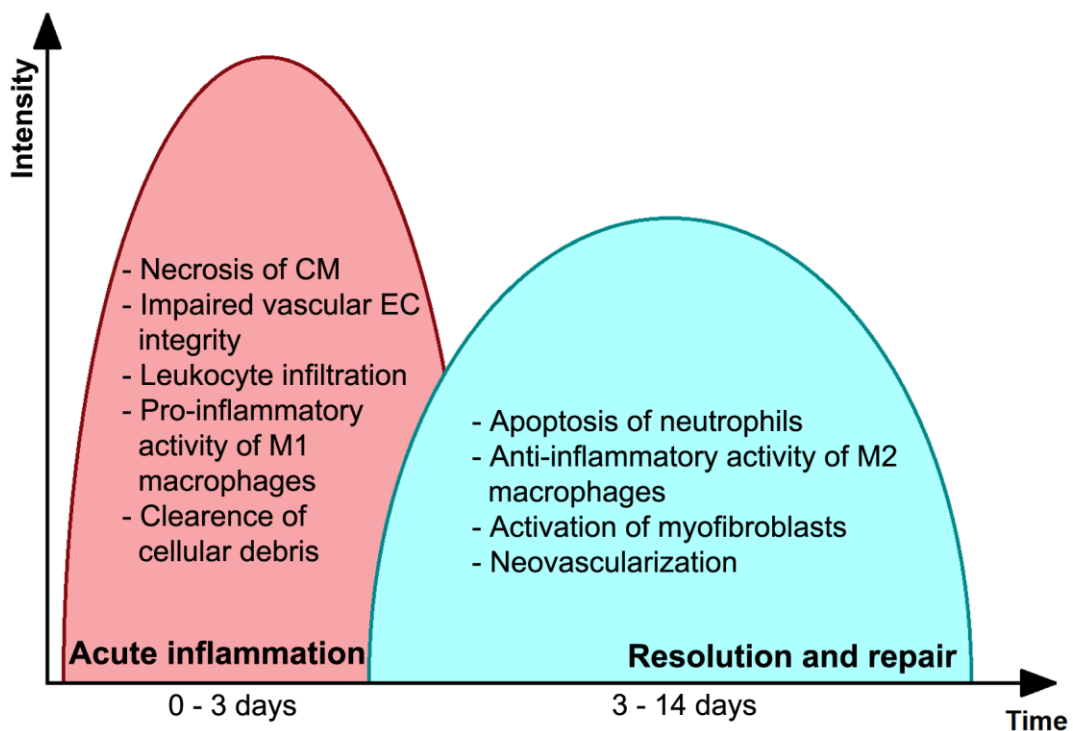
Figure 2: Temporal phases after MI and their characteristics.

The transition from a pro- to an anti-inflammatory program is mainly driven by changes in the molecular composition of the cardiac microenvironment. One of the key players that affect the resolution of inflammation in multiple ways are apoptotic neutrophils (Figure 2), which upon uptake polarize Mφ to an M2-like phenotype. M2-like Mφ are characterized by the secretion of anti-inflammatory and profibrotic factors such as interleukin 10 (IL10) and transforming growth factor beta (TGF-β), which

promote tissue repair. IL10 is known as a potent anti-inflammatory mediator, that inhibits inflammation and attenuates left ventricular remodeling post-MI (Krishnamurthy et al., 2009). TGF-β, a major pro-fibrogenic cytokine, becomes rapidly induced and activated in the infarcted heart (Bujak and Frangogiannis, 2007). The exact role of TGF-β in cardiac repair still remains to be elucidated, but accumulating evidence suggests three main functions of TGF-β in healing infarcts: repression of inflammation, modulation of FB phenotype, and induction of interstitial fibrosis (Euler, 2015). Immune cells have been identified as key players in the fibrotic cascade, with the capacity to exert either injury-inducing or repair-promoting effects. In particular Mφ, that can be found in close proximity with collagen-producing myofibroblasts, play a crucial role in fibrosis (Wynn and Barron, 2010). The accumulation of pro-fibrogenic myofibroblasts is a central feature of tissue fibrosis and upregulation of collagen production and promotion of extracellular matrix (ECM) deposition results in the formation of a collagen scar to stabilize contractile function of the damaged ventricle (Sutton and Sharpe, 2000). The scar formation is accompanied by myocyte hypertrophy and neovascularization (Nelissen-Vrancken et al., 1996). Nevertheless, the developing microvascular networks are not capable to fulfill the demands of the growing tissue, resulting in inadequate oxygenation and nutrient supply (Kocher et al., 2001). As a result, there is dilatation of the chamber arising from the infarct region, which bears the risk of heart failure.

Nonetheless, the knowledge about the exact molecular and cellular mechanisms and regulatory networks involved in cardiac repair is limited and further research is needed to decipher this multifaceted process as a requirement for the development of efficient target treatments that improve cardiac repair.

3. THE DIFFERENT CELL TYPES OF THE HEALTHY HEART AND AFTER MYOCARDIAL INFARCTION

The tissues of the mammalian body are composed of a wide variety of cell types that closely interact to maintain and regain homeostasis in case of tissue injury, such as MI. The mammalian heart is composed of different cell types and around 70% of the cells in the healthy heart are nonmyocytes, including primarily FBs and ECs (Zhou and Pu, 2016). A recent study reassessed the cardiac cellular composition and revealed that ECs constitute more than 60% of the adult mouse heart, followed by FBs (< 20%), and hematopoietic-derived cells (5-10%) (Pinto et al., 2016). Only recently it

has been shown that Mφ also populate the healthy myocardium, interspersed between CMs, FBs, and ECs (Heidt et al., 2014; Pinto et al., 2012).

3.1. Cardiac macrophage activation and function

Mφ reside in virtually every tissue of the body and are very heterogeneous. Many tissue-resident Mφ populations arise from embryonic precursors and circulating monocytes contribute to only a few tissues, including the gut, dermis and heart (Ginhoux and Guilliams, 2016). Tissue Mφ, including cardiac Mφ, have remarkable proliferative capacity and maintain themselves through local proliferation with tissue-dependent turn-over rates (Heidt et al., 2014; Lavine et al., 2014). The functions of tissue resident Mφ are tissue specific and range from tissue homeostasis and iron processing to wound healing after inflammation (Figure 3). Mφ are highly influenced by the microenvironment in which they reside and *in vivo* Mφ transplantation experiments demonstrated that the functional phenotype of tissue-resident Mφ is not terminal. Transplanted Mφ can be reprogrammed and adopt the transcriptional signature of the new microenvironment they reside in (Lavine et al., 2014).

Tissue heterogeneity

Clearence of apoptotic neurons

Elimination of dust, allergens and microorganisms

Clearence of pathogens and toxins

Clearence of senescent red blood cells by red pulp Mφ

Recognition and removal of enteric pathogens

Bone resorption

Polarization spectrum

+ LPS & IFNγ — M1 pro-inflammatory

+ IL4 & IL13

+ IC, LPS, IL-1β — M2 anti-inflammatory

+ IL10, GC
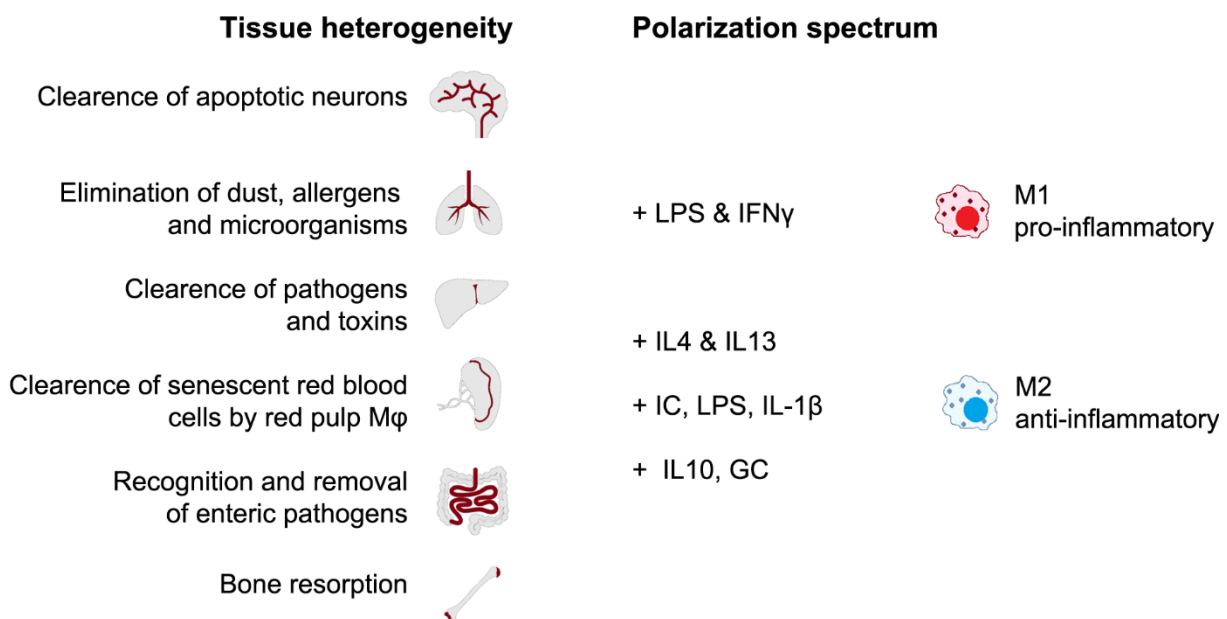
Figure 3: Overview of tissue specific functions of resident Mφ and typical stimuli of Mφ activation. LPS, lipopolysaccharide; IFNγ, interferon gamma; IL4, interleukin 4; IL13, interleukin 13; IC, immune complex; IL-1β, interleukin 1-beta; IL10, interleukin 10; GC, glucocorticoid.

Depending on their surroundings Mφ adapt different functional phenotypes and have been classified according to a simplified bipolar classification system with pro-

and anti-inflammatory macrophages on opposite ends of the activation spectrum (Martinez and Gordon, 2014). Mφ activated with pro-inflammatory signals, such as lipopolysaccharides (LPS) and interferon gamma (IFNγ), are termed M1 or "classically-activated" Mφ, whereas anti-inflammatory signals, such as interleukin 4 (IL4) and other stimuli lead to M2 or "alternatively-activated" Mφ (Mackaness, 1962; Nathan et al., 1983; Stein et al., 1992)(Figure 3). M1-like Mφ contribute to immune response, whereas anti-inflammatory M2-like Mφ support the resolution of inflammation and tissue remodeling mainly through the production of IL10. The M1/M2 classification system derives from the pre-genomic era and recent findings have shown that Mφ activation is best described with a multi-dimensional model (Xue et al., 2014). Studies of *in vivo* Mφ in different disease contexts have shown that the different Mφ populations do not exhibit either of the M1/M2 polarization states (Daley et al., 2010; Novak et al., 2014; Varga et al., 2016).

Cardiac tissue- resident Mφ (CRM) display typical Mφ characteristics, such as phagocytosis, and express markers associated with an anti-inflammatory phenotype (Pinto et al., 2012). Although only a few functional studies of cardiac Mφ and their role in tissue homeostasis exist, transcriptional analyses suggest a role in angiogenesis, fibrosis, and maintenance of immune quiescence (Pinto et al., 2014; Pinto et al., 2012). However, the exact mechanisms remain still elusive and further studies are needed to improve the knowledge of CRMs.

Intensive cell tracking studies showed a complete loss of tissue-resident Mφ in the heart following sterile tissue injury with subsequent infiltration of inflammatory monocytes to replenish the Mφ pool (Heidt et al., 2014). These Mφ resemble an M1-like phenotype and are characterized by their phagocytic, inflammatory, and fibrolytic properties (Heidt et al., 2014; Lambert et al., 2008). Within hours after MI the microenvironment is dominated by inflammatory mediators, such as IFNγ. Various studies established IFNγ as an immune-activating cytokine for Mφ (Flynn et al., 1993). Although Mφ can also be a source of IFNγ production (Darwich et al., 2009) the major sources of IFNγ are T-cells, specifically Th1, and natural killer cells (NK) (Hansson et al., 2006). Mφ bind IFNγ and the IFNγ-induced signaling is mainly mediated by signal transducer and activator of transcription 1 (STAT1) and janus kinase 2 (JAK2), resulting in the activation of the JAK/STAT signaling cascade (Martinez and Gordon, 2014). However, T-cells and NK cells are not the only cells or environmental factors capable

to activate Mφ. A common feature of inflammation sites are low levels of oxygen which trigger necrotic CM death. Necrotic CMs and the damaged ECM of the infarcted area release endogenous molecules (DAMPs) into the extracellular environment (Chen and Nuñez, 2010). DAMPs trigger an inflammatory response and activate immune cells through engagement with membrane-bound pattern recognition receptors. In order to fulfill the demands of the energy-intensive inflammatory response, pro-inflammatory Mφ are known to undergo a metabolic switch to favor glycolysis (Bordbar et al., 2012; Freemerman et al., 2014; Rath et al., 2015). The pro-inflammatory response is sustained by Mφ secreted molecules but intercellular programs as well as changes in the molecular composition of the microenvironment lead to an attenuation of inflammation and the onset of anti-inflammatory transcriptional programs (Martinez and Gordon, 2014; Sedlyarov et al., 2016). A recent study related to skeletal muscle injury has shown that the subsequent shift of Mφ to a M2-like phenotype is accompanied by the increased production and secretion of ECM components (Varga et al., 2016). Although many studies have demonstrated the importance of Mφ during wound healing (Diegelmann and Evans, 2004; DiPietro, 1995) the exact mechanisms and functions of these Mφ are not well known. However, the secretion of ECM components and the reported function of Mφ in fibrosis (Wynn and Barron, 2010) suggest that Mφ mainly act through the activation of myofibroblasts.

3.4. Fibroblasts, fibrosis and myocardial infarction

FBs are one of the most abundant cell types in the healthy myocardium (Pinto et al., 2016) and are responsible for maintaining the integrity of the cardiac matrix network due to their elevated production of ECM proteins. MI and other heart diseases lead to the expansion and activation of cardiac FBs, which play critical roles in the reparative response of the tissue and are implicated in left ventricle remodeling (Porter and Turner, 2009). It is now evident that FBs are more than just matrix-producing cells, performing a variety of functions ranging from the activation of the inflammasome during the inflammatory phase to cell migration, cell proliferation, and endothelial to mesenchymal transition during the proliferative phase of infarct healing (Chen and Frangogiannis, 2013). Since the adult mammalian heart has only a limited regenerative capacity, necrotic CMs are replaced by a collagen-based scar. FB are less susceptible to low oxygen levels than CM but hypoxic conditions polarize cardiac FBs to a

fibrogenic phenotype with increased collagen production (Tamamori et al., 1997). FBs, like MΦ, undergo dynamic phenotype alterations during the process of cardiac repair and, mediated by various factors such as TGF-β/ SMAD Family Member 3 (SMAD3) signaling (Dobaczewski et al., 2010), transdifferentiate into myofibroblasts during the proliferative phase of cardiac repair. The contractile force produced by myofibroblasts effectively promotes tissue remodeling and is reinforced by the deposition of collagen (Baum and Duffy, 2011). Once the tissue repair is terminated myofibroblasts undergo apoptosis and disappear (Desmouliere et al., 1995). While MΦ are the key players of the inflammatory response, modulated FBs (myofibroblasts) become the dominant cell type during the reparative phase (Hinz, 2007).

3.5. Endothelial function and myocardial infarction

Cardiac ECs can be found in the endocardium, cardiac valves, and the interior lining of blood vessels (Xin et al., 2013). The endothelium senses the sheer stress of flowing blood and contributes significantly to cardiac homeostasis through dynamic regulation of vascular permeability, blood vessel caliber, and the maintenance of blood fluidity (Brutsaert, 2003). The capillaries are in very close proximity to CM and EC-CM interactions are not only essential for normal heart development and growth but seem also to be relevant to promote cardiac repair (Hsieh et al., 2006). Cardiac EC are characterized by an extensive secretome, including vasoconstricting and vasodilating factors, pro- and anticoagulant factors, and many other mediators that directly impact cardiac metabolism, growth, contractile performance, and rhythmicity of the adult heart (Zhang and Shah, 2014).

Following MI circulating ECs can be detected in the blood, indicating severe damage to the vasculature and cardiac endothelial dysfunction (Mutin et al., 1999). The rapture of the vasculature results in reduced coronary vasodilator function post-MI in both, the infarct and the remote zone (Uren et al., 1994), limiting the oxygen and nutrient supply of the myocardium. Endothelial dysfunction also affects the coronary microcirculation (Sellke et al., 1990). Hence, the revascularization of damaged tissue is one of the crucial events of cardiac remodeling. The formation of new blood vessels does not only salvage ischemic myocardium but is also essential to prevent the transition to heart failure (Cochain et al., 2013). It has been shown that the formation of new microvessels starts as early as 3 days post-MI and occurs first at the border

zone of the infarct (Zhao et al., 2010). The same study proposed that vascular endothelial growth factor (VEGF) signaling is responsible for the initiation of the cardiac angiogenic response but might not be crucial for angiogenesis at later time points. Although angiogenesis is often associated with VEGF-signaling many different, VEGF-independent, signaling pathways exist, which are highly connected (Ferrara, 2010; Shibuya, 2008). Due to the importance of angiogenesis in cardiac remodeling EC-based proangiogenic therapies seem to be a promising strategy. Nevertheless, the lack of success of these approaches indicates the involvement of multiple cell types (Cochain et al., 2013) and further studies are needed to decipher the exact regulatory interactions and mechanisms.

3.6. Cardiomyocytes and myocardial infarction

CMs take up the largest cell volume of the healthy myocardium and are characterized by a high mitochondrial density, which allows them to fulfill the energy demand of the muscle metabolism. The sudden onset of ischemia following MI leads to a massive necrotic death of CMs, which release endogenous factors into the extracellular environment due to decreased plasma membrane integrity, triggering an inflammatory response. Recently, interleukin 1 alpha (Il-1α) and RNA, released by necrotic CMs, have been identified as key danger signals that induce an inflammatory response post-MI (Lugrin et al., 2015). The pro-inflammatory effect of necrotic CMs might be amplified by surviving CMs in the infarct border zone that produce and secrete pro-inflammatory cytokines (Prabhu and Frangogiannis, 2016). These cytokines support the recruitment of leukocytes and polarize them to a pro-inflammatory phenotype, establishing a strong inflammatory response.

The loss of CMs in the infarcted area is irreversible and results with time in the formation of scarred tissue. The number of dead CMs defines the size of the infarct which directly impacts the outcome of cardiac repair. Smaller infarcts have been associated with reduced remodeling and improved cardiac repair (Chareonthaitawee et al., 1995). For this reason, the development of efficient therapies predominantly focused on limiting infarct size. In order to do so many studies tried to identify the crucial factors that impact CM survival. It has been shown that CM- EC interactions significantly decrease myocyte death, implying a crucial role for the endothelium in formation and maintenance of myocardial structure (Narmoneva et al., 2004).

Moreover, it has been shown that granulocyte colony-stimulating factor (G-CSF) treatment improved cardiac function through the induction of anti-apoptotic proteins and inhibition of apoptotic death of CMs (Harada et al., 2005). The treatment also led to increased vascularization, caused by reduced apoptosis of ECs, indicating a reciprocal communication between CMs and ECs. These findings indicate that CMs are involved in functional communication during cardiac repair and most likely not only with ECs but also other non-CM.

4. POST-TRANSCRIPTIONAL REGULATION IN THE HEALTHY HEART AND AFTER MYOCARDIAL INFCARTION

Heart development and infarct healing are highly orchestrated processes incorporating different cell types and different layers of regulation. Only 1.5% of the genome encodes for protein coding genes (Alexander et al., 2010) and it is becoming increasingly apparent that non-coding RNAs (ncRNAs) play key roles in normal development and in regulating complex diseases such as MI. The non-coding genome is broadly divided into two subcategories based on the length of the transcripts. All transcripts with a length < 200 nucleotides (nt) are considered as small ncRNAs, whereas lncRNA are RNA molecules with > 200 nt. The relevance and function of ncRNAs has mainly been studied for small ncRNAs, especially miRNAs, whereas the analysis of lncRNAs is still in its infancy. The network of mediators is extended by RNA-binding proteins, which contribute significantly to the resolution of inflammation through degradation of pro-inflammatory cytokines.

4.1. Modulation of mRNA stability by RNA binding proteins

The timed shut down of the inflammatory response following MI is necessary to ensure effective cardiac repair. In contrast to anti-inflammatory mediators most cytokines and chemokines are primarily regulated by changes in mRNA abundance (Schott et al., 2014). The expression of these inflammatory signaling molecules is suppressed by RNA-binding proteins such as tristetraprolin (TTP, symbol = Zfp36) at a post-transcriptional level, as demonstrated by the development of generalized inflammation in TTP- knockout mice (Taylor et al., 1996). TTP accelerates the degradation of cytokine mRNAs by binding to AU-rich elements (ARE) in the 3'-untranslated region (3'UTR) of its target mRNAs. Recent studies have shown that TTP

significantly contributes to the resolution of inflammation through the degradation of approximately one third of inflammation induced mRNAs in Mφ, shifting their functional phenotype to a more anti-inflammatory state (Kratochvill et al., 2011; Sedlyarov et al., 2016). It has been shown that a timed phenotype transition improves cardiac repair (Harel-Adar et al., 2011), which underlines the importance of TTP activity and post-transcriptional regulation of the immune response. On a more global scale it has been shown that mRNA stability stronger correlates with structural features of genes than their function (Sharova et al., 2009). mRNAs coding for regulatory proteins, such as transcription factors (TF), cytokines, and chemokines, are predominantly less stable than mRNAs related to metabolism and structure, such as ECM and cytoskeleton components (Sharova et al., 2009). Nevertheless, RNA-binding proteins are not the only modulators of mRNA stability. mRNA degradation can also be initiated by miRNA binding to the 3'UTR of target genes.

4.2. microRNA structure, function, and computational analysis

miRNAs are ~22 nt endogenous, single-stranded, non-coding RNAs that regulate gene expression by mRNA binding to direct transcript destabilization, translational repression, or both (Bartel, 2004; Friedman et al., 2009; Preusse et al., 2016). Different studies have shown that the majority of miRNA-induced gene repression can be explained by reduced expression levels of targeted mRNAs (Lu et al., 2008). To date, 1193 murine and 382 porcine miRNAs are annotated in the miRBase database (miRBase version 21). miRNAs are predicted to regulate hundreds of genes in mammals and are evolutionary highly conserved (Bartel, 2004). Consequently, miRNAs are implicated in nearly all developmental and pathological processes in animals. A single miRNA is capable of regulating several mRNAs, interfering with a wide range of functions and pathways at the same time. On the other hand, one mRNA can be targeted by multiple miRNAs and the regulatory effect might depend on combined miRNA actions (Preusse et al., 2016). miRNAs capture tissue and cell type specific effects and their expression profiles can be used to distinguish between samples of different physiological and pathological conditions (Liang et al., 2007).

The integration of mRNA and miRNA expression data might add an additional regulatory layer to reconstructed GRN and has the capability to reveal regulatory

mechanisms which otherwise would go unnoticed. The main requirement for such integration is the accurate identification of miRNA target genes. Based on the high preservation of miRNA- mRNA pairings, miRNA targets can be predicted by searching for conserved 6-8mer matches to miRNA seed regions (Figure 4A)(Friedman et al., 2009). Nevertheless, perfect sequence complementarity alone is not always sufficient for repression. A combination of computational and experimental approaches has been used to identify further features of site context, including positioning of the miRNA seed within high local AU composition, proximity to sites for co-expressed miRNAs and specific positioning of miRNA binding sites within the 3'UTR of their target genes (Grimson et al., 2007).
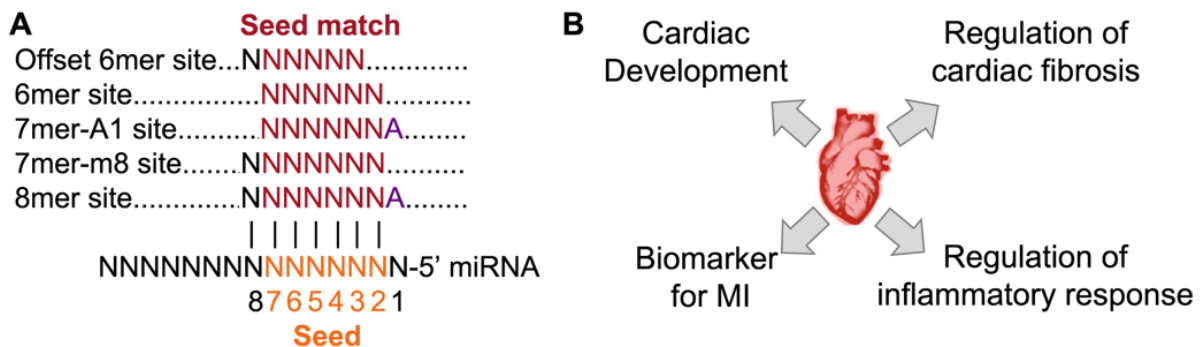
Figure 4: miRNA- mRNA pairing and the role of miRNAs in the heart. A) Sites matching the miRNA seed region. B) Functional impact of cardiac miRNAs.

Different target prediction algorithm have been developed, including TargetScan (Agarwal et al., 2015) and miRWalk (Dweep and Gretz, 2015). miRWalk provides the largest collection of predicted and experimentally verified miRNA- target interactions (~949 million) including three different organisms: human, mouse, and rat. Target prediction can be carried out applying multiple established algorithms (e.g. TargetScan, miRanda) and/or using the miRWalk algorithm, which relies on Watson-Crick complementarity between the miRNA seed (7mer) and the mRNA 3'UTR. TargetScan does not only rely on sequence complementarity but also requires conservation of identified 8mer, 7mer or 6mer sites in five vertebrate genomes (human, mouse, rat, chicken, dog)(Lewis et al., 2005). A comprehensive review of available target prediction algorithms can be found in (Yue et al., 2009).

miRNA activity plays a key role in many different BPs (Figure 4B), including heart and cardiovascular development (Cordes and Srivastava, 2009; Liu and Olson,

2010; Olson, 2006), acute MI (Dong et al., 2009), and cardiac fibrosis (Pan et al., 2012; Van Rooij et al., 2008; Wang et al., 2012). It is well accepted that the integration of miRNA activity into cardiac signaling and transcriptional pathways is a necessary step to gain a comprehensive understanding of the regulatory interactions that govern cardiac gene expression (Liu and Olson, 2010). In the case of MI, the cardiac miRNA expression profile undergoes changes that differ between the infarcted and non-infarcted area (Dong et al., 2009). Moreover, circulating miRNAs (e.g. miR-499, miR-208b, miR-1) have been found to be sensitive biomarkers of MI that can be used in diagnostic medicine for early detection of MI (Adachi et al., 2010; Ai et al., 2010; Wang et al., 2010).

4.3 Long noncoding RNAs

lncRNAs are endogenous RNA molecules with a transcript length > 200 nt. Although little is known about their exact function and regulatory mechanisms, growing evidence indicates that they play important roles in diverse cellular processes and diseases (McHugh et al., 2015; Xiang et al., 2014; Yang et al., 2012). Recent studies revealed changes in lncRNA expression in the infarcted heart, identifying new candidates for potential target treatment (Ounzain et al., 2015; Vausort et al., 2014; Zangrando et al., 2014). However, originally the existence of lncRNAs was attributed to transcriptional 'noise', which is supported by the facts that individual lncRNAs are transcribed at much lower levels than individual mRNAs and the low sequence conservation between species (Derrien et al., 2012). In contrast, the promotor sequences of lncRNAs show a higher conservation compared to protein coding genes. Thus, the level of lncRNA transcription seems to be highly conserved but not the nucleotide sequence itself.

LncRNAs are usually located close to protein coding genes in the genome and can be categorized into five criteria (Ponting et al., 2009): sense, antisense, bidirectional, intronic and intergenic (Figure 5). Due to their close proximity to protein coding genes it is assumed that neighboring lncRNAs and mRNAs are co-expressed and thus co-regulated (Rinn and Chang, 2012). Based on this assumption a method termed "guilt by association" can be applied to estimate the function of unannotated lncRNAs depending on the function of their co-expressed protein coding genes.
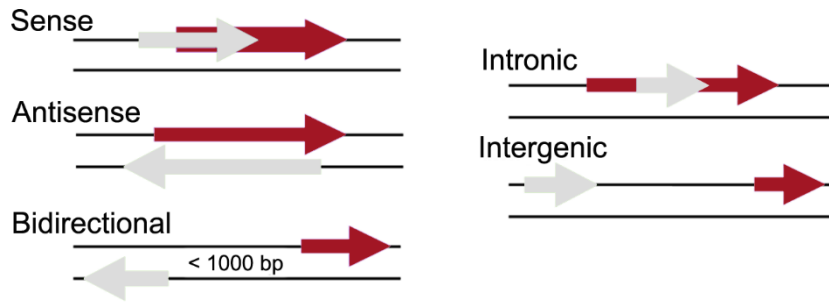
Figure 5: Categorization of lncRNAs based on genomic location. Red arrows indicate protein coding genes, grey arrows indicate lncRNAs.

Furthermore, it has been suggested that some lncRNAs are precursors to short ncRNAs, such as miRNAs. An example of this is the lncRNA *H19* which contains the exon that encodes the miRNA mir-675 (Cai and Cullen, 2007). LncRNAs share many features with mRNAs, such as transcription by RNA polymerase II, the presence of multiple exons, 5'capping, and polyadenylation, but they lack a long open reading frame (Derrien et al., 2012). Genome-wide stability analysis in mouse further revealed a comparable range of half-lives between lncRNAs and mRNAs with only a minority of unstable lncRNAs (Clark et al., 2012). Furthermore, a striking similarity between lncRNA sequences and the 3'UTR of protein coding genes in terms of structural features and sequence composition has been found (Niazi and Valadkhan, 2012). In accordance with this finding, it has been reported that lncRNAs can act as miRNA sponges, titrating miRNAs away from their respective mRNA targets (Cesana et al., 2011; Wang et al., 2013). Recently, the competitive endogenous RNA (ceRNA) hypothesis was introduced to build a large-scale regulatory network across the transcriptome, involving protein coding genes, pseudogenes, lncRNAs and miRNAs, which are all linked via miRNA response elements (MREs) (Salmena et al., 2011). It is one of the first systematic approaches to capture the intrinsic complexity of BPs by integrating different levels of regulation. Another appeal of the hypothesis is its attempt to elucidate the yet unknown function of many lncRNAs encoded in the genome. However, the hypothesis is rather controversial and experimental quantifications of the ceRNA effect do not support the proposed regulatory mechanism (Thomson and Dinger, 2016).

OBJECTIVES

OBJECTIVES

The main goal of this thesis is to decipher the transcriptional network of distinct cardiac cell types (CM, FB, EC, Mφ) in the healthy heart and post-MI through bioinformatics analysis of two sets of ad-hoc generated transcriptomic data acquired from different animal and MI models.

Specific aims:

1. Development and implementation of novel and original visualization methods for the integration and representation of functional annotations and quantitative variables, such as expression levels.

2. Characterization of the molecular changes in the transcriptome of distinct cardiac cells (EC, CM, FB, Mφ) in the healthy heart and after MI using exhaustive bioinformatics analysis of transcriptomics data of two MI and animal (mouse and pig) models.

3. Implementation of data integration approaches to achieve appropriate comparison of publicly available data of tissue resident Mφ and *in vitro* activated Mφ. The comparison aims to identify cardiac specific transcriptional programs and to determine the polarization state of post-MI Mφ.

4. Application of mathematical models to identify key regulatory elements of the transcriptional network and to simulate phenotypic changes upon perturbation of the modeled biological system.

5. Integration of different molecular and regulatory levels to elucidate the impact of post-transcriptional regulation on cardiac Mφ gene expression and to estimate its potential in controlling Mφ phenotype transition.

6. *In silico* construction of a cell- cell interaction network to shed light on the potential interplay of cardiac Mφ and other cardiac cell lineages.

MATERIALS AND METHODS

Materials and Methods – murine cardiac macrophages (project 2)

All experimental procedures were carried out by other members of the laboratory and are only described in brief to provide the necessary background for the *in silico* analysis of the gathered data.

Mice

2-3 months old C57BL/6 (males and females, Charles Rivers) and CX$_3$C chemokine fractalkine receptor knock-in (CX$_3$CR1$^{GFP/+}$) mice (36) were used in this study. All animal procedures were conducted in accordance with EU Directive 2010/526/EC, and enforced in Spanish law under Real Decreto 1201/2005.

Mice model of myocardial infarction

Cryoinjury was used as MI model in this study. The procedure was performed as previously described (van Amerongen et al., 2008). Briefly, mice were weighed, anesthetized, and intubated for artificial ventilation. A thoracotomy was performed through the fourth left intercostal space, the pericardium was opened, and the heart was exposed. Cryoinjury was induced applying a 3 mm diameter cryoprobe, cooled to -196°C with liquid nitrogen to the anterior left ventricle free wall for 10 seconds. After this, the procedure was repeated two times. The exact position of the probe was carefully set using the left atrium and pulmonary artery as anatomic landmarks. Animals were randomly sacrificed by CO$_2$ inhalation 3, 7 and 30 days post-MI. Mφ samples from healthy animals were not subjected to any surgery and were included as physiological condition (day 0).

Fluorescence-activated cell sorting (FACS) analysis and cell sorting

Single cell suspensions were obtained from heart, spleen, lung and peritoneum. Mice were euthanized by CO$_2$ inhalation and immediately perfused by intracardiac injection of ice-cold phosphate buffered saline (PBS). Right and left atria were removed and the ventricles were minced with fine scissors, and digested in collagenase IV 0.1% (528 U/mg Sigma) in PBS at 37°C for 45 min under gentle shaking. Whole spleen was collected and mechanically disrupted. Peritoneal cells were harvested by peritoneal cavity lavage (10mL of cold PBS). Alveolar cell suspension was obtained by bronchoalveolar lavage (6 times) with 1ml of FACS buffer using a blunt syringe.

MATERIAL AND METHDOS

All samples were filtered through nylon mesh of 100 µm (BD biosciences) to obtain a homogeneous cell suspension, and heart and spleen suspensions were subjected to red blood cells lysis with 1x RBC Lysis buffer solution (eBioscience, CA). The resulting single-cell suspensions were Fc-blocked using anti-mouse CD16/CD32 antibody (BD Pharmingen) for 30min at 4ºC in FACS buffer. Antibodies were incubated for 30 min at 4ºC in FACS buffer. Where appropriate, cells where further incubated with streptavidin conjugates for 30min at 4ºC. Flow cytometry studies were performed on a BD FACSCantoTM II and subsequently analysed with FlowJo Software (Tree Star). Cell sorting was performed using BD FACS-ARIA^{TM} II cell sorter (BD Biosciences) and all the samples were sorted into PBS supplemented with 10% fetal bovine serum (FBS). Within the $CD45^+$ and $CD11b^+$ population a $Ly6c^{low}/CX_3CR1^{high}$ population and a $Ly6c^{high}/CX_3CR1^{low}$ population was distinguished.

RNA isolation and quantitative Real Time PCR (q-RT-PCR)

Sorted cells were placed in Tri Reagent (Ambion) for RNA isolation. Total RNA, including small RNA, was isolated from three independent biological replicates using miRNeasy Micro Kit with RNeasy MinElute Spin Columns (Qiagen) with DNaseI treatment. RNA was analyzed with the NanoDrop (Thermo Scientific) and the Bioanalyzer (Agilent Technologies) system for measuring RNA quality and quantity. Complementary DNA (cDNA) synthesis was performed with 500 ng of total RNA by using High Capacity cDNA Reverse Transcription Kit (Applied Biosystems). For relative quantification of expression, quantitative real-time polymerase chain reaction (PCR) analysis was performed using Sybr Green probes (genes analysed) in AB7900 FAST 384 Detection System (Applied Biosystems), according to the manufacturer´s instructions. Gene expression values were normalized to the housekeeping genes 36b4 and cyclophilin, and expressed as relative mRNA level. Data were analyzed by qBASE program (Biogazelle, Zwijnaarde, Belgium) obtaining the cycle threshold (Ct) of the amplification products. Primer sequences can be provided by request.

Cell culture

Peritoneal thioglycollate-elicited Mφ were isolated from the peritoneal cavity 3 days after injection of thioglycollate. Cells were plated in Roswell Park Memorial Institute

(RPMI) medium supplemented with 10% of heat-inactivated FBS and 1% penicillin-streptomycin solution. Cells cultured in normoxia were incubated in the presence or the absence of 10 ng/mL IFNγ (ThermoFisher) for 24h.

Hypoxic conditions

Cells were routinely cultured in 21% O_2 and 5% CO_2 (normoxic conditions). To expose the cells to hypoxia, they were placed in an *in vivo* SCI-tive Hypoxia Workstation (Baker Ruskinn) that was infused with a mixture of 0.5% O_2, 5% CO_2 and 94.5% N_2. Cells cultured in hypoxia were incubated in the presence or the absence of 10 ng/mL IFNγ (ThermoFisher) for 24h.

RNA Sequencing

For RNASeq 2 ng of total RNA from three independent biological replicates was used. cDNA was amplified using the Ovation® RNA-seq System v2 (NuGEN® Technologies, San Carlos CA). Amplified cDNA (1 μg) was sonicated to an average size of 100-300 bp and used with the TruSeq DNA Sample Preparation v2 Kit (Illumina) to generate index-tagged sequencing libraries. Libraries were sequenced using the Genome Analyzer IIx (Illumina) followed by standard RNA sequencing protocol to generate single reads of 75 bps. Fastq files containing reads for each library were extracted and demultiplexed using Casava (Ilumina) pipeline. Sequencing adaptor contaminations were removed from reads using cutadapt software (version 1.3) and the resulting reads were mapped and quantified on the transcriptome (GRCm38) using RSEM (version 1.2.20).

mRNA abundance and differential gene expression

TMM normalization method was applied to estimated counts from RSEM. The resulting $\log_2$ counts per million (CPM) were used as a proxy of gene expression in each sample. Genes were kept if they were expressed in at least six samples. Gene expression differences were assessed using the edgeR package with correction for multiple testing (Benjamini-Hochberg). Genes with an adjusted p-value < 0.05 and an absolute $\log_2$ fold-change (logFC) > 1 were considered differentially expressed.

MATERIAL AND METHDOS

Exploratory analysis of mRNA expression profiles

Due to the high dimensionality of high-throughput data, unsupervised exploratory analysis techniques are used to analyze gene expression data and to obtain a first insight into the dataset. Classical techniques include principal component analysis (PCA) and different clustering algorithms such as hierarchical clustering (HC) and k-means clustering. PCA performs an orthogonal transformation of the data into a new set of linearly uncorrelated variables (the principle components), reducing the dimensionality of the data while capturing most of its variation. Here PCA was applied to the $\log_2$ CPMs of filtered genes and Mφ samples from the healthy heart and post-MI.

Normalized Mφ samples were clustered applying HC with average linkage as clustering method and Euclidean distance as distance measure. To identify groups of genes with similar expression profiles k-means clustering was used. Whereas HC determines the number of clusters automatically, k-means clustering requires this information as an input. Here the R package clValid (Brock et al., 2011) was used to determine the optimal number of clusters (often referred to as *k*) based on internal measures. K-means clustering was performed on normalized $\log_2$ CPMs (z-score) of genes DE in at least one condition using GENESIS software (Sturn et al., 2002). The result was visualized as a heatmap of normalized expression values for each cluster, created with ggplot2.

Functional analysis

To identify overrepresented biological categories PANTHER classification system version 10.0 (Mi et al., 2016), based on the GO database (version 1.2), was applied with default settings for mouse using the annotation dataset 'GO biological process complete'. Bonferroni correction was used to correct for multiple testing. If not indicated otherwise, terms with a fold enrichment > 2 and an adjusted p-value < 0.01 were considered for further analysis.

Data integration and comparison with publicly available datasets

Comparison with *in vitro* polarized Mφ

For the comparison of *in vivo* Mφ from the healthy heart and post-MI with *in vitro* activated murine Mφ, two gene expression data series were downloaded from the

MATERIAL AND METHDOS

National Center for Biotechnology Information (NCBI) Gene Expression Omnibus (GEO): GSE32690 and GSE53321. The data was normalized, $\log_2$ transformed and adjusted for batch effects using the comBat function implemented in the R package sva (Leek et al., 2012). Whole gene expression profiles were clustered using average linkage and the result was visualized as an unrooted dendrogram using the R package ape (Paradis et al., 2004).

Comparison with other tissue resident Mφ

To compare *in vivo* cardiac Mφ with other tissue resident Mφ and immune cells, gene expression data series for brain, peritoneum, spleen, liver, lung, large intestine and small intestine tissue Mφ (GSE15907, GSE63340), monocytes and neutrophils (GSE15907) were downloaded from the NCBI GEO. The data was normalized, $\log_2$ transformed and adjusted for batch effects using the comBat function implemented in the R package sva. Samples with and without batch correction were clustered applying HC, to underscore the necessity of batch removal techniques. A correlation matrix of all samples (batch corrected) was calculated and visualized with the heatmap.2 function of the R package gplots (Warnes et al., 2013). DE analysis of quantile normalized data was carried out with the edgeR package, where experiment batches were included as covariates in the statistical model. Genes DE in at least one of the contrasts (adjusted p-value < 0.05) were further grouped by k-means clustering (k = 15). A heatmap of normalized expression values for each cluster was created using the ggplot2 package.

Computational deconvolution of post-MI Mφ gene expression profiles

The R package CellMix (Gaujoux and Seoighe, 2013) was used for *in silico* gene expression deconvolution analysis (Figure 1). Gene expression deconvolution has been mostly used to identify the contribution of different cell types within heterogeneous samples, like brain and blood (Capurro et al., 2015; Kuhn et al., 2012; Shen-Orr et al., 2010). Although the exact relationship between cell type specific gene expression and gene expression of mixed samples is not well defined, the deconvolution of mixed gene expression profiles is assumed to be linear (Shen-Orr et al., 2010). Hence, gene expression deconvolution methods are formulated as linear models, where the global expression value of gene *i* in sample *j* is the sum of its

expressions in the *r* cell types:

$$x_i = \sum_{k=1}^{r} w_{ik} h_{kj} + \varepsilon$$

where w_{ik} is the specific gene expression in cell type *k*, and h_{kj} the proportion of cell type *k* in sample *j*. Considering all genes together, the following matrix decomposition problem arises:

$$X \approx WH$$

where *X* is the gene expression matrix, *W* is the signature matrix, containing cell type specific expression profiles, and *H* is the cell type proportion matrix. To solve the matrix decomposition problem, different methods exist that also depend on the availability of additional data such as known marker genes or cell type proportions. If neither the signature matrix *W* nor the proportion matrix *H* is available, then complete deconvolution methods estimate both the cell signatures and proportions directly from the provided gene expression data (Repsilber et al., 2010). If at least one of the matrices is available, then partial deconvolution methods can be applied.
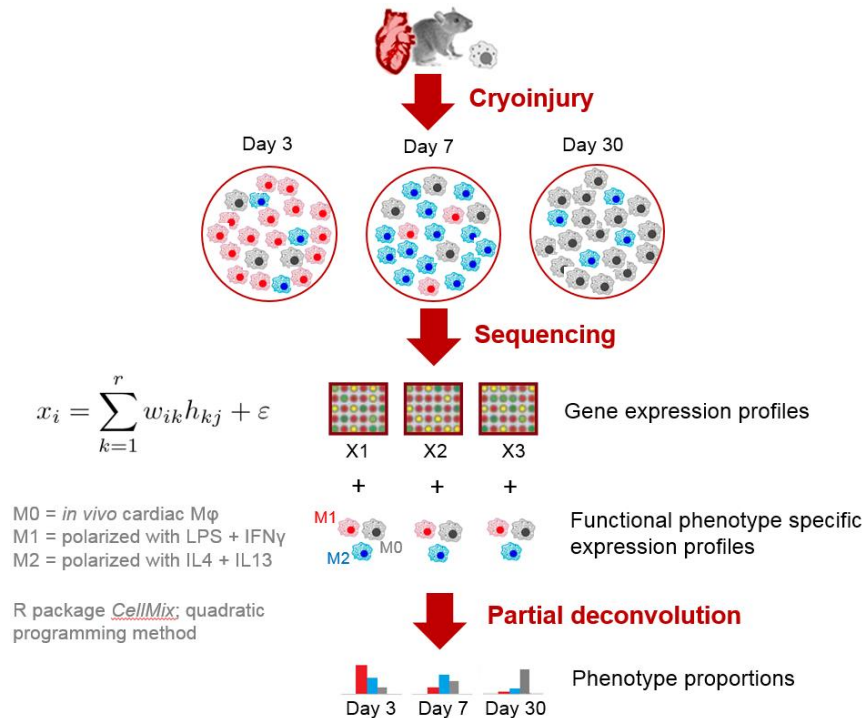

Figure 1: Workflow to computationally estimate phenotype proportions in post-MI Mφ gene expression profiles. Transcriptional profiles of *in vivo* cardiac Mφ isolated from the healthy heart and *in vitro* activated Mφ (GSE53321) were used as signatures.

Here we were interested in estimating the contribution of M1/M2 transcriptional

programs in our ad-hoc generated transcriptomics data of post-MI Mφ. For that purpose, we used quadratic programming (Gong et al., 2011) to estimate phenotype proportions using the *in vivo* control sample and *in vitro* derived, phenotype-specific expression profiles as expression signatures (Figure 1). The advantage of the quadratic programming approach is that it efficiently identifies the global optimum of the matrix decomposition while at the same time preserving non-negativity of the phenotype proportions. In gene expression deconvolution, non-negativity of the phenotype proportions is a necessity to obtain biologically relevant results.
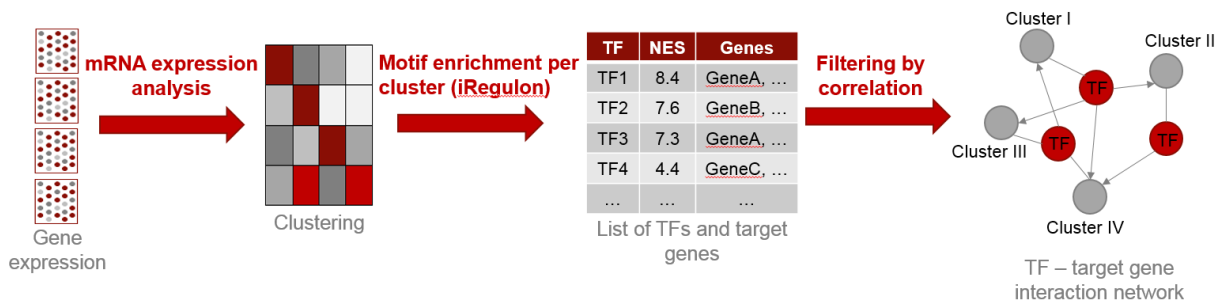
Identification of transcriptional regulators

Figure 2: Workflow to identify transcriptional regulators of co-expressed genes.

In order to efficiently identify transcriptional regulators of co-expressed genes we followed the workflow depicted in Figure 2. The iRegulon App (Janky et al., 2014) was applied to each gene cluster to search for enriched motifs 20kb centered around the transcription start site (TSS) of the co-expressed genes and to link enriched motifs to known TF binding sites. The resulting list of enriched motifs was filtered and only motifs that are potentially recognized by at least one DE TF were kept. Enriched motifs were ranked by decreasing normalized enrichment score (NES) applying the default iRegulon NES cutoff of 3.0. Identified TFs were linked to their target genes and the resulting list of TF – target gene pairs was imported into cytoscape. In order to enhance and to simplify the resulting network, target genes were grouped according to their cluster membership. Although gene products can influence the expression of their regulators, the network only represents interactions going from the TFs to the target genes and not vice versa. Hereby we took into account that TFs can be activators or repressors and filtered the list of predicted interactions by correlation between the TF and its target gene. Only interactions with an absolute correlation coefficient (CC,

spearman) > 0.7 were kept. As a subgroup of transcriptional regulators we focused on the identification of nuclear receptors and the GOCluster function of the R package GOplot (project 1) was used to visualize hierarchical clustering and expression profiles of DE nuclear receptors (adjusted p-value < 0.05).

In silico analysis of the secretome and receptome

To estimate the extracellular signaling potential of cardiac Mφ, genes DE in at least one comparison were classified according to their cellular location and a list of secreted molecules (ligands; SM) and membrane proteins (receptors; MP) was curated semiautomatically. As a preliminary step, the list of DEGs was filtered, excluding all genes that were not annotated with one of the following terms from the GO_CC hierarchy: "extracellular region" (GO:0005576), "extracellular space" (GO:0005615), "cell surface" (GO:0009986) and "extracellular matrix" (GO:0031012). Subsequently, the Human Protein Atlas (Uhlen et al., 2015) was used to classify cellular location of the proteins encoded by our list of selected genes more precisely. The cellular localization of the encoded proteins was manually confirmed in the literature. PANTHER classification system was used to perform the functional analysis of the SMs and MPs per cluster. We were further interested in estimating the homeotypic paracrine signaling potential of the identified SMs and hence used the STRING database (Szklarczyk et al., 2015) to extract predicted interactions for all SMs and MPs. The active prediction methods "co-expression", "experiments", "databases" and "text mining" and a score > 0.8 were selected. Subsequently, the list of possible interactions for SMs was crossed with the list of predicted MP-ligand pairs to distinguish *in silico* between heterotypic and homeotypic paracrine signaling. Homeotypic paracrine signaling pairs and their expression were visualized using the GOChord() function of GOplot.

miRNA microarray data analysis

Intensity data from microarray images were extracted with Feature Extraction Software (Agilent Technologies). The total gene signal was quantile normalized and miRNAs were kept if they were expressed in at least six samples. PCA was applied to the whole miRNA expression profile of all samples. Limma (Smyth, 2005) was used to perform the DE analysis for miRNAs with correction for multiple comparisons (Benjamini-

Hochberg). miRNAs with an adjusted p-value < 0.05, an absolute logFC > 1 and an average expression value > 4.0 were considered differentially expressed.

miRNA – mRNA interactions

miRNA – mRNA interactions were analyzed through three different approaches, following the workflow depicted in Figure 3.
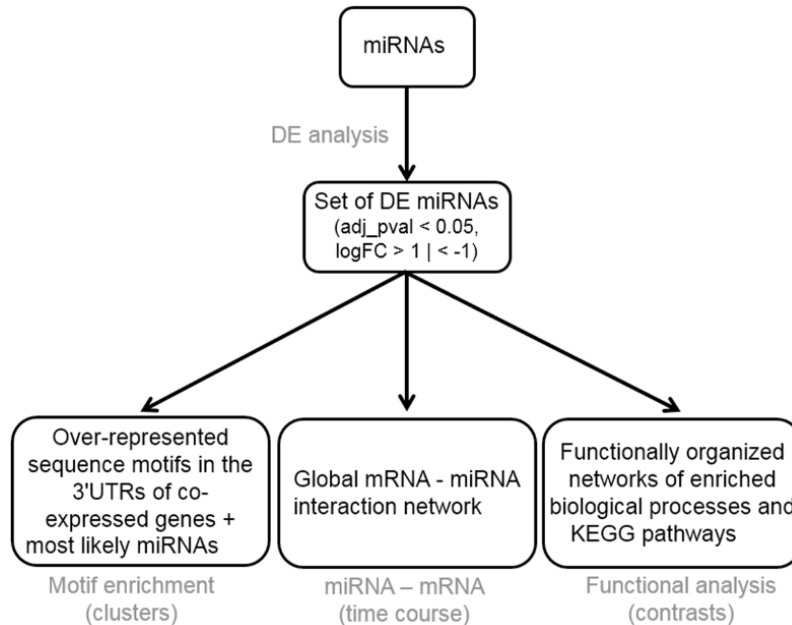

Figure 3: Computational analysis of miRNA – mRNA interactions.

Motif enrichment

miRvestigator (Plaisier et al., 2011) was used to search for enriched motifs within the 3'UTR of co-expressed genes and to identify the most likely miRNAs regulating these genes. The parameters used were default settings except: seed models = 6mer, 7mer and model wobble base – pairing = 'yes'. In brief, miRvestigator determines *cis*-regulatory signatures within the 3'UTR of co-expressed genes using the Weeder software package (Pavesi et al., 2006). A hidden Markov model is then used to systematically compare enriched motifs as a matrix (position specific scoring matrix) to miRNA seed sequence strings, which leads to a more probabilistic solution in identifying the most likely complementary miRNA seed. The resulting list of potential mRNA – miRNA interactions was filtered by expression and only miRNAs anti-correlated (CC < -0.7) to the median expression profile of the target cluster were kept.

MATERIAL AND METHDOS

Temporal miRNA – mRNA interaction network

All DE miRNAs were used as input for mirWalk (Dweep et al., 2011) to predict mRNA targets based on the mirWalk and TargetScan algorithm. Only predicted mRNA target genes that were DE in at least one of the comparisons were kept and the remaining list of miRNA – mRNA pairs was filtered based on expression (anti-correlation, CC < -0.9). Subsequently, the resulting list of 31196 miRNA – mRNA interactions was imported into cytoscape to visualize and analyze the miRNA - mRNA interaction network. Due to the high complexity of the network, the perfuse force directed layout was applied to improve comprehensibility. The algorithm assigns forces among the set of edges and the set of nodes and reduces the number of crossing edges by minimizing the energy (Kobourov, 2012). Node color (genes and miRNAs) was mapped to the normalized expression values (z-score) at various temporal stages, to highlight the dynamical changes in transcription.

Functional analysis of miRNAs

To identify the role of miRNAs in Mφ transition, miRNAs DE in the contrast Day 7 vs Day 3 were used as input for mirWalk to predict mRNA targets. The interactions were filtered as described before and they were automatically split into two networks according to miRNA expression (miRNA up-regulation at day 3 or day 7). Functional analysis of the networks was performed with the cytoscape plugin ClueGO (Bindea et al., 2009). ClueGO performs common enrichment analysis based on the hypergeometric distribution and creates functionally organized GO/pathway term networks. Here we selected as ontologies/pathways GO Biological process and Kyoto Encyclopedia of Genes and Genomes (KEGG) Pathway databases with evidence on the level 'All_experimental'. Optionally ClueGO also simplifies the resulting network by fusing GO terms that are in a parent-child relation and preserving the most representative term. The 'GO Term Fusion' option was applied and only terms with an adjusted p-value < 0.05 (Bonferroni step down) were considered. ClueGO then connects the selected terms based on their shared genes, which serves as a similarity measure. The actual strength of the connection is calculated based on corrected kappa statistics. Similar to clustering approaches, functional groups are finally created by iteratively merging the different groups. In this analysis the initial group size was set to 2 and a 35% overlap was set as threshold to merge groups with fixed group coloring.

For each group the most significant term was displayed.

lincRNA analysis

In order to get a first impression of the number of lincRNAs in our data, Ensembl biotype information from biomaRt (Durinck et al., 2005) was used to classify DEGs as long intergenic non-coding RNAs (lincRNAs), protein coding genes and pseudogenes. Based on the ceRNA hypothesis, which proposes that the different RNAs are linked through MRE, we aligned mRNA 3'UTR sequences with lincRNA sequences and searched for common miRNA seed sequences (7mer, perfect match, starting at 1st position). Extracted mRNA - lincRNA - miRNA triangles were further filtered by expression and only interactions with CC > 0.7 or CC < -0.7 were kept. The nature of the interactions was determined by plotting the CC values between mRNA and lincRNA expression profiles on the x-axis, the CC values between lincRNA and miRNA expression profiles on the y-axis, and mapping the CC values between mRNA and miRNA expression profiles to the fill color of the displayed points. The four different cases of lincRNA – miRNA – mRNA interactions were subsequently summarized in the middle of the figure as small graphics. Based on the available literature, lincRNA – miRNA – mRNA interactions of interest were selected and the R package HiveR (HiveR Version 0.2.55, academic.depauw.edu/~hanson/HiveR/HiveR.html) was used to create a hive plot of these interactions.

Based on the "guilt by association" principle, the BEDOPS closest-features program (Neph et al., 2012) with --no-overlaps option was used to identify the closest protein coding genes upstream and downstream of each lincRNA. The reported list was further filtered to exclude protein coding genes that were not DE. Subsequently, cytoscape was used to create small networks where two protein coding genes were connected through at least one lincRNA. ClueGO was used to perform the functional analysis of the networks with the same settings as described above.

Network-based analysis of cardiac Mφ mRNA expression

To obtain a more detailed understanding of the regulatory mechanisms that drive cardiac Mφ gene expression we used a network-based approach following the workflow depicted in Figure 4.
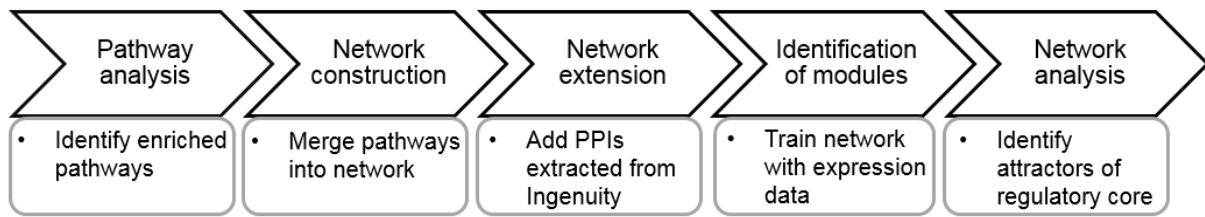
Figure 4: Workflow of network-based analysis of cardiac Mφ mRNA expression.

The initial step of the analysis aimed at the identification of pathways enriched in any post-MI stage compared to control. The pathway analysis was performed using PathVisio (version 3.2.2)(Kutmon et al., 2015). The mouse pathway collection from WikiPathways (Kelder et al., 2012) was used to perform an over-representation analysis with the transcriptomics data set. Subsequently, the pathways were ranked based on a standardized difference score (z- score). Pathways with a z-score > 2.0, p value < 0.05 and minimum number of four measured genes were considered significant. Enriched pathways were imported as networks into cytoscape using the WikiPathways app (Kutmon et al., 2014) and subsequently merged into one network.

In order to increase the number of DEGs in the network, the network was extended with protein – protein interactions (first neighbours) extracted from Ingenuity software (Ingenuity Systems, Mountain View, CA) between the genes in the pathways and DEGs. Next, the jActiveModules app (Ideker et al., 2002) was used to identify active modules, i.e., small, connected subnetworks with significant changes in expression, within the molecular interaction network. The details of the method can be found in (Ideker et al., 2002), in brief, the method is comprised of a rigorous statistical measure for scoring subnetworks and a search algorithm to identify high scoring subnetworks. First, an aggregated z-score is calculated per subnetwork, summarizing the individual z-scores, which are converted p-values obtained with the program VERA (Ideker et al., 2000), over all genes in the subnetwork. In order to estimate the significance of an obtained aggregated z-score, the value is compared to the distribution of scores for random gene sets of similar size. After scoring the different subnetworks, a simulated annealing approach is used to find the subnetworks with the highest scores. Here, the subnetwork with the highest score was selected for further analysis.

The topology of the selected subnetwork was analyzed and the SCC was calculated using the BiNoM app (Zinovyev et al., 2008). Within the SCC every pair of genes is

connected through a directed path and changes in the state of one gene might affect the genes of the remaining SCC. Hence, a Boolean dynamical model with a synchronous updating scheme (Garg et al., 2007), as described before, was used to identify stable states (attractors) of the SCC.

Materials and Methods – Porcine cardiac cells (Project 3)

All experimental procedures were carried out by other members of the CardioNext project and are only described in brief to provide the necessary background for the *in silico* analysis of the gathered data.

Pig

Experiments were performed in male Large-White pigs weighing 30 kg to 40 kg. The study was approved by the Institutional Animal Research Committee and conducted in accordance with the recommendations of the Guide for the Care and Use of Laboratory Animals.

Pig myocardial infarction model

Closed-chest ischemia-reperfusion was used as MI model in this study. The procedure was performed following the protocol described in (Garcia-Prieto et al., 2014). Briefly, pigs were anesthetized, intubated, and mechanically ventilated with oxygen. An angioplasty balloon was introduced via the percutaneous femoral route and the left anterior descending coronary artery was occluded for 30 minutes. Following reperfusion pigs were sacrificed at 3 days and 7 days post-MI. Control pigs were sacrificed without any intervention.

Cell isolation

Single cell suspensions were obtained for CM, Mφ, FB, and EC. In brief, the heart was harvested from sacrificed pigs and immediately perfused. The heart was chopped into small pieces and digested in collagenase at 37°C with maximal shaking. Following digestion, the suspension was centrifuged for 4 minutes at 500 revolutions per minute. The supernatant was collected for the isolation of EC, Mφ, and FBs. CMs were extracted and further purified, by repeated steps of digestion and centrifugation, from

the pellet. ECs, Mφ, and FBs were isolated from the collected supernatant through FACS. CD45^{high}/CD68^{high} cells were selected as Mφ, and within the CD45$^-$ cell population CD31^{high}/CD46^{high} cells were selected as ECs and CD31^{low}/CD46^{high} cells were selected as FBs.

RNA Sequencing

For RNASeq 2 ng of total RNA were used and amplified cDNA (1 μg) was sonicated to an average size of 100-300 bp and used with the TruSeq DNA Sample Preparation v2 Kit (Illumina) to generate index-tagged sequencing libraries. Libraries were applied to Genome Analyzer IIx (Illumina) followed by standard RNA sequencing protocol to generate single reads of 75 bps. Fastq files containing reads for each library were extracted and demultiplexed using Casava (Illumina) pipeline. Sequencing adaptor contaminations were removed from reads using cutadapt software (version 1.7.1.) and the resulting reads were mapped and quantified on the transcriptome (Sscrofa10.2.73) using RSEM (version 1.2.20.).

mRNA profile and exploratory analysis of porcine cardiac cells

Log2 TPM values from RSEM were used as a proxy of gene expression in each sample. The gene expression profiles were further filtered and only genes which were expressed in at least six samples were kept. As described for murine cardiac Mφ, PCA was applied to the whole gene expression profile of all samples. Due to the lack of biological replicates, we selected genes with expression intensities ranked above the 95th percentile (i.e., top 5% of expression intensities) for each cell type and time point for downstream analysis. The selected top expressed genes were clustered applying HC with average linkage and Euclidean distance.

Functional analysis

Ensembl gene IDs (Sus scrofa) of top expressed (top 5%) genes were provided as input for the PANTHER classification system to determine overrepresented biological categories. PANTHER was applied with default settings for pig, using the annotation dataset 'GO biological process complete'. Bonferroni correction was used to correct for multiple testing. Terms with an adjusted p-value < 0.05 were further considered.

MATERIAL AND METHDOS

Secreted molecules and membrane proteins

For each cell type a list of SMs and MPs was curated semiautomatically, based on the top 5% expressed genes per time point. The Human Protein Atlas was used to classify cellular location of the proteins encoded by the top expressed genes. Subsequently, the cellular localization of the molecules was confirmed in the literature. Venny (Oliveros, 2013) was used to create Venn diagrams of SMs and MPs of the different cell types per time point. As described in the paragraph above, PANTHER was used to perform the functional analysis of the SMs and MPs. In an attempt to reconstruct a cell-cell interaction network, Ingenuity software (IPA®, QIAGEN Redwood City, www.qiagen.com/ingenuity) was used to extract experimentally validated interactions between identified SMs and MPs. The resulting list of interactions was imported into cytoscape, with nodes representing SMs (circle) and MPs (arrowhead). Nodes were manually arranged in a circular pattern based on their shared expression between cell lineages.

miRNA sequencing

1 ng of total RNA was used and amplified cDNA (1 µg) was used with the TruSeq Small RNA Sample Preparation Kit (Illumina) to generate index-tagged sequencing libraries. Libraries were applied to Genome Analyzer IIx (Illumina) followed by standard RNA sequencing protocol to generate single reads of 75 bps. Fastq files containing reads for each library were extracted and demultiplexed using Casava (Illumina) pipeline. Sequences were trimmed, size selected and miRDeep2 software (Friedländer et al., 2012) was used to map the reads to all miRBase mature pig miRNAs (Sscrofa10.2) for quantification.

miRNA analysis

PCA was applied to the whole miRNA expression profile of all samples. The miRNA expression profiles were further filtered and only miRNAs which were expressed in at least six samples were kept. EdgeR was used to identify cell type- specific miRNAs. miRNAs with an expression intensity above the 95th percentile were considered as top expressed. miRNA – mRNA interaction networks were created considering only top expressed miRNAs and mRNAs. Based on expression, a correlation matrix (rows = miRNAs, columns = mRNAs) of all miRNAs and mRNAs was calculated and only

possible interactions with CC < -0.8 were kept. The resulting list of miRNA – mRNA pairs was further filtered based on perfect sequence complementarity between 3'UTR of mRNAs and miRNA seed region. Only 6mer and 7mer-m8 sites (Friedman et al., 2009) were taken into consideration. miRNA – mRNA interaction networks were visualized with cytoscape and node fill was mapped to z-score of mRNA and miRNA expression. Functional analysis of resulting subnetworks was performed applying PANTHER.

RESULTS

PROJECT 1: GOplot: AN R PACKAGE FOR VISUALLY COMBINING EXPRESSION DATA WITH FUNCTIONAL ANALYSIS

Despite the plethora of methods available for the functional analysis of *omics* data, obtaining comprehensive-yet detailed understanding of the results remains challenging. This section introduces the R package GOplot which is available via CRAN- The Comprehensive R Archive Network: https://cran.r-project.org/web/packages/GOplot/index.html. A detailed manual of the package can be found at https://wencke.github.io/.

1.1. Package description

GOplot uses ggplot2, one of the three graphic systems in R, as a scaffold to create a collection of pre-specified and multilayered charts. In order to customize the provided charts, two input datasets are needed: a list of selected molecules with their expression levels and the results of a functional analysis. The package takes the output of any general enrichment analysis and generates visualizations of gene expression data and enriched biological functions with varying levels of complexity and detail. Although it is not mandatory to use the implemented preprocessing functions before using the plotting functions, it is highly recommended to ensure an easy and smooth workflow.

So far the package includes three preprocessing functions: `circle_dat()`, `reduce_overlap()`, and `chord_dat()`. The `circle_dat()` function was designed to easily integrate the gene expression data with the results of the enrichment analysis and to transform the datasets into the appropriate format for the majority of plotting functions. The function does not only combine the two datasets it also computes the z-score for each enriched process. This z-score has to be clearly differentiated from the standard score from statistics and is calculated as follows:

$$z-score = \frac{(up - down)}{\sqrt{count}}$$

Where *up* and *down* are the number of assigned genes up-regulated (logFC > 0) or down- regulated (logFC < 0) in the data, respectively; and *count* is the overall number of genes assigned to the enriched process.

`reduce_overlap()` is a function that can be applied to the data if the created plots are difficult to comprehend due to overplotting. The function eliminates redundant terms that share more than a user- defined number of genes (parameter *overlap*) and takes as an input a data frame created with `circle_dat()`. The exclusion of highly similar terms significantly improves the readability of plots without losing informational value. The third preprocessing function, `chord_dat()`, generates a binary matrix that assigns the genes to each predefined functional term, which is elementary to display their relationship with, for example, a chord diagram. The exact input format for the different preprocessing functions can be checked with the help function in R.

After the preprocessing step the user can choose between seven plotting functions with different levels of complexity. In general, the exploratory data analysis starts at a very general level to gain a global overview of the dataset(s). At the entry level `GOBar()` and `GOBubble()` provide intuitive comparative charts that focus on the significance of the enrichment (-log10 of the adjusted p-value) and the z-score of the terms. Displayed terms in the bar plot (`GOBar()`) can be sorted according to their significance or z-score to answer different research questions. The bubble plot (`GOBubble()`) additionally provides the information of the count as the displayed circles are area-proportional to the number of genes in the given category. Based on these charts a list of relevant terms can be selected. In the next step the user can add quantitative information of gene expression to the plots through the application of one of the more elaborated charts created with `GOCircle()`, `GOChord()`, `GOHeat()` and/or `GOCluster()`. Due to the fact that the calculated z-score is a rather crude measure of process activation it is sometimes difficult to interpret the obtained result. The circular plot created with `GOCircle()` facilitates the interpretation by displaying the logFC value of each gene assigned to a specific term. `GOChord()` creates a chart that shows the relationship between the list of selected genes and enriched terms and is based on the Circos plot developed by Martin Krzywinski (Krzywinski et al., 2009). `GOHeat()` serves a similar purpose as `GOChord()` and generates a heatmap of the relationship between genes and terms. `GOCluster()` on the other hand groups genes

either according to their expression profile or based on the assigned functions and creates a circular dendrogram of the provided data. Furthermore, we implemented with `GOVenn()` a Venn diagram that does not only display the number of overlapping elements but also the expression pattern (commonly up-regulated, commonly down-regulated, contra-regulated). This addition to a common Venn diagram makes a significant difference when comparing list of genes because it is not only important to identify genes that are commonly altered under different conditions but also how the expression changes.

1.2. Examples

The package and its original visualization styles was used throughout the different projects in order to gain a better insight into the different datasets. It was not only used to produce figures that summarize obtained results but was also widely applied during the exploratory phase of the data analysis process to guide further analyses. The following paragraph will briefly exemplify some of the functionalities of the GOplot package and create visualizations that have not been used for the analysis of the ad-hoc generated transcriptomic data of cardiac cells. For that purpose, I will use the manually compiled sample dataset of GOplot.

The calculated z-score is only a crude measure to estimate the level of activation for each enriched process and might sometimes be difficult to interpret. The Circle plot (Figure 1) tries to improve the understanding by displaying a scatter plot of gene expression for each selected term. By default, up-regulated genes are displayed in red and down-regulated genes in blue, respectively. The inner ring is a barplot where the height of the bar indicates the significance of the term (-log10 adjusted p-value), and color corresponds to the z-score. The plot was created with the following the R code:

```
library(GOplot)
# Load the dataset
data(EC)
# Generate the plotting object
circ ← circle_dat(EC$david, EC$genelist)
# Generate a circular visualization of the results of gene- annotation enrichment analysis
GOCircle(circ)
```
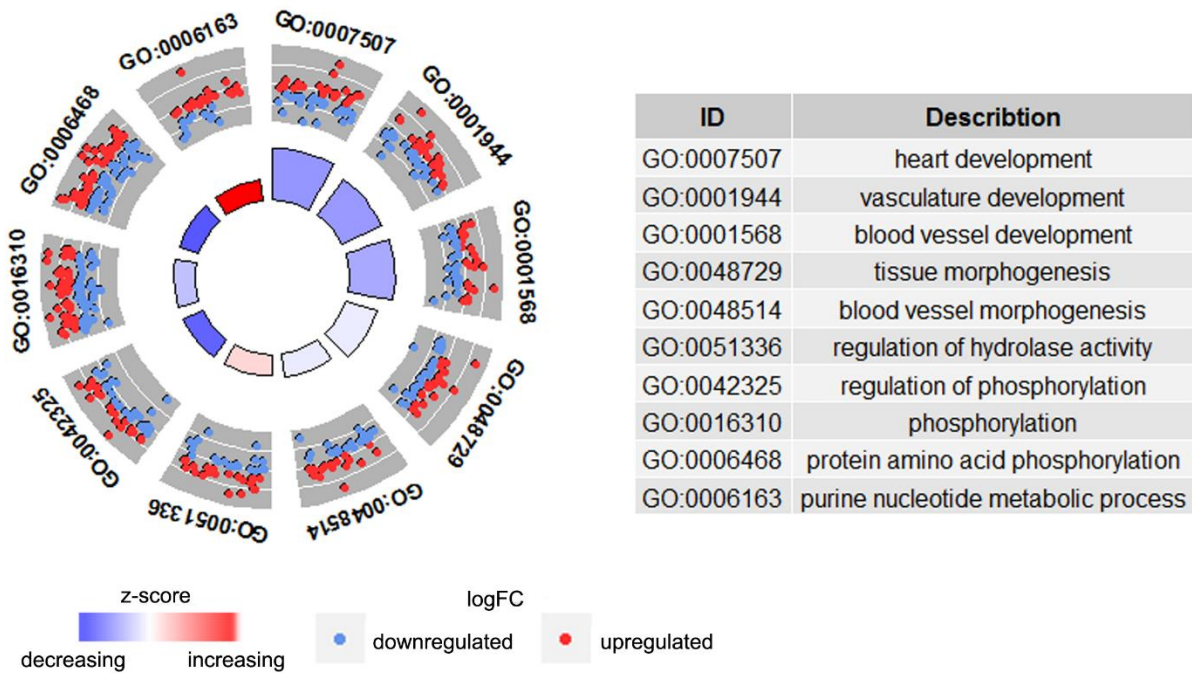
ID	Describtion
GO:0007507	heart development
GO:0001944	vasculature development
GO:0001568	blood vessel development
GO:0048729	tissue morphogenesis
GO:0048514	blood vessel morphogenesis
GO:0051336	regulation of hydrolase activity
GO:0042325	regulation of phosphorylation
GO:0016310	phosphorylation
GO:0006468	protein amino acid phosphorylation
GO:0006163	purine nucleotide metabolic process

Figure 1: Output of `GOCircle()`. The outer circle shows a scatter plot for each term of the logFC of the assigned genes. Red circles display up- regulation and blue ones down-regulation. The inner ring is a bar plot where the height of the bar indicates the significance of the term (-log10 adjusted p-value), and color corresponds to the z-score.

Another chart that will not appear in the later sections is the heatmap of enriched processes (Figure 2). The `GOHeat()` function generates a heatmap of the relationship between genes (columns) and terms (rows). Each column is divided into smaller cells and the coloring of the cells depends on the presence or absence of logFC values in the input data. This information is passed to the function through the *nlfc* argument. If the logFC is provided, the cells are colored according to the logFC of the genes, otherwise the cells are colored according to the number of assigned genes per term (count). In order to highlight groups of genes with similar annotated functions, a column-wise hierarchical clustering is performed.

```
library(GOplot)
# Load the dataset
data(EC)
# Generate the plotting object
circ ← circle_dat(EC$david, EC$genelist)
chord ← chord_dat(data = circ, genes = EC$genes, process = EC$process)
```

Generate a circular visualization of the results of gene- annotation enrichment analysis
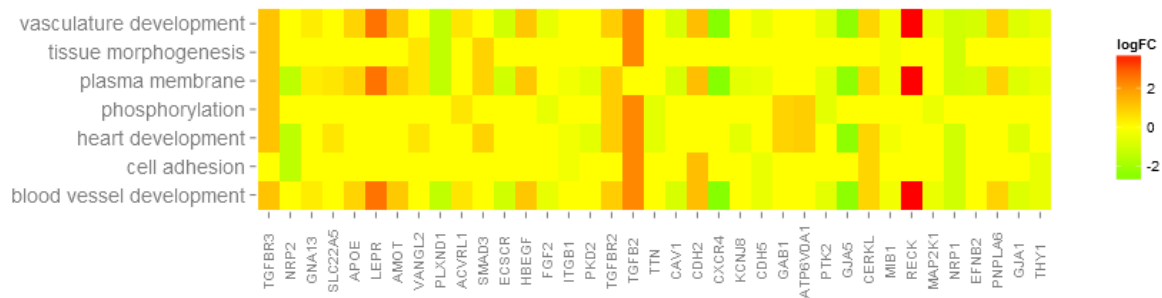**GOHeat**(chord, nlfc = 1, fill.col = c('red', 'yellow', 'green'))

Figure 2: Output of `GOHeat()`. Heatmap displaying the relationship between genes (columns) and terms (rows). Cells are colored according to the logFC values of the assigned genes.

We tracked GOplot downloads through CRAN download logs provided by R Studio to get an idea of its usage. The daily download statistics of GOplot were downloaded starting from its release (31 January 2015) to the first week of December 2016. The overall number of downloads for this period accumulates to 17 343. The median number of downloads per week is 53 (Figure 3A). To get an impression of the worldwide usage of GOplot a world map was colored according to the overall absolute number of GOplot downloads per country (Figure 3B). China, India and the United States are the countries with the highest downloads, followed by various countries from Europe. Since only 9.3% of all internet users are inhabitants of African countries (www.internetworldstats.com), the number of GOplot downloads was very low for these countries. To put the downloads of GOplot into perspective we compared the absolute number of weekly downloads to the R package BACA (Fortino et al., 2015), a package that allows the user to combine multiple annotation charts into one output graph, and RCircos (Zhang et al., 2013a), the R implementation of the Circos plots developed by Martin Krzywinski.
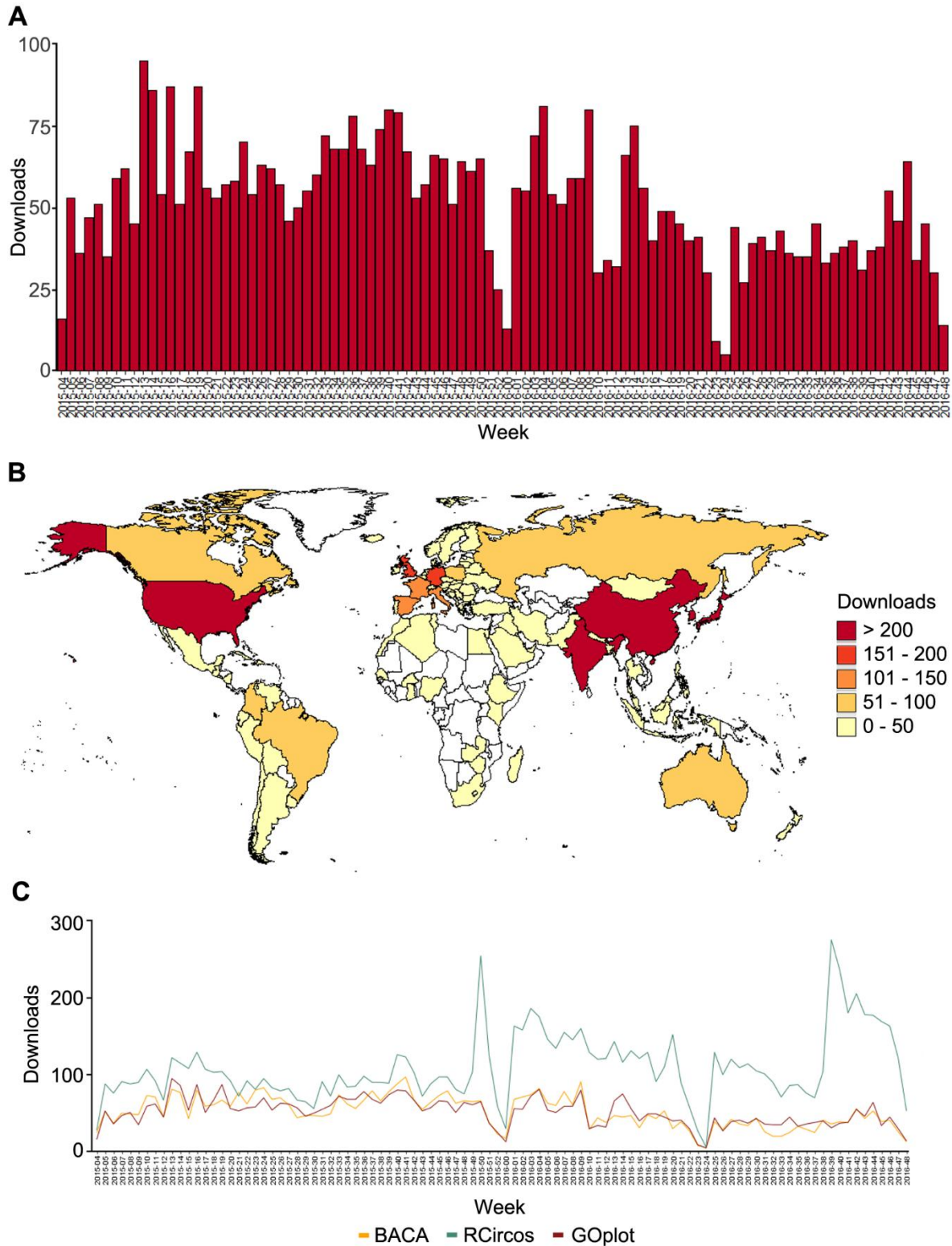
A

B

C

Figure 3: Download statistics of GOplot. Daily downloads of GOplot in the period from late January 2015 to early December 2016 were obtained from CRAN download logs provided by R Studio. (A) Barplot displaying absolute numbers of weekly downloads of GOplot. (B) Overall downloads of GOplot per country. (C) Comparison of weekly downloads of the R packages BACA, RCircos and GOplot.

PROJECT 2: TRANSCRIPTIONAL ANALYSIS OF MURINE MΦ FROM THE HEALTHY HEART AND AFTER MYOCARDIAL INFARCTION

2.1. Phenotypical characterization of cardiac Mφ in the healthy heart and after MI

To investigate the specific characteristics of *in vivo* cardiac Mφ green fluorescence protein positive (GFP+) cells were isolated from $CX_3CR1^{GFP/+}$ knock-in mouse hearts at different post-MI stages. The CX3CR1$^{GFP/+}$ reporter mouse has been used to identify resident Mφ in a wide variety of tissues (Jung et al., 2000; Lee et al., 2010; Soos et al., 2006) and also enabled the detection of CRMs in the healthy heart (Pinto et al., 2012). Firstly, we performed a temporal study of the chosen mouse model by flow cytometry and analyzed the kinetics of GFP$^+$ and Ly6c$^+$ cells within the CD45$^+$ and CD11b$^+$ cells (Figure 4).
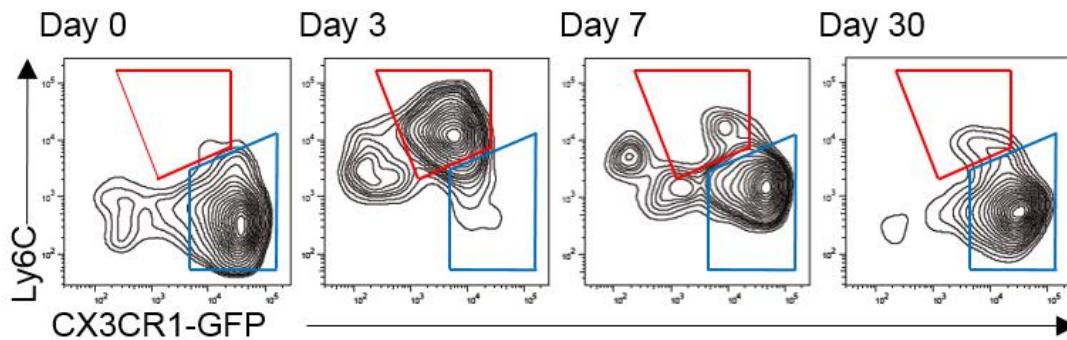

Figure 4: Characterization and isolation of cardiac Mφ in $CX_3CR1^{GFP/+}$ mice. Cardiac cell suspensions from healthy or cryoinjured hearts of $CX_3CR1^{GFP/+}$ mice were analyzed by FACS. Representative contour plots depict the kinetics of the different subsets of murine tissue/resident Mφ in the healthy heart and after cryoinjury. Within the CD45$^+$ and CD11b$^+$ population we distinguished a Ly6c^{low}/CX_3CR1^{high} population (red) and a Ly6c^{high}/CX_3CR1^{low} population (blue).

Ly6c^{low}/CX_3CR1^{high} cells were selected to investigate CRMs and the same population was chosen to assess the functions and characteristics of Mφ in the reparative phase (7 and 30 days post-MI). In order to characterize Mφ in the inflammatory phase (3 days post-MI) Ly6c^{high}/CX_3CR1^{low} cells were selected. The Mφ populations were sorted from single cell suspensions of digested hearts at different post-MI stages using FACS.

Collectively, the obtained data confirms the existence of CRM in the healthy

heart and proves that the applied strategy can be used to identify Mφ populations at different post-MI stages.

2.2. Gene expression analysis of cardiac Mφ in the healthy heart and after MI

Mφ respond to a broad spectrum of external stimuli and the accompanied Mφ activation is orchestrated by intricate transcriptional regulatory networks which still remain mostly elusive. Comprehension of the process is further hindered by the lack of available transcriptome data of *in vivo* Mφ. Here we present the gene expression profile of CRMs and post-MI Mφ obtained by RNA-seq.

PCA of the global transcriptional profiles of all samples revealed clear separation between the different temporal stages (Figure 5A). Pairwise comparison of each post-MI stage to the healthy heart and between each other led to the identification of 4988 DEGs with an adjusted p-value < 0.05 and |logFC| > 1 in at least one comparison (Figure 5B).
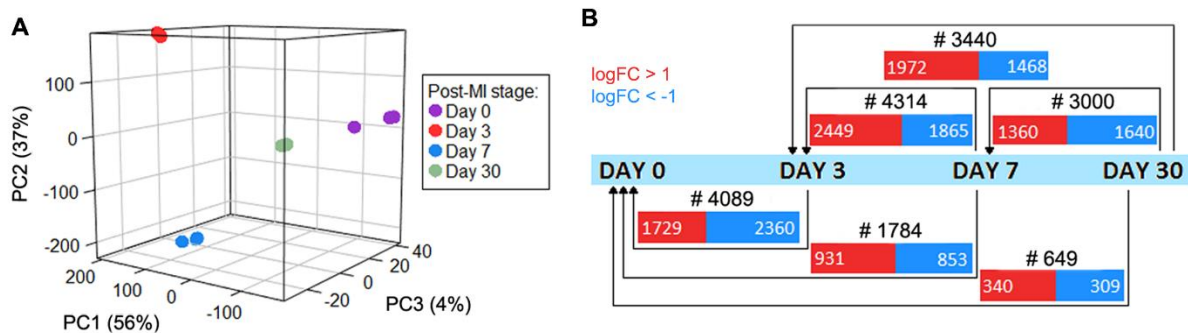

Figure 5: Global gene expression analysis. (A) PCA of gene expression. Numbers in parentheses indicate the percentage of variation explained by each of the three first principal components. (B) Number of differentially expressed genes (DEG) for every comparison across time. Numbers in blue rectangles indicate down-regulated genes (logFC < -1); numbers in red rectangles indicate up-regulated genes (logFC > 1).

The observed dissimilarity of Mφ 3 days post-MI to other temporal stages in PCA and DE analysis, indicated major transcriptional changes in cardiac Mφ at this temporal stage. It was interesting to note, that both analyses revealed a high similarity between the latest post-MI stage monitored (30 days) and CRMs, which might indicate a reestablishment of resting conditions. PCA and DE analysis also showed that Mφ isolated 7 days post-MI could be clearly distinguished from the other time points but were more similar to CRMs than to 3 days post-MI Mφ.

We performed unsupervised k-means clustering for the 4988 genes DE in at least one comparison to better characterize the global dynamic changes in gene expression and to identify groups of co-expressed genes (k = 6, Figure 6A). In order to gain a better understanding of the grouped genes, PANTHER was used to perform functional analyses of each cluster (Figure 6B). The clustering revealed three clusters (clusters I, II, and III) that exhibited a time point specific expression profile. Genes assigned to cluster I showed an elevated expression in the healthy heart and included cardiomyocyte structural genes like *Myl2* (Figure 6B, C) associated to the enriched processes heart development and myofibril assembly. The cluster was further enriched for biological adhesion associated to genes like *Lyve-1* and cell adhesion molecules such as *Esam*, *Bcam*, and *Mcam*, which might indicate close interactions between Mφ and other cardiac cells, such as CMs and ECs in homeostasis, as previously suggested (Pinto et al., 2012).

Genes with primarily elevated expression 3 days post-MI were assigned to cluster II and enriched for immune response, programmed cell death, apoptotic signaling pathway, and regulation of ROS metabolic process, suggesting a pro-inflammatory phenotype for these Mφ population (Figure 6B). Interestingly, a query of the interferome database v2.01 (Rusinova et al., 2013) revealed, that approximately 20% of the genes assigned to cluster II were potential targets of IFNγ – induced signaling (e.g. *Stat1*, *Zfp36*, *Il6*). Although Mφ can also be a source of IFNγ production (Darwich et al., 2009), the major sources of IFNγ after MI are T-cells, specifically Th1, and natural killer cells (Hansson et al., 2006), indicating a T-cell mediated IFNγ -priming of cardiac Mφ after infarct (Mosser, 2003). In addition, we found an up-regulation of *Hif1a* and its target genes *Vegfa*, *Glut1,* and *Pgk1*, which might indicate a hypoxic environment at 3 days post-MI, a common microenvironmental feature at the site of inflammation (Murdoch et al., 2005).

Genes assigned to cluster III showed a primarily elevated expression 7 days post-MI and were associated with ECM and collagen fibril organization (e.g. *Lum*, *Col3A1*), indicating an active role in tissue remodeling (Figure 6A, B, C). The identification of regulators of cell proliferation (e.g. *Sox9*, *Sox4*) together with the enrichment of the process indicate proliferative capacity of 7 days post-MI Mφ, in accordance with previous findings in Mφ isolated after skeletal muscle injury (Varga et
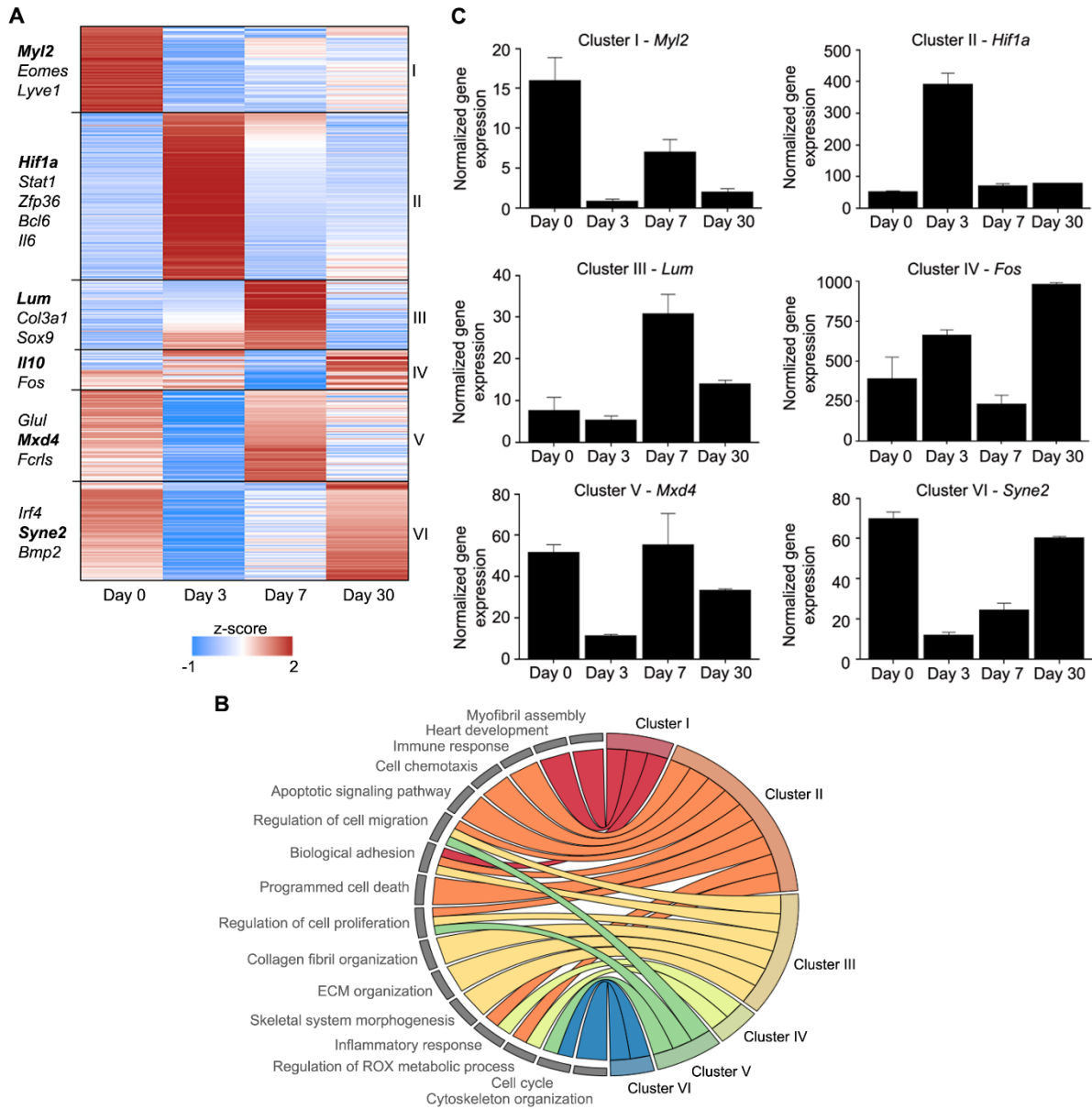
al., 2016).

Figure 6: Analysis of dynamic gene expression of cardiac Mφ in the healthy heart and after MI. (A) K-means clustering (k = 6) of the 4988 genes differentially expressed in at least one time point compared to control. (B) Chord diagram of a manually curated selection of significantly enriched (B-H adj-p < 0.01, Fold-Enrichment > 2) PANTHER biological processes. Biological processes are displayed on the left and clusters on the right side. (C) Gene expression profile of selected genes from each cluster. Y-axis displays normalized counts. Error bars indicate standard error.

The highly specific gene signature found for CRMs, 3 and 7 days post-MI Mφ contrasted with the absence of genes specifically expressed 30 days post-MI. Genes of the latest post-MI stage were either co-expressed with CRMs (cluster VI) or at both, day 0 and day 3 (cluster IV). Genes assigned to cluster IV were also associated with

inflammatory response and included a high number of TFs like *Atf3*, *Fos* and *Jun* and the cytokine *Il10*. Recently it has been shown that Mφ up-regulate the expression of *Il10* as early as 3 days post-injury in the context of skeletal muscle injury (Novak et al., 2014). Additionally, cluster V contained genes with comparably high expression values at 0 and 7 days post-MI. The cluster was characterized by cell cycle and cell proliferation (e.g. *Glul*, *Mxd4*, *Fcrls*) associated processes, confirming self-renewal potential of CRMs (Heidt et al., 2014) and proliferative capacity of Mφ involved in tissue repair (Varga et al., 2016). Already the PCA (Figure 5A) and the overall number of DEGs (Figure 5B) showed that CRMs and 30 days post-MI Mφ were the most similar samples. K-means clustering (Figure 6A) confirmed that these two time points shared a high number of co-expressed genes (cluster VI). These genes were mainly involved in cell cycle processes (e.g. *Bmp2*) and cytoskeleton organization (e.g. *Syne2*), indicating restoration of homeostasis at 30 days post-MI.

All together the transcriptional characterization of cardiac Mφ revealed very heterogeneous expression profiles that were associated with time point specific functions, indicating a highly dynamic, yet coordinated, transcriptional landscape of Mφ activation in response to MI.

2.3. Cardiac Mφ contribute to tissue heterogeneity of Mφ

Mφ reside in nearly all tissues of the body but differ in their ontogeny origin, epigenetic imprinting, and gene expression (Gautier et al., 2012; Lavine et al., 2014). The transcriptional analyses that led to these findings compared multiple tissues but did not include the heart. For this reason, we compared cardiac resident Mφ with two published datasets (GSE15907, GSE63340) of tissue-resident Mφ, including also neutrophils and monocytes. The datasets were obtained from different experiments and we applied batch correction to reduce the impact of systematic non-biological differences in later analyses (Leek et al., 2012). The HC shows the effect of the batch correction and clearly underscores the necessity of such batch effect removal technique (Figure 7). In contrast to the dendrogram of normalized but not batch corrected samples (Figure 7A), in which samples clustered primarily according to the different experimental batches, batch correction led to distinct tissue-specific clusters (Figure 7B). The data reveals a clear batch-specific bias that could be reduced through

the application of batch correction methods, emphasizing the necessity of batch correction to generate robust gene expression profiles.
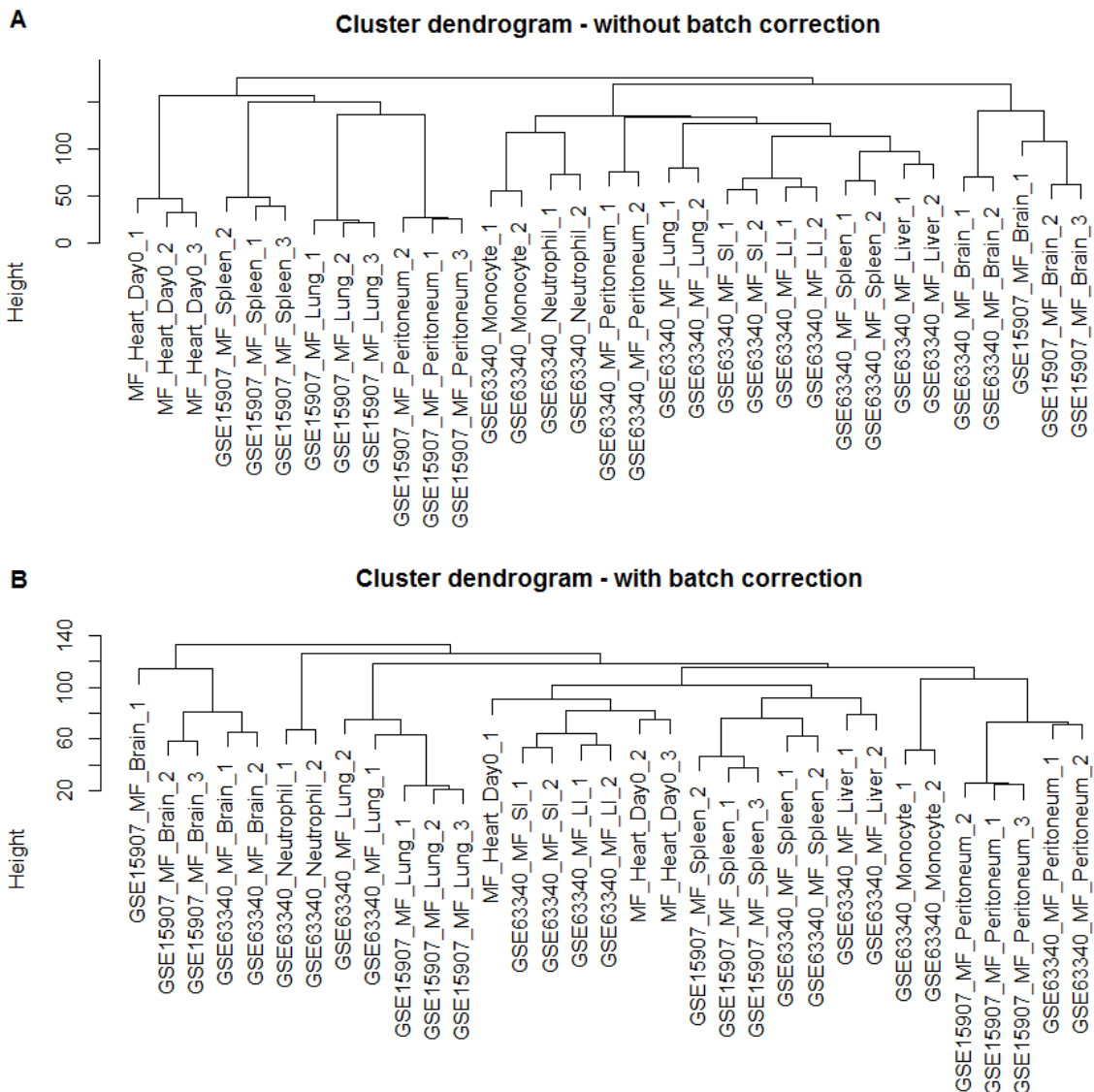

Figure 7: Hierarchical clustering of tissue resident Mφ. A) Quantile normalized dataset without batch correction. B) Quantile normalized dataset of tissue resident Mφ with batch correction.

PCA of all samples (Figure 8A) revealed that tissue- resident Mφ from the heart are most similar to Mφ from the small and large intestine, with a relatively greater distance to the other tissues. Nevertheless, pairwise correlation analysis (Figure 8B) revealed that cardiac Mφ were not only very similar to the intestine but also exhibited high CC compared to other tissues (mean = 0.84, SD = 0.03), whereas the CC between the other tissues ranged from 0.68 (lung versus brain) to 0.89 (liver versus spleen). From all the tissue resident Mφ microglia were the most dissimilar samples (Figure 8A,

Figure 8B). Interestingly, monocytes clustered together with resident Mφ from peritoneum, heart, and gut, which might suggest an increased monocyte influx to these populations in homeostasis.
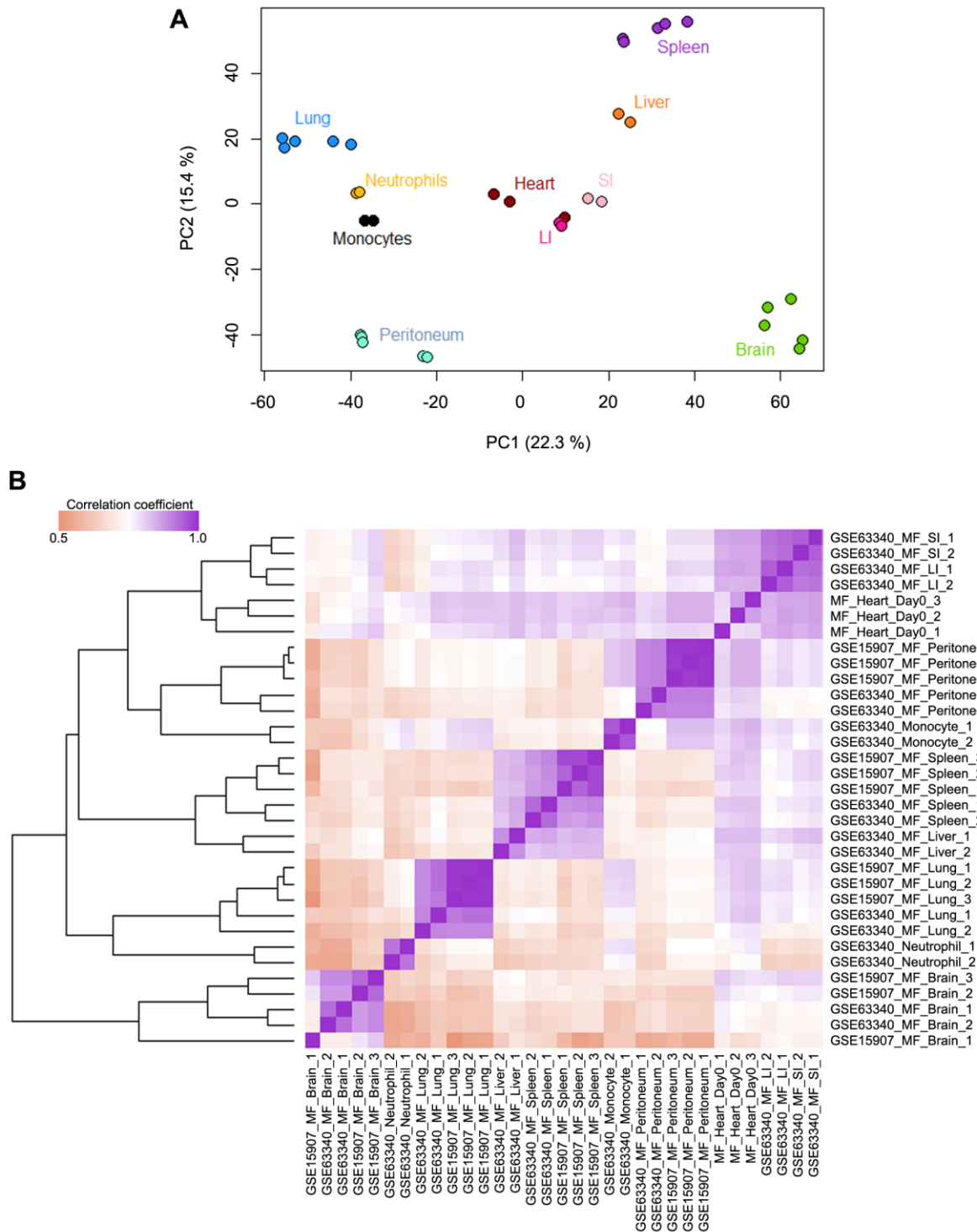

Figure 8: Global gene expression comparison of tissue resident Mφ, monocytes and neutrophils. A) PCA of gene expression of all samples. Numbers in parentheses indicate the percentage of variation explained by each of the principle components. B) Pairwise spearman

correlation of transcriptional profiles of all samples. Labels indicate origin of data, cell type, and tissue of origin.

In order to explore the heterogeneity of tissue resident Mφ in more detail, k-means clustering (k = 15, Figure 9A) was used to identify sets of co-expressed genes. The clustering revealed tissue specific gene signatures for resident Mφ, including previously described tissue specific genes such as *Siglech* in microglia, *Tgfb2* and *Gata6* in peritoneal Mφ, *Pparg* and *Spi-c* in splenic red pulp Mφ and *Car4* in lung Mφ (Lavine et al., 2014). The clustering further revealed a yet undescribed set of cardiac specific genes (Figure 9A, cluster XII). Amongst these genes, three surface markers were selected and tested via real-time polymerase chain reaction (qPCR). The experiments confirmed the cardiac specific expression of *Osmr*, *Lifr* and *Egfr* compared to Mφ from lung, spleen, and peritoneum (Figure 9B). Previously a set of 35 heart specific genes had been identified comparing the transcriptional profile of cardiac resident Mφ to spleen and brain (Pinto et al., 2012). Our integrated analysis showed that several genes of this signature (e.g. *Tnnt2*, *Myh6*, *Steap4*) were indeed specifically expressed in the heart (Figure 9B, cluster XII), but around 20% (e.g. *Stab1*, *Mmp13*, *Sdc4*, *Retnla*) were expressed in heart and intestine, consistent with the observed high similarity between the global gene expression profile of heart and gut (Figure 8A, Figure 8B). As already indicated by the correlation analysis, k-means clustering showed that cardiac Mφ shared gene sets with many other tissues. Brain and heart shared one of the larger clusters (Figure 9A, cluster II), including the TF *Mef2c*, the F-box protein *Fbox11*, which is associated with metal ion binding, members of the Toll-like receptor family (*Tlr3*, *Tlr5*), and the chemokine receptor *Ccr5*. Genes commonly expressed in the peritoneum and heart included the pro-angiogenic factor *Lyve1* which was previously proposed as a cardiac specific Mφ surface marker (Pinto et al., 2012) and the TF *Crem,* which binds to the cyclic adenosine monophosphate (cAMP) responsive element in the promoters of its target genes, regulating various complex processes. The surface markers *Cd163* and *Mrc1*, which are associated with a M2-like phenotype, were commonly expressed by spleen and heart (Figure 9A, cluster XI).

Collectively, these data support the heterogeneity of tissue resident Mφ, which possess significant differences in their transcriptional profiles. The detected high similarity between intestine and heart might suggest a high percentage of mature but monocyte-derived cardiac Mφ in the healthy myocardium.
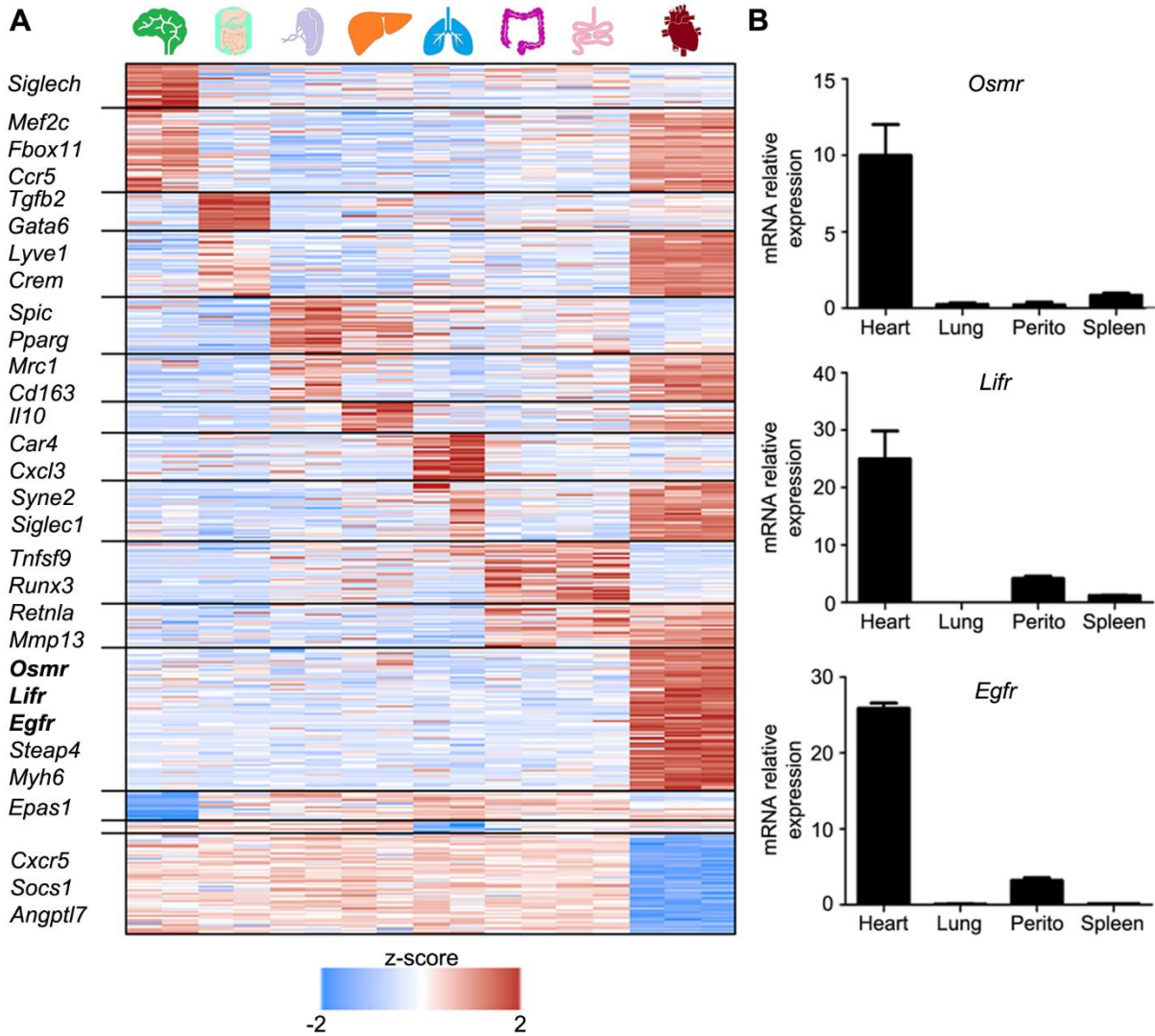
Figure 9: Gene signatures of tissue resident Mφ. A) K-means clustering (k = 15) of genes differentially expressed in at least one tissue comparison. Genes highlighted in bold were selected for qPCR. B) Gene expression profile of cardiac specific membrane proteins obtained by qPCR. Data represent the mean + standard error (SE) of three independent experiments.

2.4. The hybrid phenotype of cardiac Mφ during infarct healing

In order to globally determine the functional phenotype of the *in vivo* samples and to place them within the M1/M2 activation spectrum, the gene expression profiles of *in vivo* cardiac Mφ isolated at different post-MI stages were compared to two *in vitro* datasets (Li et al., 2015; Riquelme et al., 2013). In both *in vitro* studies bone marrow-derived Mφ (BMDM) were cultured for several days in the presence of Mφ colony-stimulating factor (M-CSF), followed by treatment of the mature Mφ with different stimuli. HC of the samples was performed and the resulting tree was visualized (Figure

10). The length of the branches corresponds to the Euclidean distance between the samples.
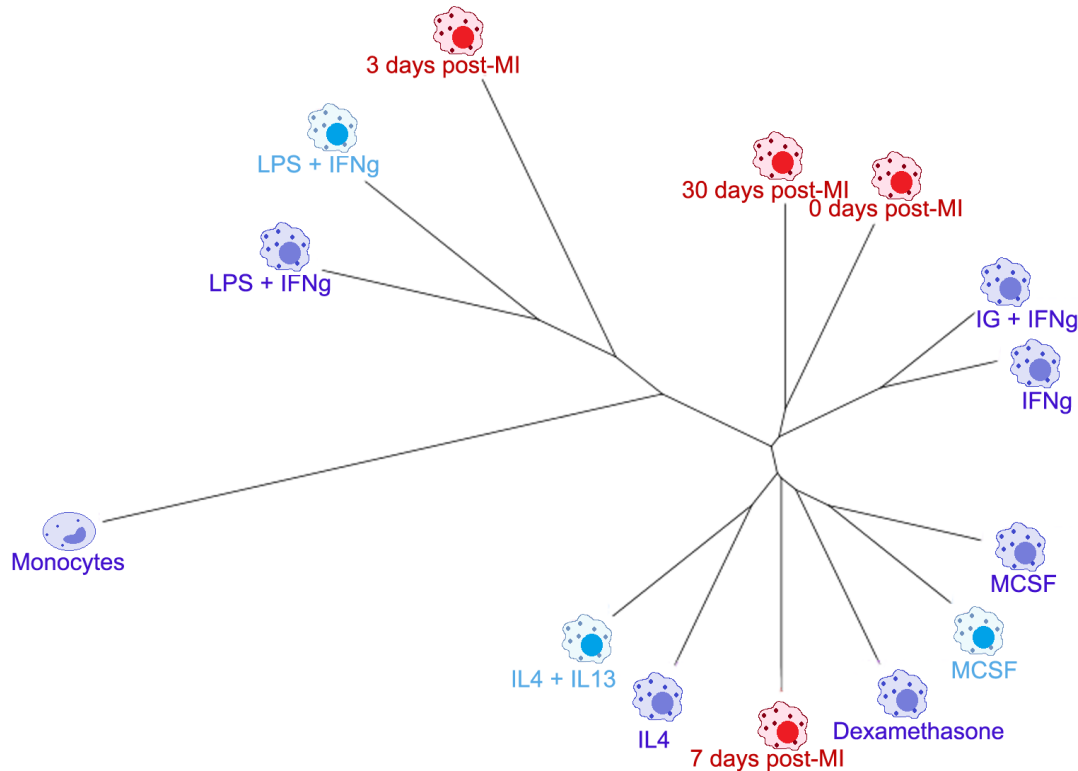

Figure 10: Comparison of the global gene expression profile of cardiac Mφ with *in vitro* activated Mφ. Clustering of mouse Mφ samples isolated from the heart at various post-MI stages (*in vivo*, red font color) and bone marrow-derived Mφ treated *in vitro* with various stimuli (light blue and purple font color). Both *in vitro* datasets were downloaded from the NCBI GEO with the accession numbers GSE32690 (purple) and GSE53321 (light blue), respectively. The labels of the *in vitro* samples indicate the applied stimulus. For the *in vivo* samples the labels indicate the post-MI stage at which the cells were isolated.

Isolated monocytes without stimulation were clearly distinguishable from the Mφ samples and formed a separate part of the tree (Figure 10), which further supports the Mφ identity of our samples. Taking the monocytes apart, a dichotomous structure developed, indicating significant differences in gene expression and function between the subtrees. As indicated by PCA and DE analysis (Figure 5A, B), CRMs clustered closely together with the latest post-MI stage monitored (30 days). These samples also clustered together with BMDMs activated with IFNγ and BMDMs stimulated with immune complex (IC) and IFNγ. These Mφ populations have been shown to exhibit an immunosuppressive phenotype (Riquelme et al., 2013), suggesting a similar phenotype for CRMs, as previously described (Pinto et al., 2012), and Mφ at 30 days

post-MI. Interestingly, non-activated BMDMs were not part of this cluster, but were grouped together with cardiac Mφ 7 days post-MI amongst others. Mφ from day 7 clustered closely together with samples treated with dexamethasone, IL4, and a combined treatment of IL4 and IL13, further indicating a M2-like phenotype for these post-MI Mφ. Mφ isolated at 3 days post-MI clustered together with BMDMs activated with LPS and IFNγ, supporting the assigned M1-like phenotype for 3 days post-MI Mφ.
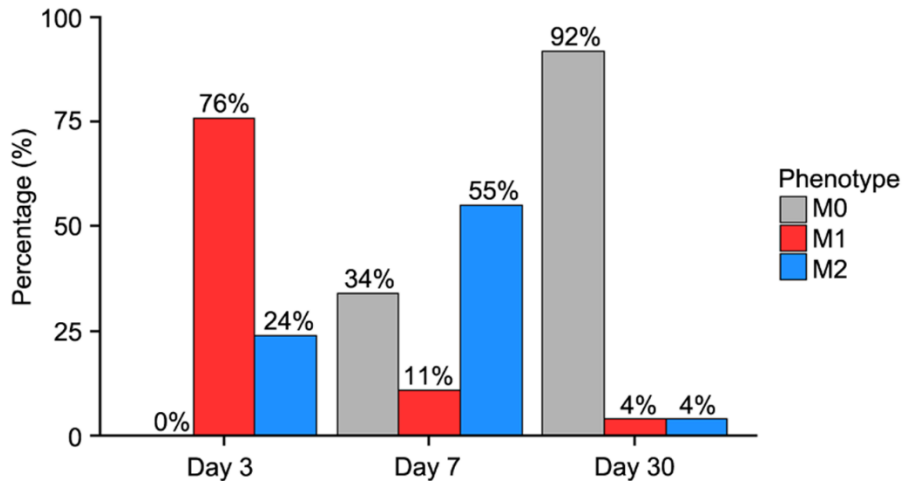

Figure 11: The hybrid phenotype of *in vivo* Mφ. Frequency of functional phenotypes within *in vivo* samples at different post-MI stages estimated using CellMix.

Nevertheless, results of the DE analysis revealed a mixture of M1 and M2 signature genes within the *in vivo* transcription profiles, suggesting that *in vivo* Mφ are a mix of described *in vitro* phenotypes. In order to test this hypothesis computationally, partial deconvolution was used to estimate the M1 and M2 phenotype contribution to the *in vivo* samples. Mouse BMDMs cultured for 7 days in M-CSF and activated with LPS + IFNγ or IL4 + IL13 were used as reference profiles for a M1 and M2 functional phenotype, respectively. In addition to the *in vitro* data, our samples of CRMs were used as reference for tissue- resident Mφ (M0). The barplot in Figure 11 shows the frequency of the M0, M1, and M2 phenotype within post-MI Mφ. In agreement with the HC (Figure 10), the transcriptional profile of Mφ isolated at 3 days post-MI was predominated by M1 associated genes (76% M1) but already included activated anti-inflammatory programs (24% M2). On the other hand, the profile held no gene expression pattern reminiscent of CRMs (0%). Mφ gene expression at 7 days post-MI was mainly characterized by M2-associated genes (55%) but still held transcriptional traces (11%) of a M1-like profile. This result might suggest a transition from pro-
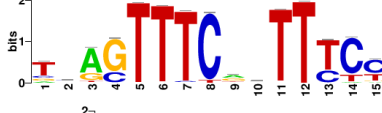
inflammatory to anti-inflammatory further continuing to resting Mφ, as indicated by the contribution (34%) of the M0 profile. The latest post-MI stage was completely dominated by the M0 phenotype (92%).

Both, the partial deconvolution approach and the inter-experimental comparison pointed towards a hybrid nature of *in vivo* Mφ phenotypes and support a dynamical phenotype alteration of Mφ in cardiac repair.

2.5. Global network of transcriptional regulation in Mφ

Mφ are phenotypically very heterogeneous and the individual cells exhibit a remarkable plasticity, swiftly changing their phenotype to cope with changing microenvironments. The identity of Mφ is specified by a complex interplay between external signals and activated transcriptional programs. In order to explore TF activities and to identify master regulators of cardiac Mφ in the healthy heart and after MI, we applied sequence-based discovery of regulons per cluster (Janky et al., 2014). The program identified enriched motifs per cluster and linked the motif to known TF binding sites.

Table 1: Motif enrichment analysis of co-expressed genes. For each cluster, the motifs with the highest normalized enrichment score (NES) up to a maximum of three are displayed. The selected motifs were linked to their corresponding TF, considering only DE TFs.

Cluster	Motif	TF	NES
I		*Max*	3.5
II		*Stat1*	9.1
		Fosl1	5.1
		Cebpb	3.6
III		*Runx2*	4.1
		Pura	4.0

		Zbtb18	3.1
V		*Patz1*	4.4
		Hinfp	3.5
		Rora	3.2
VI		*Nilf3*	4.0
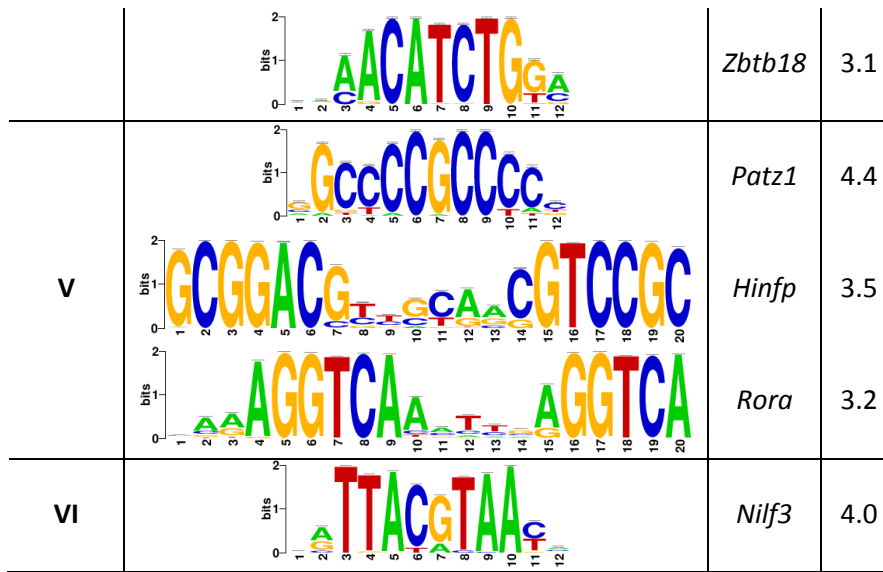
The motif enrichment analysis led to the identification of 66 DE TFs, revealing a highly complex regulatory program of *in vivo* Mφ. The top enriched motif for cluster I was linked to *Max* (Table1), a TF that forms heterodimes with *Myc* or *Mad* and depending on the combination functions as an activator or repressor of transcription. In cluster II two of the top enriched motifs were linked to mediators of IFNγ- induced signaling (*Stat1*, *Cebpb*), supporting the finding that many genes of this cluster are targets of IFNγ-signaling. The top three enriched motifs for cluster III were linked to TFs associated to cell maturation (*Runx2*), cell differentiation (*Pura*) and skeletal muscle tissue development (*Zbtb18*). Surprisingly, no enriched motif could be found for cluster IV. The TFs linked to the top enriched motifs of genes in cluster V were involved in cell cycle processes, consistent with the enriched BPs identified for this cluster (Figure 6B). The top enriched motif of cluster VI was linked to the survival factor Nfil3, which was recently associated with Mφ activation (Roy et al., 2015).

The identified 66 DE TFs were linked to their target genes from different clusters and the list of TF – target gene pairs was imported into cytoscape. To simplify the resulting network, target genes were grouped according to their associated k-means clusters. Taking into account that TFs can be activators and repressors the list of predicted interactions was filtered by correlation between the TF and its target gene. Only interactions with an absolute CC > 0.7 were kept, reducing the list of potential regulators to 40 TFs (Figure 12). Interactions with anti-correlation were considered as

repressive functions of the TFs, whereas TFs with positive correlation to the targeted cluster were considered as activators.
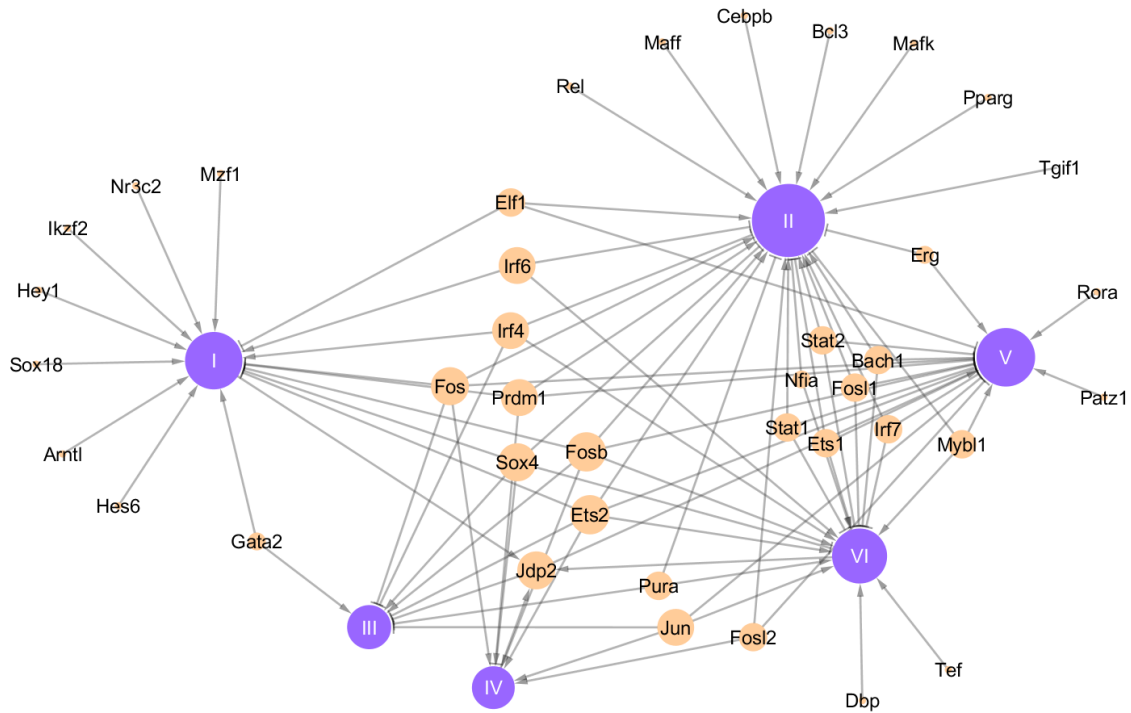
Figure 12: Global network of potential regulatory effects of TFs on the different clusters. TFs are highlighted in light orange and clusters in purple. Negative interactions are indicated by flat line ends, whereas activating interactions are indicated by solid arrows. The node size corresponds to the node degree.

Approximately half of the TFs potentially regulated multiple (> 1) clusters and only the clusters III and IV were not linked to cluster-specific TFs. Seven TFs had the potential to specifically regulate genes in the healthy heart, including the clock-controlled *Arntl* gene, angiogenesis-related genes (*Sox18*, *Hey1*), and regulators associated with developmental processes (Hes6). The identified transcriptional regulators are in line with the determined functions of this cluster (Figure 6B) and support the proposed pro-angiogenic function of CRMs (Pinto et al., 2012). Cluster II contained the highest number of identified TFs, including regulators of metabolic processes (e.g. *Rel*, *Pparg*), negative regulators of cell proliferation (e.g. *Prdm1*, *Tgif1*, *Fosl1*), regulators of programmed cell death (e.g. *Bcl3*, *Fosl1*), and genes involved in immune response reactions (e.g. *Stat1*, *Stat2*, *Cebpb*). The high number of identified TFs matches the observed massive changes in Mφ gene expression 3 days post-MI (Figure 5A, 5B). TFs that belonged to cluster III (*Spib*, *Sox4*, *Cebpa*) were linked to cell maturation and cell differentiation, in accordance with the identified motifs. Despite the

small number of genes assigned to cluster IV, the cluster included many TFs, such as *Jun* and *Fos*, known regulators of cell life and death (Shaulian and Karin, 2002). The TFs linked to the top enriched motifs of genes in cluster V (Table 1), were involved in cell cycle processes, consistent with the identified functions for this cluster (Figure 6B). TFs commonly expressed in in the healthy heart and at 30 days post-MI (cluster VI) were linked to cell differentiation (e.g. *Mybl1*, *Pura*) and apoptotic processes (*Pura*, *Irf6*), indicating possible differentiation of blood monocytes into tissue Mφ (Schwerk and Schulze-Osthoff, 2003).

The data, taken together, revealed a complex regulatory network of cardiac Mφ in homeostasis and in response to tissue injury. The result emphasizes the complexity of Mφ activation, reflecting the multifaceted interplay between different intrinsic pathways and received activating signals from neighboring cells (Gordon and Taylor, 2005).

1.6. Receptome and Secretome contribution to Mφ identity and function

Mφ are highly influenced by the microenvironment in which they reside in and depending on its molecule composition execute specific effector functions (Martinez and Gordon, 2014). They also interact with other cardiac cells (e.g. CMs, FBs, ECs) to maintain and to regain homeostasis in case of tissue injury (Frantz and Nahrendorf, 2014). The intercellular crosstalk is most likely mediated through the secretion of distinct signaling molecules. Hence, we classified DEGs according to their cellular location and analyzed SMs (macrocrines) and MPs (receptome) of cardiac Mφ to estimate their cell-cell signaling potential at the different temporal stages.

After a pre-selection process (*Materials & Methods*), clustered genes were classified as SMs and MPs according to the Human Protein Atlas. Interestingly, the highest relative abundance of genes encoding for SMs could be identified for cluster III, which was nearly twice as high as the relative abundance of MPs (Figure 13A).

Functional analysis associated the identified macrocrines with ECM-related processes, indicating a key role of Mφ in cell-cell signaling through the secretion of ECM components (e.g. *Col3a1*, *Lox*, *Postn*) during the reparative phase of cardiac repair (Figure 13B).
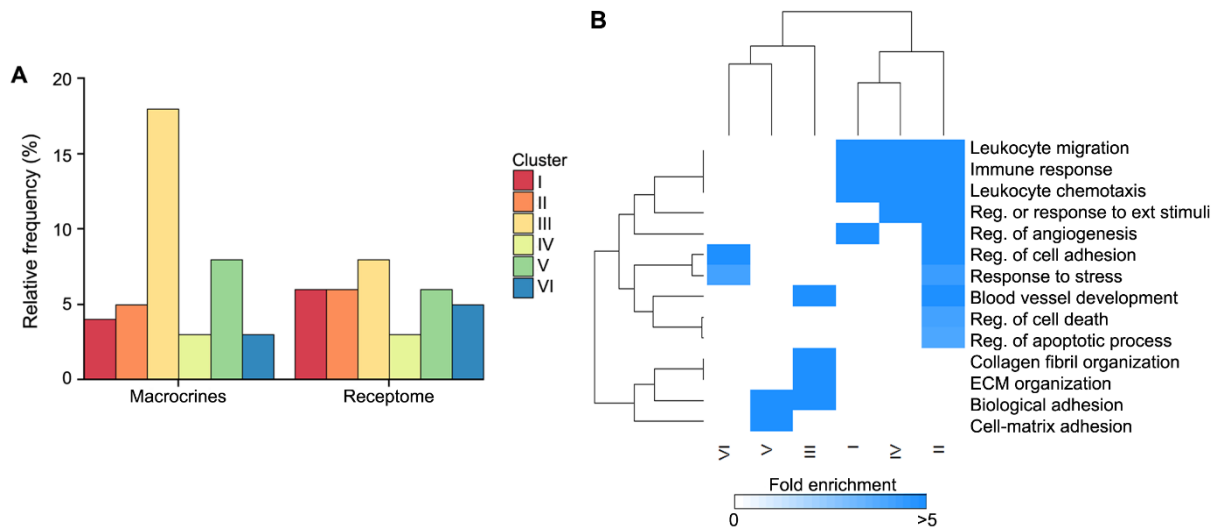
Figure 13: Transcriptional characterization of macrocrines and the receptome of cardiac Mφ. (A) Relative abundance of secreted molecules (SM, macrocrine) and membrane proteins (MP, surface marker) in each cluster (Figure 1C). (B) Hierarchical clustering of a manually curated selection of significantly enriched (B-H adj-p < 0.01, Fold-Enrichment > 2) PANTHER biological processes for secreted molecules.

Molecules secreted by Mφ during the inflammatory phase were consistently associated with immune response (e.g. *Il18bp*, *Cxcl10*, *Ccl2*), blood vessel development (e.g. *Thbs1*, *Mmp19*, *Vegfa*), and apoptotic processes (e.g. *Spp1*, *Osm*, *Serpine1*), suggesting maintenance of the inflammatory response through secretion of pro-inflammatory factors. In addition, we found a similar relative abundance of SMs and MPs for cluster II (Figure 13A), suggesting homeotypic paracrine signaling potential of Mφ at 3 days post-MI. The macrocrine of CRMs was associated with the regulation of angiogenesis (e.g. *Pf4*, *Cx3cl1*, Figure 13B), indicating a contribution of Mφ to angiogenesis in the healthy myocardium, most likely carried out through reciprocal paracrine signaling with ECs, as previously suggested (Pinto et al., 2012). The importance of such signaling has been shown for vascular network formation in developing organs (Sunderkötter et al., 1994) and in disease (Ahmad et al., 2002). As already indicated by the absence of a time point-specific gene cluster for day 30, we couldn't define either a secretome or a receptome that distinguishes day 30 from the other temporal stages. SMs and MPs with elevated expression at day 30 were co-expressed in day 0, and supported the M2-like phenotype (e.g. *Mrc1*) of CRMs.

We further aimed at defining surface markers specific for the different Mφ populations at the different temporal stages. The expression of selected surface

markers for the clusters I, II, III and VI was tested via qPCR (Figure 14). As previously reported (Pinto et al., 2012) we found a high expression of *Lyve-1* in CRMs (Figure 14), which might suggest a role of CRMs in angiogenesis as already indicated by the macrocrines. 3 days post-MI Mφ expressed high levels of *CD40*, which is associated with pro-inflammatory signaling upon binding with *CD154* on activated CD4+ T cells (Stout and Suttles, 1996) supporting the pro-inflammatory character of post-MI Mφ at day 3. The anti-inflammatory character of 7 days post-MI Mφ was supported by the elevated expression of *Trem2*, which might also contribute to the resolution of inflammation by suppressing the production of pro-inflammatory cytokines (Neumann and Takahashi, 2007). Additionally, *Mrc1* was primarily expressed in CRMs and at 30 days post-MI, consistent with its association to alternatively activated Mφ (Stein et al., 1992).
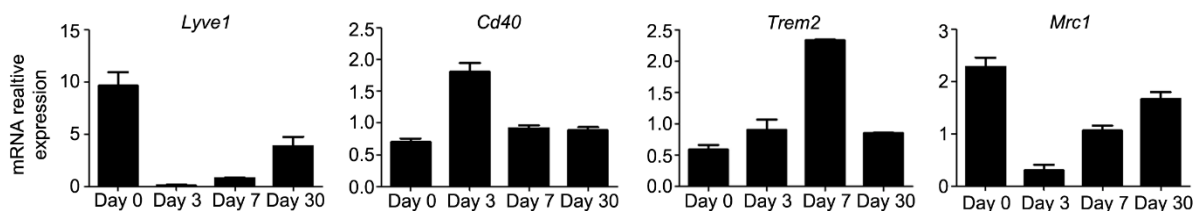
Figure 14: Gene expression profile analysis of selected surface marker of cardiac macrophages. Data represent the mean ± SEM of 3 independent experiments.

To fully understand the macrocrine – receptome interaction at each temporal stage, STRING was used to identify SM - MP pairs within the list of selected molecules as an indication for homeotypic paracrine signaling. By filtering the list for co-expression, 28 SM - MP pairs, assigned to three different clusters, were identified (Figure 15).

The majority of SM - MP pairs could be identified for cluster II, indicating a high potential for homeotypic paracrine signaling. We found that 3 days post-MI Mφ expressed both, the chemokine receptor *Ccr2* and its ligand *Ccl2* (Figure 14), which might indicate the recent infiltration of circulating monocytes (Lavine et al., 2014) and also facilitates further recruitment of monocytes to the site of inflammation (Kuziel et al., 1997). Elevated expressions of *Cd44* and *Spp1* have been previously observed in M1-like Mφ and are associated with the regulation of chemotaxis (Marcondes et al., 2008; Zhu et al., 2004). *Cd44* has also been linked to the phagocytosis of apoptotic neutrophils, indicating a crucial role in the removal of inflammatory cell debris (Vivers

et al., 2002). Together with the expression of other chemokine receptor ligand pairs, the result suggests that Mφ sustain the inflammatory response through potential homeotypic paracrine signaling (Figure 16).
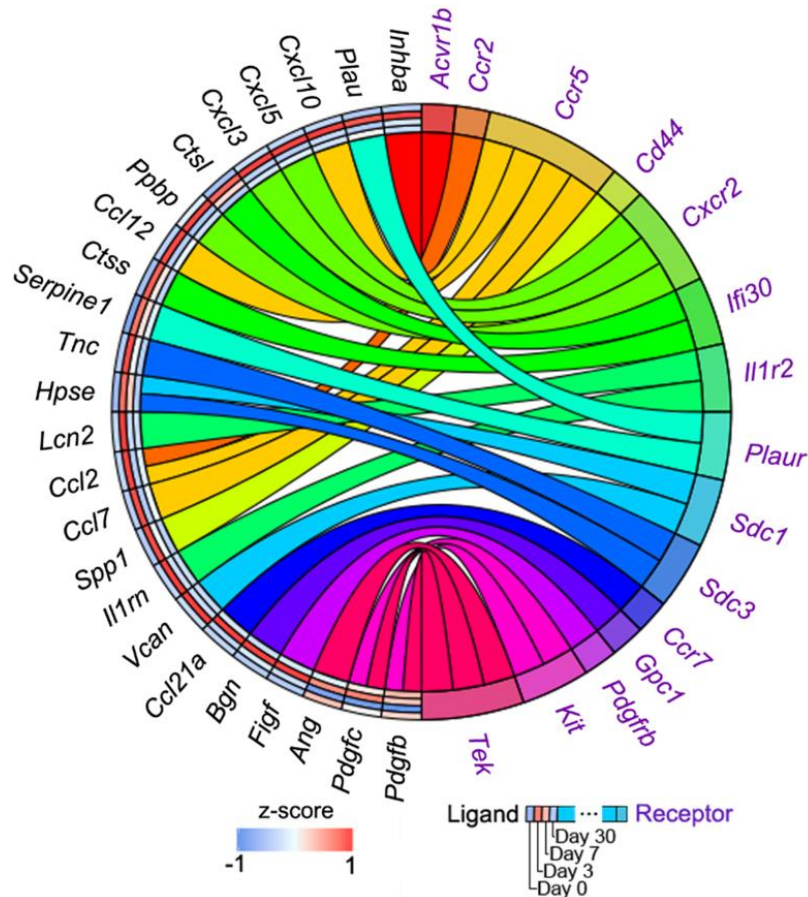
Figure 15: Potential homeotypic paracrine signaling of cardiac Mφ. Chord diagram of SM (black) – MP (purple) pairs. Squares following gene symbols of SMs indicate the z-score 0, 3, 7, 30 days post-MI.

We further identified SM- MP pairs of angiogenic factors (e.g. *Ang*, *Pdgfb*, *Pdgfc*) expressed in CRMs and at 7 days post-MI, indicating a contribution of Mφ to the process of angiogenesis. Despite the extensive macrocrine of cluster III, few SM – MP pairs could be identified. Together with the established BPs for the secretome of 7 day post-MI Mφ it indicates a strong involvement of these cells in intercellular signaling and ECM organization through the secretion of ECM components (Figure 16). The low number of potential homeotypic paracrine signaling pairs in the healthy heart and at 30 days post-MI (Figure 15) suggests that the extensive receptome primarily serves for immune surveillance (Figure 16), a widely proposed function of tissue resident Mφ (Davies et al., 2013; Mosser and Edwards, 2008).
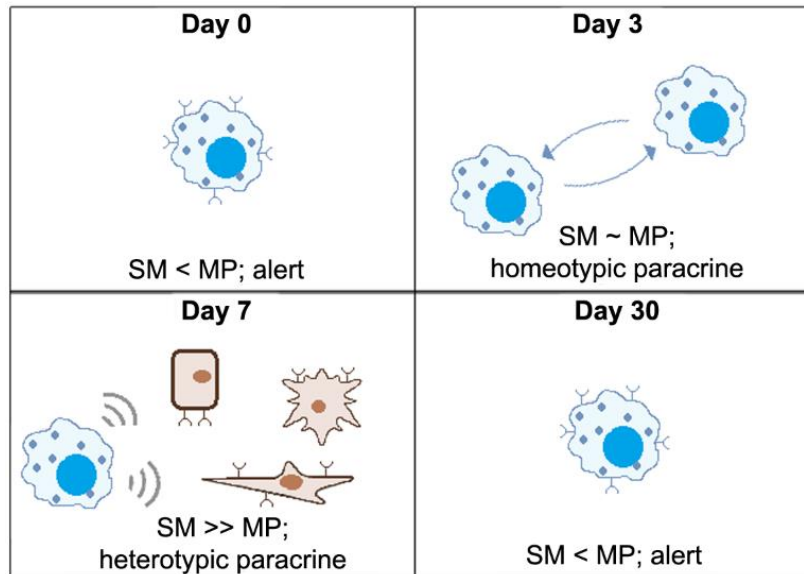
Figure 16: Pictographic summary of the potential role of the identified secretome and receptome of cardiac Mφ. MP, membrane protein; SM, secreted molecule

All together the result suggests a strong extracellular signaling potential of Mφ 3 and 7 days post-MI as opposed to a more receptive role of Mφ in the healthy heart and at 30 days post-MI. The result further suggests a high homeotypic paracrine signaling potential of Mφ 3 days post-MI, whereas Mφ 7 days post-MI seem to be strongly involved in cell-cell signaling by the secretion of ECM components.

2.7. Specific destabilization of inflammatory mRNAs by TTP-directed mRNA decay

Mφ are critical mediators of inflammation but excessive inflammation can lead to pathological conditions (Taylor et al., 1996). RNA-binding proteins, such as TTP, limit inflammatory cytokine production through destabilization of their mRNA and it has been shown that TTP is responsible for the destabilization of one third of inflammation-induced unstable mRNAs in Mφ *in vitro* (Kratochvill et al., 2011). TTP also plays an important role in Mφ polarization (Sedlyarov et al., 2016).

The DE analysis had shown that TTP was significantly up-regulated 3 days post-MI (Figure 4A), indicating TTP activity at this temporal stage. TTP enhances mRNA decay through binding to AU-rich 3'UTRs. Hence, we tested the clusters of co-expressed genes for an enrichment of AU-pentamers ("AUUUA") and AU-heptamers ("UAUUUAU"). We found two clusters with an enrichment for ARE: cluster II and VI. Genes with an elevated expression 3 days post-MI (cluster II) were associated with

immune response and showed a significant enrichment for ARE (Table 2), indicating an increased possibility of TTP-directed regulation of inflammation – induced mRNAs as previously described (Kratochvill et al., 2011). Additionally, we found an enrichment of AREs for genes up-regulated in the healthy heart and at 30 days post-MI. These genes were enriched for cell cycle-related processes (Table 2), which is in line with the finding that many cell cycle regulators are coded by ARE-mRNAs (Barreau et al., 2005).

The median mRNA half-life of co-expressed genes was calculated in hours based on the mRNA degradation rates database from the National Institute of Aging (Sharova et al., 2009). For all clusters, the calculated AU- content of 3'UTRs was anti-correlated to the estimated median half-lives (spearman correlation coefficient = -1). In accordance with the results from the AU-motif enrichment analysis the mRNAs of the clusters II and VI had a half-life below the reported overall median of 7.1 h (Sharova et al., 2009). Genes up-regulated 3 and 30 days post-MI, although not enriched for AU elements, had the shortest median mRNA half-life among all clusters (4.7 hours). The cluster was enriched for processes such as regulation of transcription, cytokine activity, and TF activity, which were previously linked to unstable mRNAs (Sharova et al., 2009). Interestingly, the mRNAs from cluster III showed a prolonged median half-life (9.6 hours) and were enriched for ECM organization and collagen fibril organization (Table 2), structural processes that are linked to stable mRNAs.

Table 2: Overview of mRNA stability parameters. Fisher's exact test was applied to test mRNA 3'UTRs for an enrichment of AU-pentamers ("AUUUA") and AU-heptamers ("UAUUUAU"). Obtained p-values were corrected for multiple testing (Benjamini - Hochberg).

Cluster	Median 3'UTR length	ARE pentamer	ARE heptamer	Median half-life (h)	Top biological process
I	964 nt	1	0.87	7.4	Myofibril assembly
II	908 nt	0.017	0.87	6.6	Immune response
III	834 nt	1	0.99	9.6	ECM organization
IV	1043 nt	1	0.87	4.7	Inflammatory response
V	710 nt	1	0.99	8.1	Cell cycle, M phase
VI	1204 nt	4.7e-22	1.04e-06	5.9	Cell cycle

Abbreviations: 3'UTR, 3-untranslated region; lincRNA, long intronic RNA; ECM, extracellular matrix; nt, nucleotides

The 3'UTR of mRNAs contain not only binding sites for regulatory proteins but also for miRNAs. Longer 3'UTRs are associated with lower levels of gene expression due to increased post-transcriptional modifications (Stark et al., 2005). Therefore, the

median length of the 3'UTRs per cluster was calculated to determine the possible regulatory effects of RNA binding proteins and miRNAs (Table 2). We found that the median 3'UTR length was highest for genes expressed in the healthy heart and 30 days post-MI, indicating a higher probability for post-transcriptional modification. Interestingly, genes with an elevated expression at 7 days post-MI (cluster III and cluster V) possessed comparably shorter 3'UTRs, reducing the likelihood of post-transcriptional regulation.

In agreement with reported findings (Kratochvill et al., 2011; Sedlyarov et al., 2016), our data indicates that inflammation-induced mRNAs are less stable and more prone for post-transcriptional regulation due to longer 3'UTRs and an enrichment for ARE in their 3'UTRs, targeting them for rapid degradation.

2.8. The miRnome of cardiac Mφ

Another level of post-transcriptional regulation that might affect mRNA stability is miRNA-mediated gene silencing. miRNAs mediate translational repression and degradation of targeted mRNAs and have been shown to play important roles in immune response and Mφ polarization (Essandoh et al., 2016; Graff et al., 2012; Wang et al., 2013). Hence, we analyzed the miRNA expression following the depicted workflow in Figure 17A.

PCA of the global transcriptional profiles revealed well separated miRNA expression signatures at the different post-MI stages (Figure 17B), supporting the idea of time point- specific post-transcriptional regulation. DE analysis of miRNAs was performed comparing each post-MI stage to the control sample and between each other (Figure 17C). Statistical analysis revealed a set of 258 non-redundant miRNAs DE in at least one of the comparisons (adjusted p-value < 0.05, logFC > 1|< -1, and average expression > 4.0). Only a small number of miRNAs were altered comparing CRMs with 7 day post-MI Mφ. The gene expression of the miRNA machinery (Drosha, Dicer1, Xpo5, Ran, Dgcr8, Tarbp2) 7 days post-MI was not significantly changed compared to all other time points, indicating that the miRNA biogenesis was not perturbed but the detected low number of DE miRNAs was due to a low level of post-transcriptional regulation at that temporal stage, as indicated by the mRNA stability analysis. Interestingly, we found similar numbers of DE miRNAs comparing 3 and 30 day post-MI Mφ to CRMs. It has been proposed that miRNA targeting of ARE is crucial

in ARE-mediated mRNA degradation (Jing et al., 2005), which matches the observed AU enrichment for clusters II and VI (Table 2).
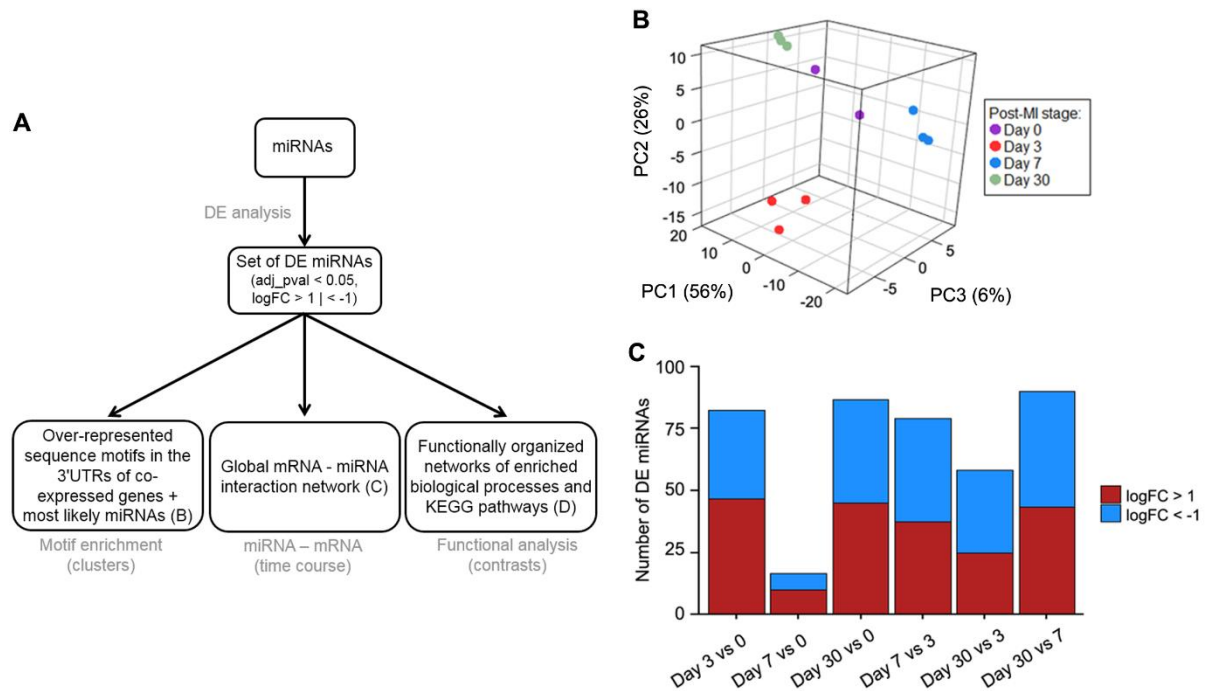
Figure 17: Global analysis of miRNA expression. (A) Workflow of integrated miRNA analysis. (B) PCA of miRNA expression. Number in parenthesis indicate the percentage of variation explained by each of the three first principle components. (C) Number of DE miRNAs for every comparison across time.

A first approach to integrate miRNA data with mRNA expression profiles aimed at the identification of miRNAs that have the potential to regulate the clusters of co-expressed genes. 3'UTRs of clustered genes were searched for enriched motifs and subsequently linked to miRNAs, based on matching seed sequences and an anti-correlated miRNA expression profile (Figure 18A). The target genes and expression profile of the identified miRNAs (Figure 18B) implied regulatory functions in cell cycle-related processes, apoptosis, the maintenance of immune quiescence and the recovery of homeostasis.
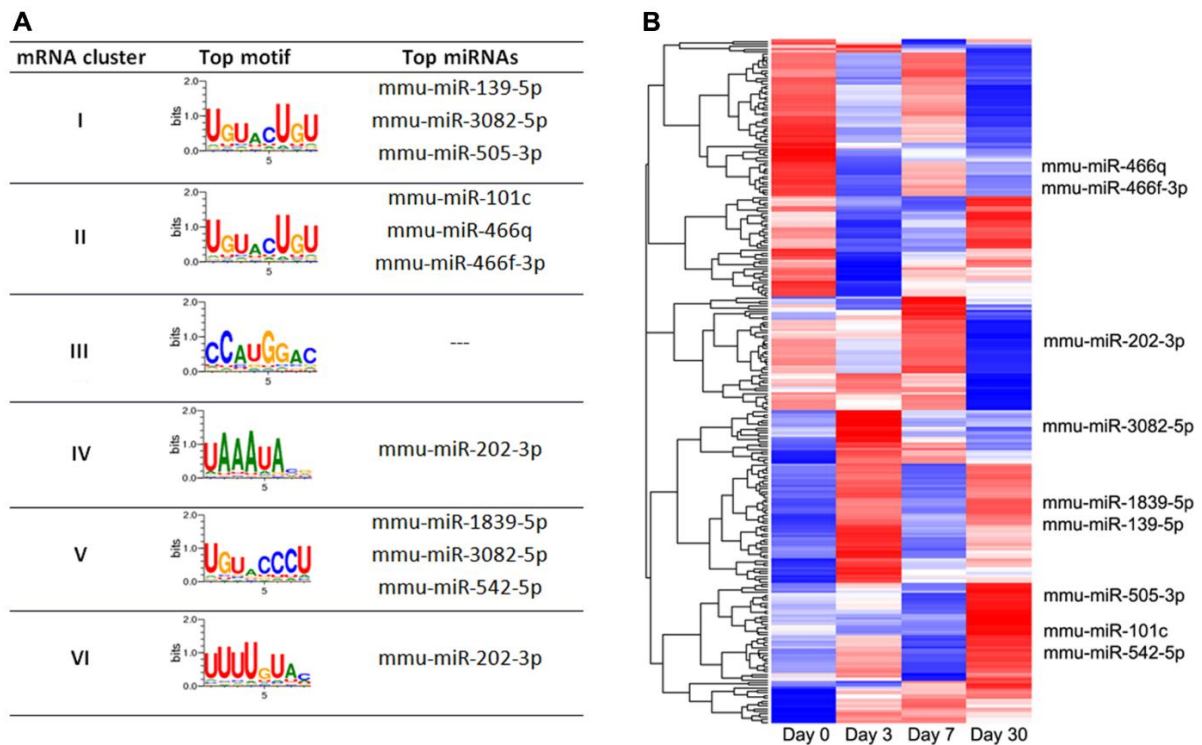
Figure 18: Cluster-specific miRNA-mediated regulation. (A) Over-represented sequence motifs in the 3'UTRs of co-expressed genes. The top miRNAs (maximum of three) corresponding to these motifs are displayed. (B) Hierarchical clustering of the 258 miRNAs differentially expressed in at least one time point compared to control. Highlighted are miRNAs identified as potential regulators of co-expressed genes by miRvestigator (Plaisier et al., 2011).

Although the over-represented motifs for clusters I and II were the same, the clusters were potentially regulated by different miRNAs based on their divergent expression profiles. miR-139-5p, miR-3082-5p, and miR-505-3p were detected as the three most probable miRNAs to regulate genes with low expression at all temporal stages compared to the healthy heart. BPs associated to the targeted cluster and the expression profile of these miRNAs imply regulatory functions in cell cycle- related processes and cell proliferation. For cluster II the highest ranked motif was linked to the miRNAs miR-101c, miR-466q, and miR-466f-3p. Based on their anti-correlation, the miRNAs were all characterized by a down-regulation at 3 days post-MI and up-regulation at other temporal stages. In combination with the biological function of their target genes it seems to be likely that these miRNAs are involved in the maintenance of immune quiescence or the recovery of homeostasis. The top miRNAs for cluster V included miR-1839-5p, miR-3082-5p and miR-542-5p. miR-542-5p has been identified as a putative tumor suppressive microRNA (Bray et al., 2011) and the functions of the targeted cluster indicate a regulatory role of these miRNAs in cell proliferation. Despite

divergent over-represented motifs the clusters IV and VI were potentially regulated by the same miRNA, miR-202-3p. It has been observed that miR-202 targets genes with a wide variety of different biological functions, such as cell proliferation, apoptosis, and inflammatory response (Kumar and Nerurkar, 2014; Zhang et al., 2014; Zhao et al., 2013).

The second approach of our integrated analysis focused on the overall temporal pattern of post-transcriptional regulation. We constructed a global miRNA-mRNA interaction network of all DE genes and miRNAs and mapped the normalized gene expression data to the node fill color (Figure 19A). The topology of the networks led to the identification of three clusters (S1, S2, S3) with different expression profiles and different biological functions (Figure 19A, Figure 19B).
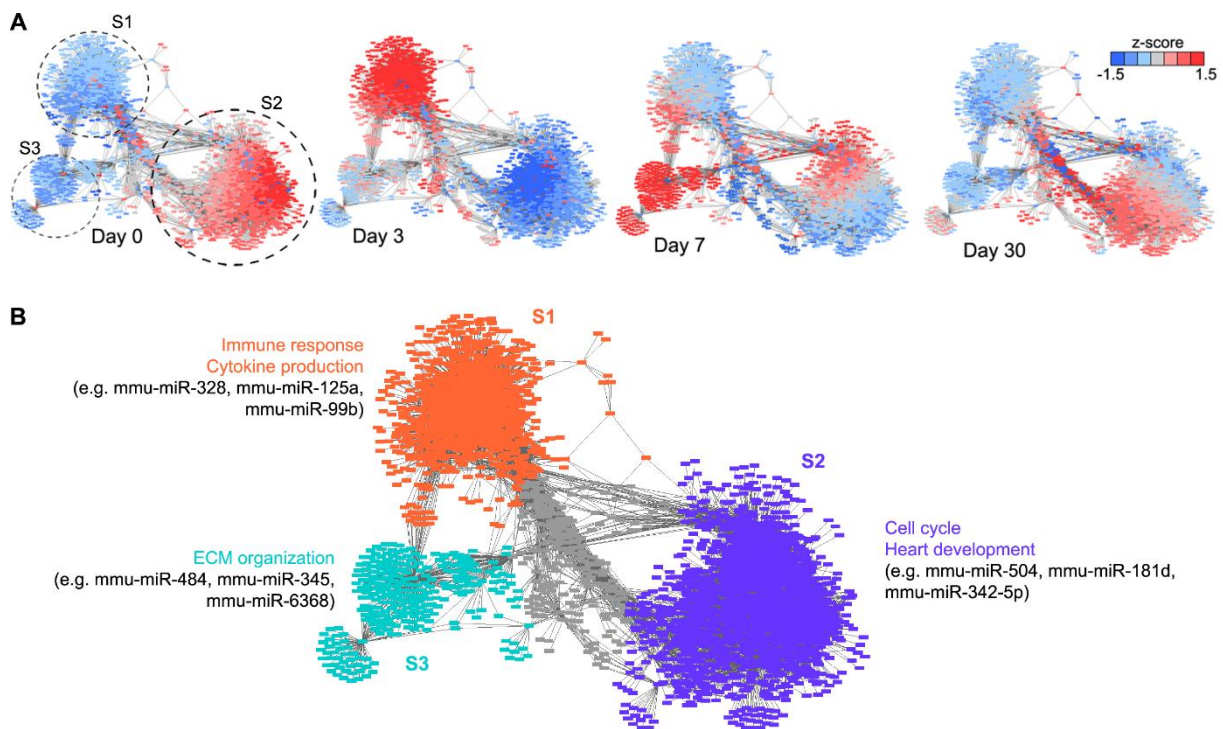
Figure 19: Global mRNA-miRNA interaction network. (A) Temporal expression profile of mRNA – miRNA interaction network. Node fill color is mapped to the normalized expression (z-score). S1, S2, S3 indicate the three hubs of the network. (B) BPs associated to the three hubs of the global mRNA – miRNA interaction network and exemplary miRNAs.

S1 was characterized by a down-regulation of miRNA expression 3 days post-MI and up-regulated genes at this temporal stage were associated with defense response and cytokine production (Figure 19A, Figure 19B). The result suggests miRNA-mediated repression of inflammatory processes to maintain homeostasis in

CRMs. Moreover, the result might indicate that miRNA activity contributes to the resolution of inflammation through miRNA-mediated degradation of pro-inflammatory mediators, enabling the restoration of homeostasis 30 days post-MI. The second subnetwork (S2), associated to cell cycle-related processes and cardiovascular development (Figure 19A, Figure 19B), exhibited a very heterogeneous gene expression profile. In the healthy heart miRNAs associated with heart and cardiovascular system development genes (e.g. mmu-miR-1a, mmu-miR-126a, mmu-miR-342-5p) were down-regulated, in agreement with the enriched processes for genes with elevated expression in resting conditions (Figure 6B). 3 days post-MI the genes of S2, which were mainly associated with cell cycle, were potentially down-regulated by miRNA activity (e.g. mmu-miR-504, mmu-miR-181d). Interestingly, the subnetwork exhibited opposite gene expression regulation at 7 and 30 days post-MI, which might indicate the onset of distinct cell cycle- related processes. It is also interesting to note that, in contrast to CRMs, genes related to heart development were down-regulated 30 days post-MI, indicating prolonged miRNA repression. Genes of the third subnetwork (S3) were related to ECM and collagen fibril organization and miRNAs regulating these genes were down-regulated 7 days post-MI (Figure 19A, Figure 19B), consistent with the detected up-regulation of genes coding for ECM component and collagen proteins at this time point.

The third approach focused on the comparison of day 7 with day 3 to investigate the role of miRNAs in Mφ polarization. Naturally two miRNA – mRNA subnetworks with opposite expression profiles emerged. Functional analysis elucidated BPs and pathways impacted by post-transcriptional regulation (Figure 20A, Figure 20B). miRNAs up-regulated at 3 days post-MI attenuated inflammatory response by potentially suppressing processes linked to cell cycle, tissue and blood vessel development, metabolism and mesenchymal cell proliferation (Figure 20A). At 7 days post-MI miRNAs contributed to a resolution of inflammation by down-regulation of immune response- related genes, facilitating the critical transition to an anti-inflammatory phenotype (Figure 20B). Interesting to note is the miRNA- mediated silencing of apoptotic signaling pathways at 7 days post-MI, which suggests that cell death related processes increased 3 days post-MI (Figure 6B) might subsequently be down-regulated by miRNAs.
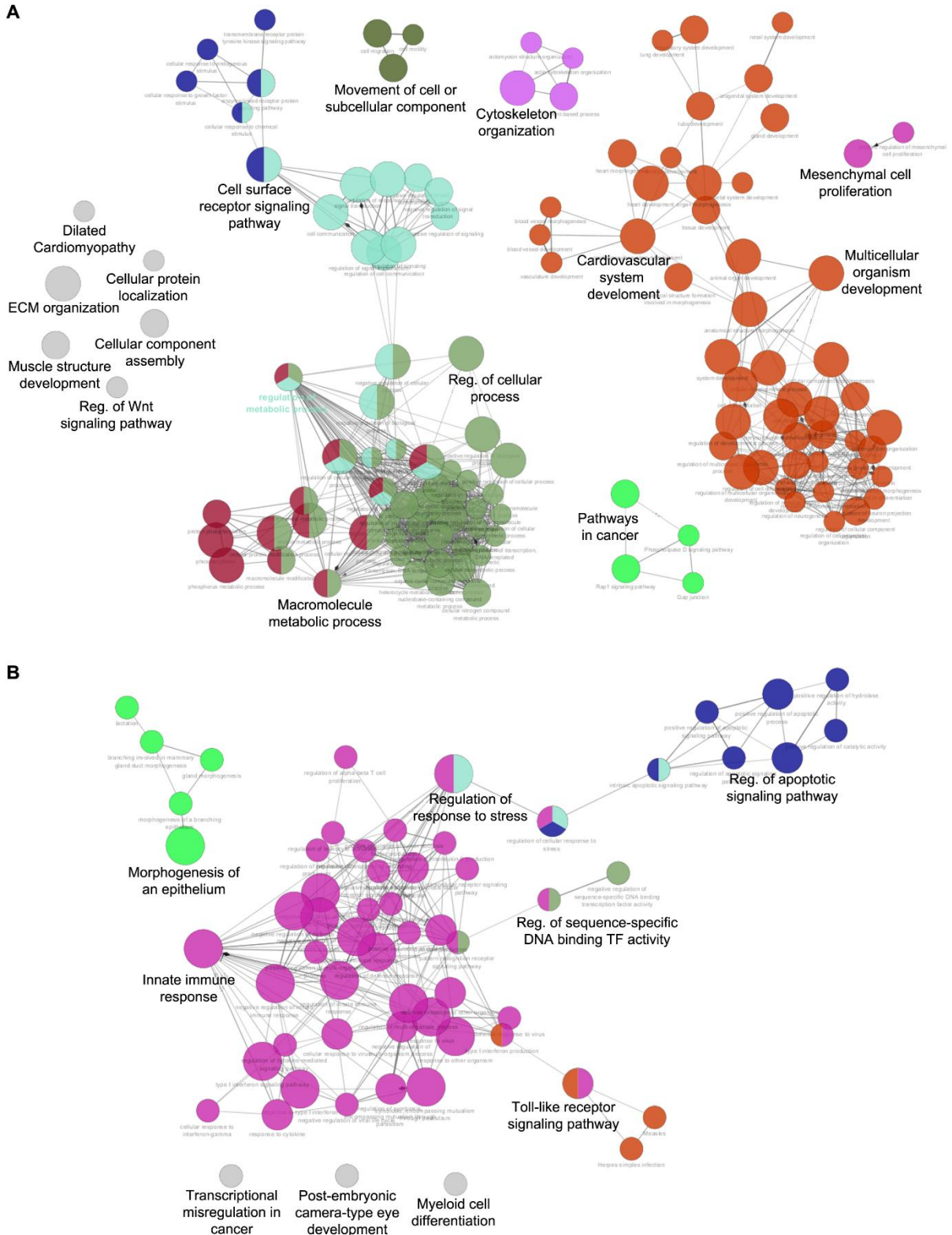
Figure 20: miRNA activity during Mφ phenotype transition. ClueGO network connecting the most significant functional terms (biological process or KEGG pathway) for the targets of those miRNAs significantly up (A) and down (B) regulated between day 3 and day 7 post-MI. The colors represent different groups. For each group the most significant term is displayed.

Taken together with the results from the mRNA stability analysis, the data indicates a critical role for TTP and miRNAs in Mφ activation and in the transition from a pro-inflammatory to an anti-inflammatory phenotype. With the important difference that TTP-driven mRNA decay of immune response related genes occurs in response to induced inflammation, whereas miRNA activity might also contribute to immune quiescence in the healthy myocardium. In addition, it seems to be likely that miRNA activity controls Mφ cell proliferation during cardiac repair.

2.9. Long non-coding RNAs in cardiac Mφ

Another set of post-transcriptional regulators are lincRNAs, which have also been recently implicated in CVDs (Ounzain et al., 2015). Based on ensembl biotype classification we identified 195 lincRNAs amongst all the clustered genes (Figure 21A).

In accordance with reported findings (Guttman and Rinn, 2012), lincRNAs were on average lower expressed than mRNAs and we found a high similarity of structural features such as length and GC content between lincRNAs and the 3'UTR of mRNAs (Figure 21B), as previously reported (Niazi and Valadkhan, 2012). Cluster specific trends on the mRNA level were mirrored in lincRNA features and the high similarity might indicate a common post-transcriptional regulation. The binding of a common regulator (e.g. a miRNA) is sequence-dependent and requires high sequence similarity between its targets. Hence, we blasted the mRNA 3'UTR sequences against lincRNA sequences to search for aligned lncRNA - 3'UTR pairs, which were subsequently scanned for common miRNA seed sequences. The emerging list of possible mRNA - lincRNA - miRNA triangles was further filtered by expression. Figure 21C displays the nature of interactions of all remaining triangles within fixed boundaries. The CCs are mapped to three aesthetics: cc between expression profiles of mRNA:lincRN on x-axis, CC of lincRNA:miRNA on y- axis, and fill colour of points corresponds to CC of mRNA:miRNA. Four different cases of mRNA - lincRNA - miRNA interactions could be identified which are summarized in the middle of Figure 21C as small graphics. The most abundant type of mRNA - lincRNA - miRNA interactions was characterized by positively correlated expression of all RNAs. No BPs were enriched for any of the clusters but we found multiple triangles that included the characterized lincRNAs *Neat1* and *Pvt1* (Figure 21D, E).
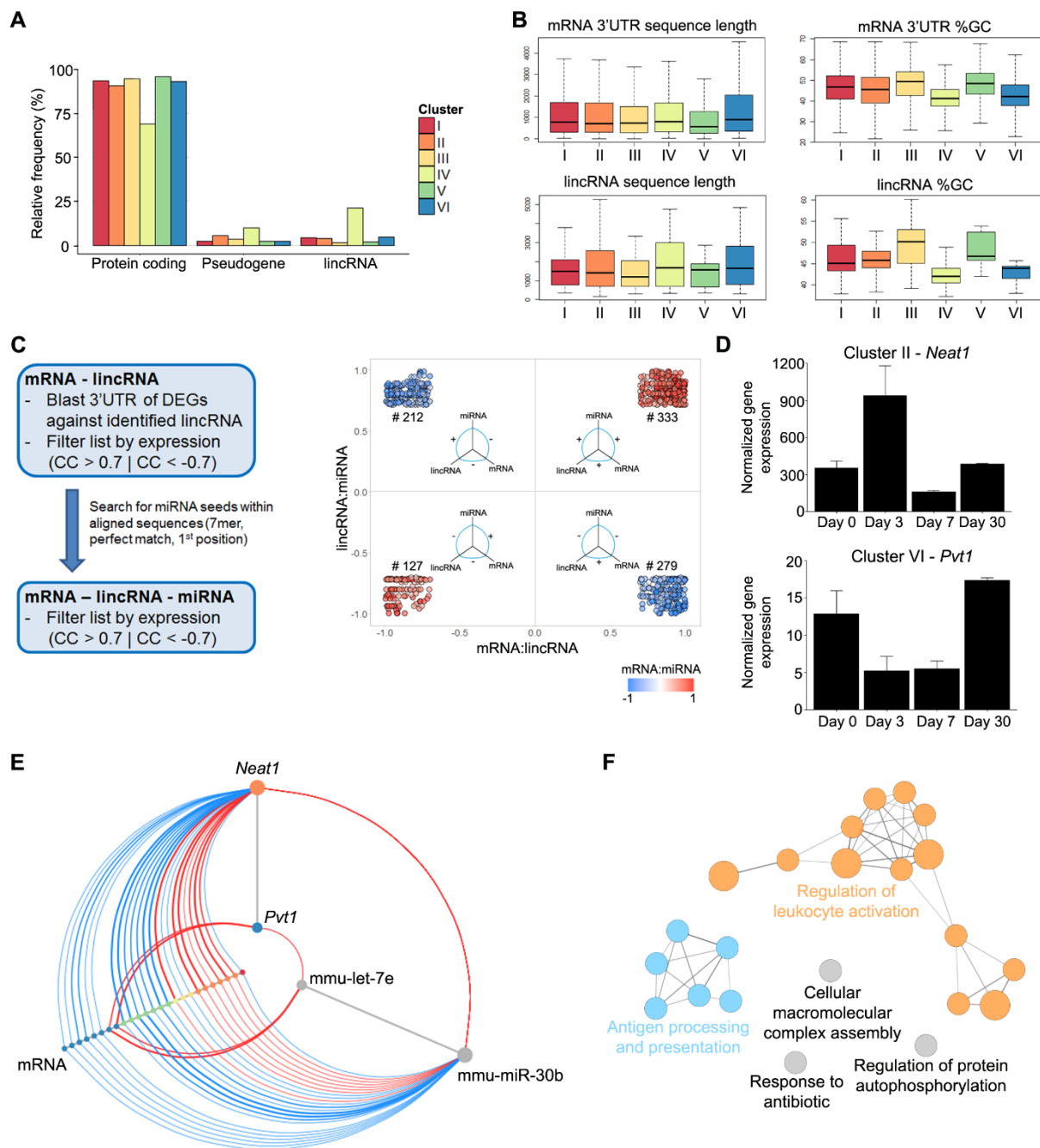
Figure 21: LincRNA profile in cardiac Mφ. (A) Percentage of various transcript biotypes per cluster (Figure 3A). (B) Structural similarities between 3'UTR of mRNAs and lncRNA sequences. (C) Correlation between mRNA – miRNA – lincRNAs expression profiles. X-axis displays CC between mRNAs and lincRNAs; Y-axis displays CC between lincRNAs and miRNAs; fill colour of points displays CC between mRNA and miRNAs. (D) Expression profiles of selected lincRNAs from various clusters. Y-axis displays normalized counts. Error bars indicate SE. (E) Hive plot presentation of mRNA – lincRNA – miRNA triangle for lincRNAs *Neat1* and *Pvt1*. Nodes representing lincRNAs and mRNAs are coloured according to clusters (Figure 3A). Red lines indicate positive correlation; blue lines indicate negative correlation. (F) ClueGO network connecting the most significant functional terms (biological process and KEGG pathway) for nearest genes of DE lincRNAs in Day 3 vs Day0.

Neat1 was up-regulated 3 days post-MI and has been associated with innate immune response (Imamura et al., 2014; Zhang et al., 2013b). *Pvt1* on the other hand was induced in the healthy heart and at 30 days post-MI and has recently gained importance as a ceRNA for *Myc* (Colombo et al., 2015), associating this lincRNA with cell cycle related processes. Both lincRNA characteristics matched the functions identified for genes with similar expression profiles (Figure 6B). The identified mRNA-lincRNA-miRNA triangles including *Neat1* were linked through miR-30b, a miRNA that has been associated with immune suppression (Gaziel-Sovran et al., 2011).

We found that cluster IV had the highest relative abundance (15.5%) of lincRNAs, including *Malat1* that is known to be induced by hypoxia and to play a relevant role in CVD (Skroblin and Mayr, 2014). Within the same cluster we found *Mir17hg*, that encodes for the miRNA 17-92 cluster. These miRNAs are associated with cell cycle and cell proliferation (Mogilyansky and Rigoutsos, 2013), indicating a potential role of *Mir17hg* in the regulation of Mφ cell proliferation. LincRNAs identified for the other time points were only poorly characterized. Hence, we tried to functionally characterize them based on association with protein coding genes (Fritah et al., 2014). The BEDOPS closest-features program (Neph et al., 2012) with the --no-overlaps option was used to identify the closest non-overlapping protein coding genes upstream and downstream of each lincRNA. Subsequently, the reported list was filtered to exclude protein coding genes that were not DE. ClueGO was used to identify enriched non-redundant biological terms of protein coding genes linked to lincRNAs DE between different post-MI stages and the control sample. Protein coding genes linked to lincRNAs DE between day 0 and day 3 were significantly enriched for processes related to antigen and leukocyte activation, suggesting a role for lincRNAs in innate immunity (Figure 21F).

All together our data suggests that lincRNAs extend the regulatory network of Mφ transcription by influencing important processes such as cell proliferation and innate immune response.

2.10. Complex regulatory network of *in vivo* Mφ

As indicated by our data, the activation of Mφ is a process orchestrated by a multitude of factors that build a highly connected network of cooperative or competing relationships. In order to gain a global understanding of the underlying regulatory

network and its dynamics we reconstructed a literature-based interaction network and computed its stable states following the workflow depicted in Figure 22A.
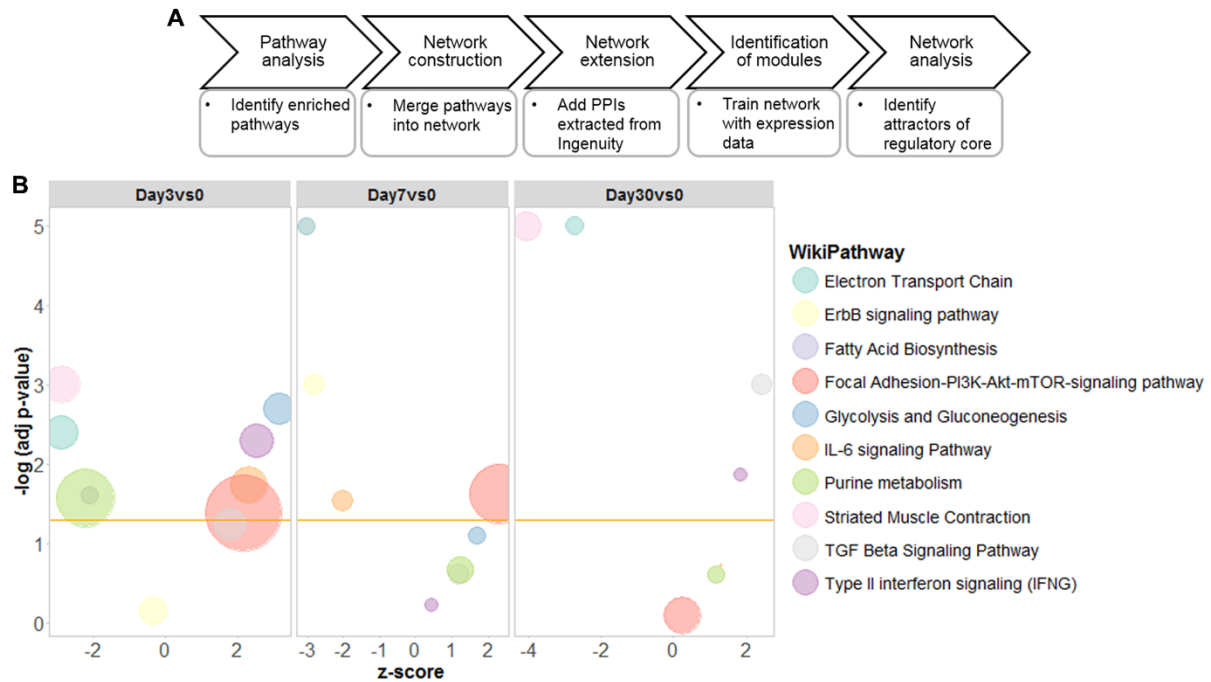
Figure 22: Pathways analysis. (A) *In silico* analysis workflow. (B) GOBubble of pathways enriched in at least one of the displayed contrasts. X-axis displays z-score of selected pathways. Y-axis corresponds to negative logarithm of the adjusted p-value. Each circle represents one pathway (legend) and the circle size correlates with number of assigned genes to pathway.

Based on the statistical analysis in PathVisio we manually selected a list of 10 pathways significantly altered in at least one of the comparisons (Figure 22B). 3 days post-MI, IL6 signaling and type II interferon signaling pathway were significantly up-regulated, confirming the pro-inflammatory phenotype of Mφ isolated at 3 days post-MI. IL6 signaling has been shown to enhance glycolysis (Ando et al., 2010), which became activated 3 days post-MI, capturing the known metabolic change of pro-inflammatory Mφ (Bordbar et al., 2012; Freemerman et al., 2014; Rath et al., 2015). In accordance with these findings striated muscle contraction, electron transport chain, fatty acid biosynthesis, and purine metabolism pathways were down-regulated in this contrast. At 7 days post-MI we observed an increase in the focal adhesion-PI3K-Akt-mTOR-signaling pathway with a strong up-regulation of ECM receptor interactions, supporting the identified involvement of DEGs and SMs in ECM organization (Figure 13B, Figure 16D) at this temporal stage. The late post-MI stage was characterized by

an increase of the TGF-β signaling pathway, consistent with the role of TGF-β signaling in cardiac remodeling (Bujak and Frangogiannis, 2007).

The pathways were imported as networks into cytoscape using the Wikipathway App and subsequently merged into one large network. The network of altered pathways contained 251 DEGs. In order to increase the number of DEGs, the network was extended by extracting experimentally validated interactions between genes of the network and remaining DEGs from Ingenuity. The extended network was submitted to the jActiveModule cytoscape App to identify active subnetworks. The most significant subnetwork, composed of 45 nodes and 123 edges, was selected for further analysis. Network structure analysis revealed a SCC consisting of 21 genes (Figure 23).
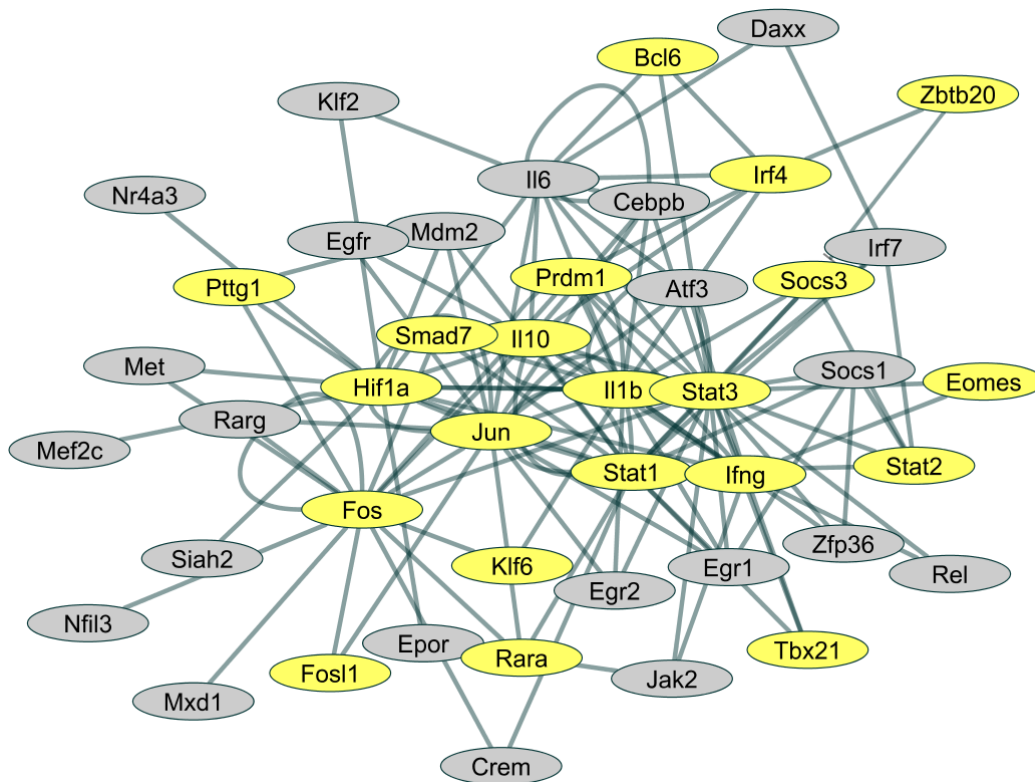
Figure 23: Network structure analysis of the most significant subnetwork. Nodes of the SCC of the module are highlighted in yellow.

A SCC is a group of genes, where every pair of genes is connected through directed paths (Albert, 2007). The high interconnectivity means that changes in the state of one gene potentially affects the state of the remaining genes of the SCC. For this reason, we proceeded to analyze the core network stability. A Boolean dynamical model with an asynchronous updating scheme was used to compute network stable states.

Despite training the network with a time series of four time points, the computation of the stability of the SCC revealed only three stable states. This result matches the observed finding of only three time point- specific clusters (Figure 6A) and the high similarity of the global transcriptional profile between the healthy heart and 30 days post-MI (Figure 10). We identified one stable state with all nodes "off", indicating a non-activated or deactivated state that might be associated with resident Mφ and Mφ isolated 30 days post-MI (Figure 24).
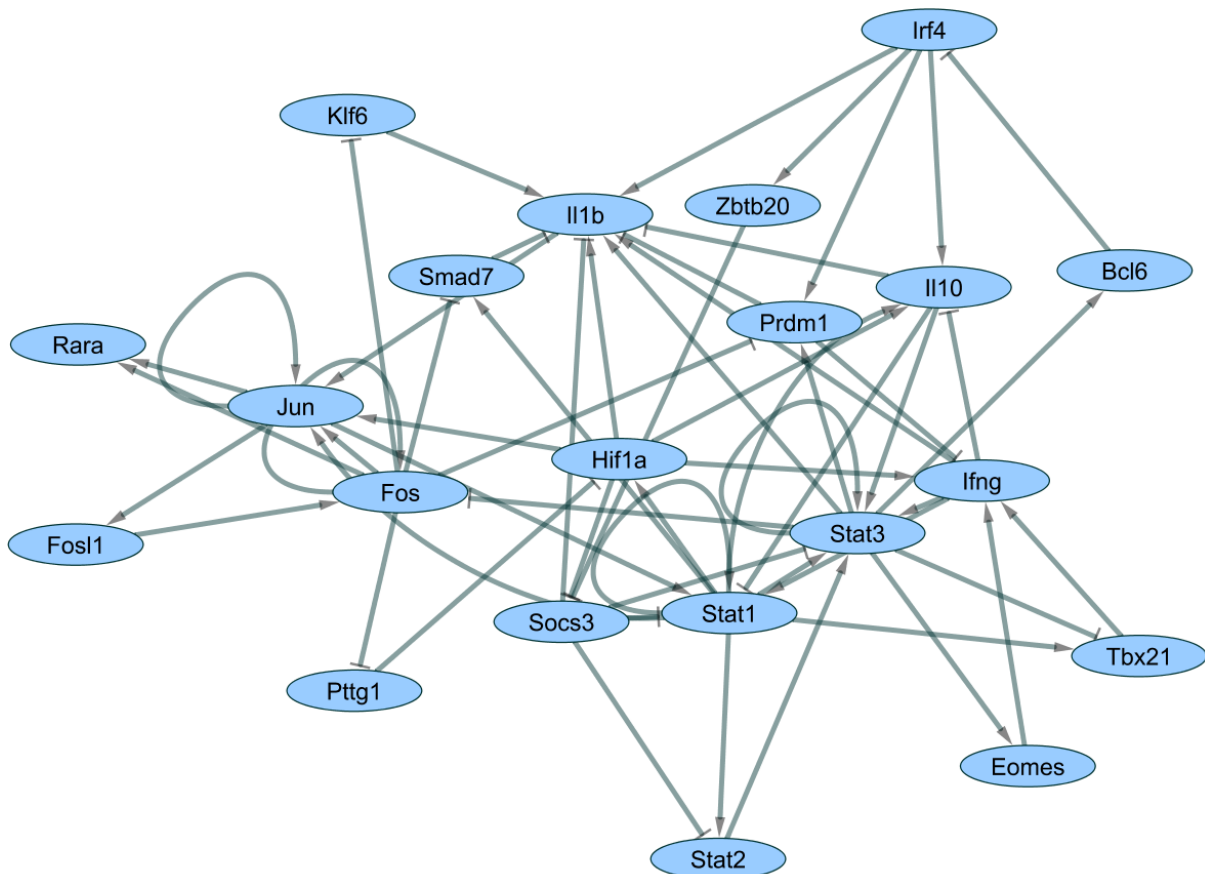
Figure 24: First point attractor of network stable state analysis. Blue nodes are "off".

Another stable state was found for the onset of *Prdm1*, *Bcl6*, *Stat3* and *Eomes* (Figure 25). *Prdm1* is a known transcriptional repressor that becomes activated in response to cellular stress in murine Mφ (Tooze et al., 2006). *Bcl6* negatively regulates Mφ proliferation by inhibition of IL6 autocrine signaling (Yu et al., 2005) and *Eomes* has been associated with cell differentiation (Pearce et al., 2003). The transcription of all three genes is regulated by *Stat3*, which can lead to the onset of a pro- inflammatory and anti-inflammatory program, depending on the strength and duration of its activation (Braun et al., 2013). The onset of these factors indicates a more repressive, anti-

inflammatory state and might be associated with Mφ at 7 days post-MI.
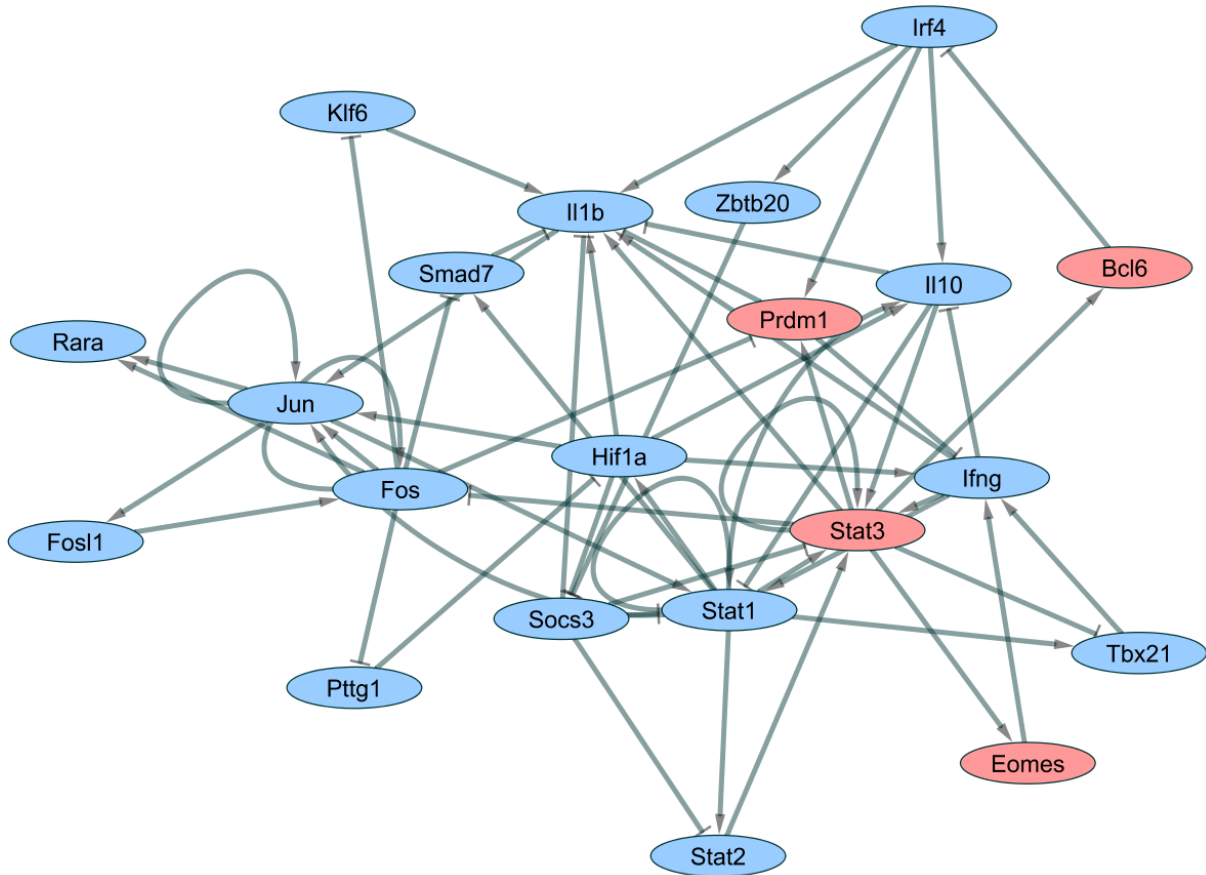
Figure 25: Second point attractor of network stable state analysis. Blue nodes are "off", red nodes are "on".

The third stable state was mainly characterized by an oscillation in activation of *Hif1a*, *Stat1* and *Il10* (Figure 26). Whereas *Hif1a* and *Stat1* are associated with a pro-inflammatory program (Mantovani et al., 2004), *Il10* is a powerful anti-inflammatory mediator, that plays a fundamental role in the transition from the inflammatory into the resolution phase of immune response (Wan et al., 2014). The up-regulated genes suggest an activation of both, pro- and anti-inflammatory programs, associating this stable state to Mφ isolated 3 days post-MI.

The oscillatory pattern of this stable state suggests that the regulation of *Il10* is tightly intertwined with the expression of *Hif1a* and *Stat1*, whereas a positive regulatory effect of *Hif1a* on *Il10* expression seems to be diminished by the presence of *Stat1*, as indicated by the changes in the node states. HIF-1α is the main mediator of hypoxic response and it has been shown that hypoxic conditions can positively alter *Il10* expression (Clambey et al., 2013; Dace et al., 2008; Murata et al., 2002; Shehade et

al., 2015), whereas IFNγ is known to have a negative effect on *Il10* expression through suppression of CREB and AP-1 activity (Hu et al., 2006). Based on this result we hypothesized that hypoxia, but not IFNγ, leads to the induction of *Il10* and tested our hypothesis *in vitro*. Peritoneal Mφ were cultured in normoxic or hypoxic conditions and incubated in the absence or presence of IFNγ. The experimental conditions were confirmed by the increased expression of target genes (Figure 27A).
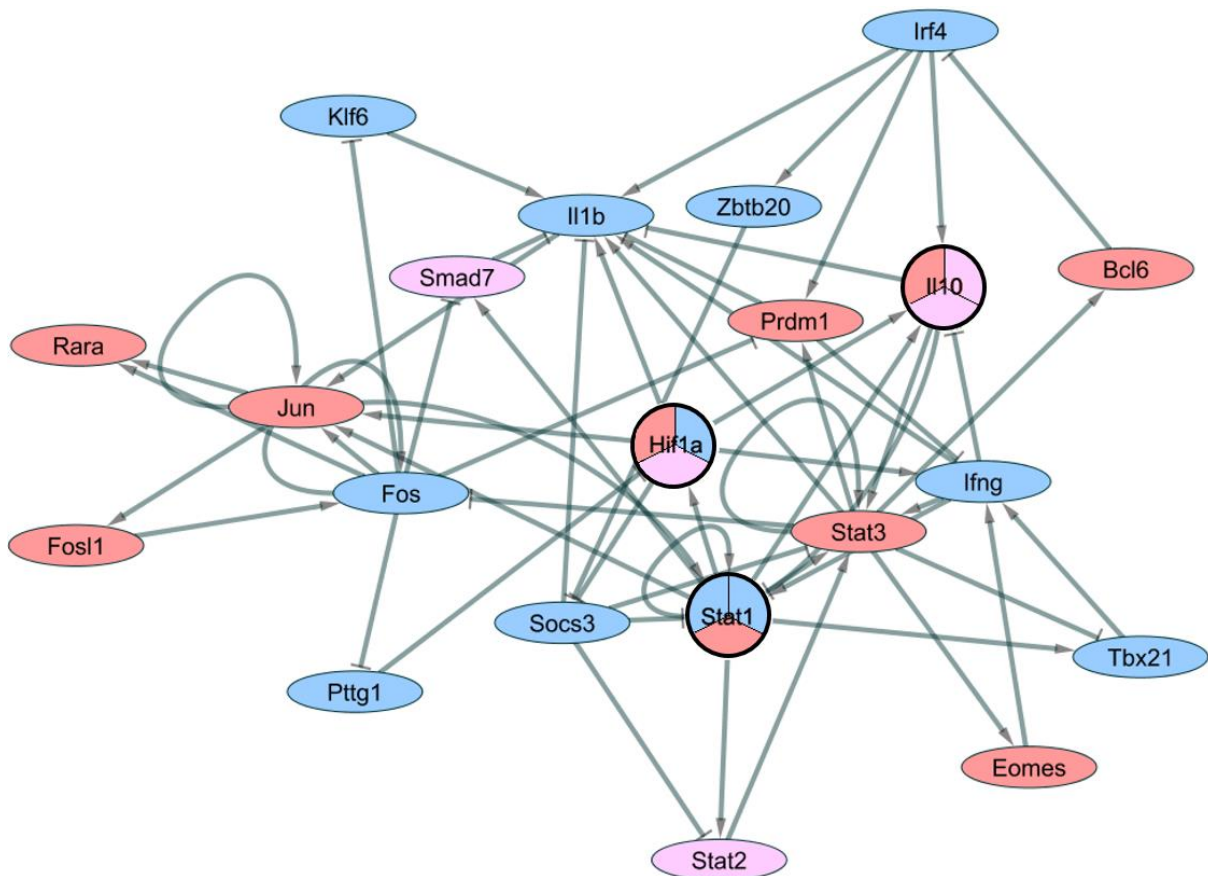
Figure 26: Cycle attractor of network stable state analysis. Blue nodes are "off", red nodes are "on", and pink nodes are "off/on". The pie charts of *Hif1a*, *Stat1* and *Il10* indicate the changing states of the genes.

To test our hypothesis, we assessed by qPCR the expression of a panel of genes from the cycle attractor (Figure 27B). As previously described (Takeda et al., 2010) we observed a strong up-regulation of *Hif1a* by IFNγ and the combined treatment of IFNγ and hypoxia, whereas we could not observe an up-regulation of *Hif1a* at the mRNA level under hypoxic conditions (Figure 24B). However, it is well known that the regulation of *Hif1a* expression occurs at the post-mRNA level (Kaelin and Ratcliffe,

2008) and the up-regulation of *Hif1a* target genes validated its activation under hypoxic conditions (Figure 24A). We further detected increased expression of *Il10* in hypoxic conditions but not in response to IFNγ treatment or the combined treatment of IFNγ and hypoxia, confirming our hypothesis. Hypoxia also induced the expression of *c-Jun*, whereas the expression of *Stat1* and *Stat3* was exclusively altered in the presence of IFNγ and did not change in hypoxic conditions.
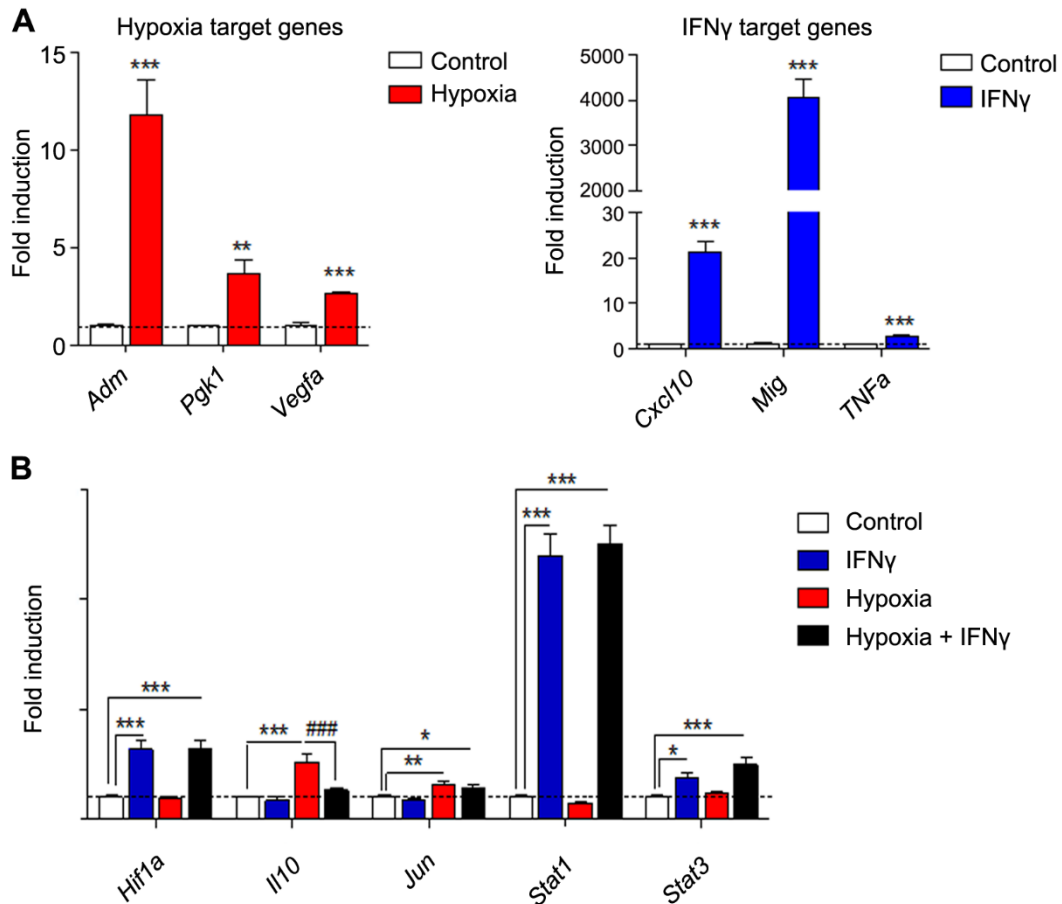
Figure 27: *In vitro* **validation of network model.** mRNA expression profile of selected HIF1α and IFNγ target genes (A) and genes of the cycle attractor (B). Data represent the mean ± SEM of 3 independent experiments; **p<0.01, ***p<0.001 (One way-ANOVA followed by Tukey's test)

Collectively, our data suggests the presence of a negative feedback-loop in post-MI Mφ that limits the initial inflammatory response through hypoxia-mediated up-regulation of *Il10*.

PROJECT 3: DECIPHERING THE TRANSCRIPTIONAL NETWORK OF THE DISTINCT HEART CELL TYPES POST-MI IN PIG

Following the characterization of cardiac Mφ in the healthy heart and post-MI, we aimed to understand their interplay with other cardiac cells. A large animal model (pig) was used to decipher the transcriptional network of distinct cardiac cells and their function in the healthy heart and after ischemia and reperfusion. For this analysis RNA-seq of CMs, FBs, ECs, and Mφ was used, integrating different levels of regulation (miRNA, mRNA).

3.1. Phenotypical characterization of distinct cardiac cells in the healthy heart and after MI
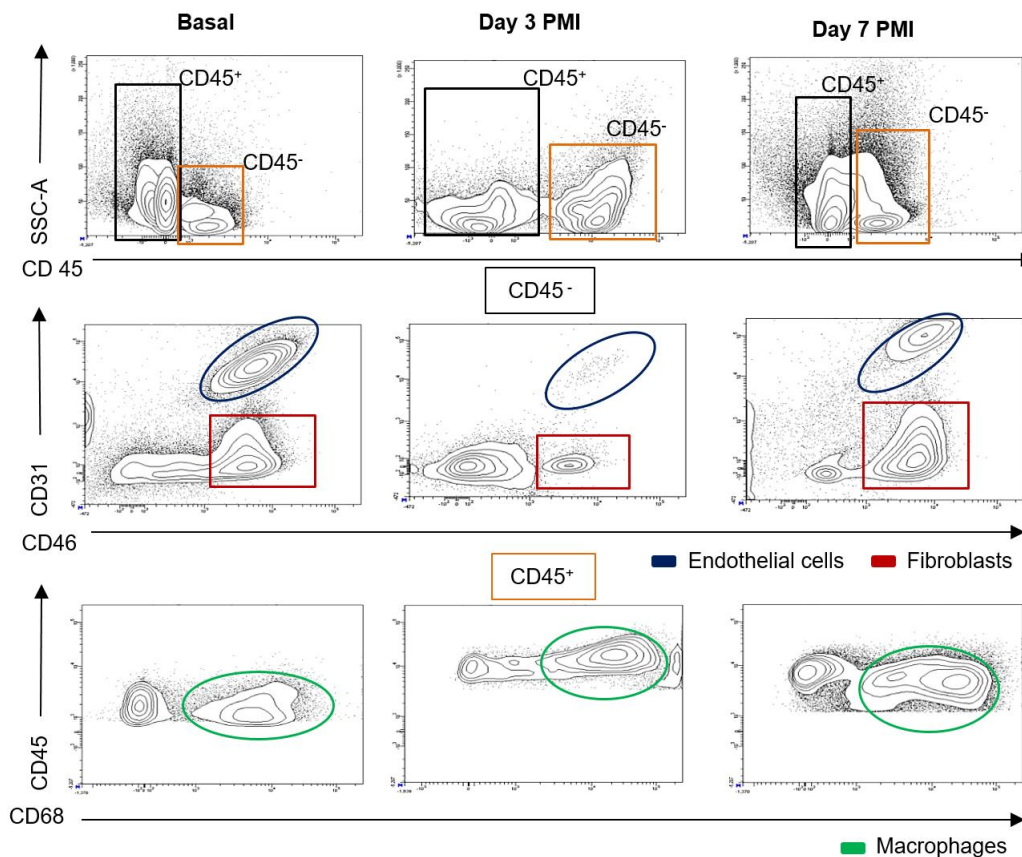
Figure 28: Characterization and isolation of distinct cardiac cells. Cardiac cell suspensions from healthy hearts or post-ischemic reperfusion were analyzed by FACS. Representative contour plots depict the kinetics of the different subsets of porcine cardiac cells.

To investigate the functional contribution of distinct cardiac cells to the process of cardiac repair, CMs, MFs, FBs, and ECs were isolated from porcine hearts at

different post-MI stages. Firstly, CM were isolated from digested porcine hearts by repeated steps of digestion and centrifugation. Secondly, MFs, FBs, and ECs were isolated by FACS. To assess the functions and characteristics of porcine cardiac Mφ CD45^{high}/CD68^{high} cells were selected. Within the CD45^{-} cell population CD31^{high}/CD46^{high} cells were selected to investigate ECs and CD31^{low}/CD46^{high} cells were selected to characterize porcine cardiac FBs.

3.2. Transcriptional characterization of porcine cardiac cells in the healthy heart and after MI

The mammalian heart consists of different cell types that all contribute to the maintenance of homeostasis in the healthy heart and to the process of cardiac repair after MI. However, the exact functions and activated transcriptional programs of the individual cell types are not well known. Here we examined the gene expression of purified CMs, ECs, FBs, and Mφ by RNA-seq.
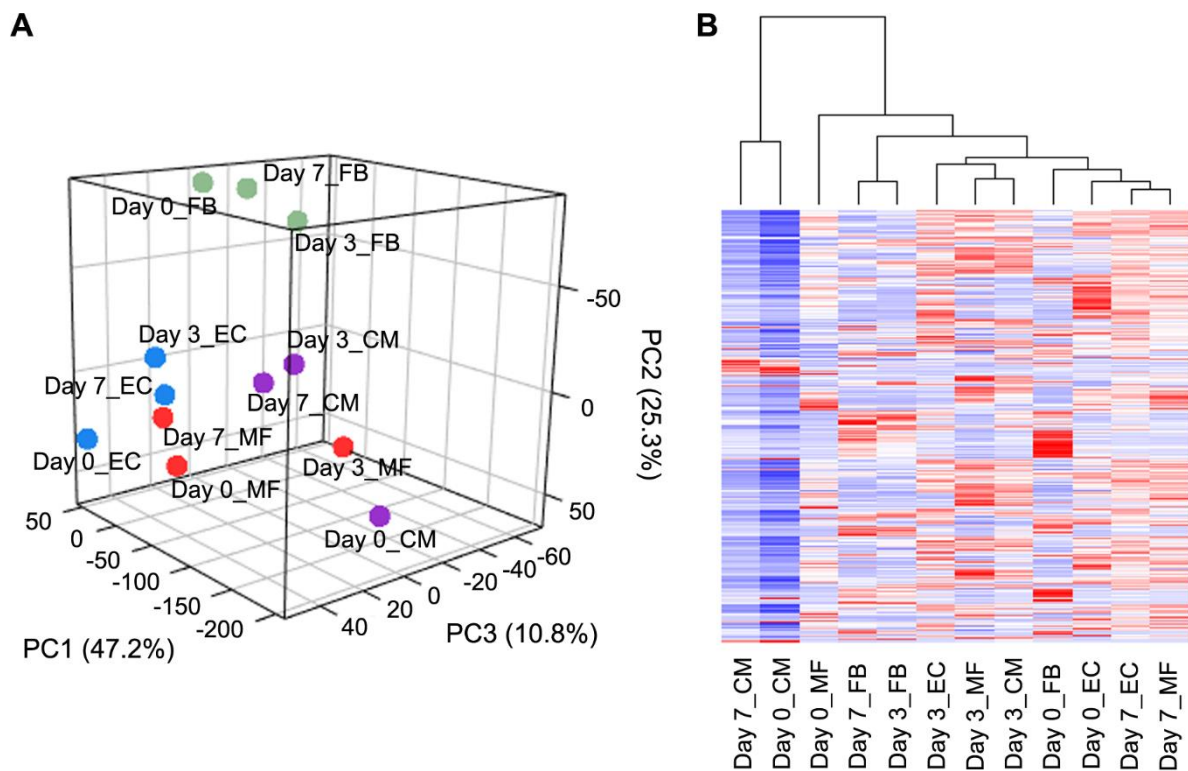
Figure 29: Transcriptional analysis of gene expression. A) PCA of the gene expression matrix. Each sample is represented by a point, and colors are assigned according to the cell type of the sample. Numbers in parentheses indicate relative scaling of the principal variables. B) HC of top 5% expressed genes.

In order to gain a global view of the different transcriptional programs we applied PCA to the whole mRNA expression profiles. The PCA (Figure 29A) shows that the different cell types are well separated and suggests that the cell type and not the time drives transcriptional regulation of cardiac cells. Next we aimed to obtain a better understanding of the functional potential of the distinct cell types at the various temporal stages, for which we selected genes with expression intensities (TPM) ranked above the 95th percentile per cell type and time point. The method was chosen due to the lack of biological replicates, which hinders population inference for DE analysis and makes any p value calculation invalid.

The HC of the top 5% expressed genes (Figure 29B) revealed that resting CMs and CMs isolated 7 days post-MI were set apart from the other samples due to a divergent expression profile. Samples of isolated FBs exhibited very similar expression profiles 3 and 7 days post-MI, indicating the onset of common transcriptional programs. Furthermore, it was interesting to note that the most abundant transcripts in ECs and Mφ post-MI showed similar expression profiles, which might indicate similar functions.

Functional analysis of the selected top 5% expressed genes (Figure 30) revealed that the different cell types shared common functions such as regulation of apoptotic process, cell migration, and metabolic process but also highlighted the functional specificity of the distinct cardiac cells. Highly abundant genes in Mφ were enriched for processes such as endocytosis, immune response, and antigen presentation, consistent with their phagocytic nature and known function in innate immune response. The result suggests further that during the reparative phase of cardiac repair (7 days post-MI) Mφ contribute to angiogenesis and ECM organization, most likely in combination with other cardiac cells such as ECs and FBs. In accordance with the literature, ECs were identified as key mediators of angiogenesis (Coultas et al., 2005; Plate et al., 1992). It is interesting to note that the VEGF signaling pathway was not enriched, implying potential VEGF-independent regulation of angiogenesis (Ferrara, 2010; Shibuya, 2008). It has been proposed that CRMs contribute to angiogenesis by non-canonical VEGF-independent pathways (Pinto et al., 2012) and the functional analysis might suggest an interplay of Mφ and ECs to promote VEGF-independent angiogenesis 7 days post-MI. Functional analysis (Figure 30) further suggests that ECs contribute to ECM organization, a process strongly enriched in FBs.

The enriched processes of FBs were very specifically centered around ECM organization (e.g. ECM organization, collagen fibril organization), in accordance with the described role of FBs in reparative fibrosis (Weber and Brilla, 1992). The functional profile of resting CMs was characterized by adenosine triphosphate (ATP) metabolic process, muscle contraction, and oxidative phosphorylation, consistent with contractile function of CMs in the healthy heart (Woodcock and Matkovich, 2005). In accordance with the described necrotic death of CMs after ischemic heart injury (Uemura et al., 2006) these functions decreased post-MI.

Altogether our data suggests, that cardiac cells exhibit cell type- specific transcriptional programs which result in divergent sets of functions. Moreover, the analysis implies that the transcriptional programs are stable enough to ensure cell type identity even in the case of disturbed homeostasis.
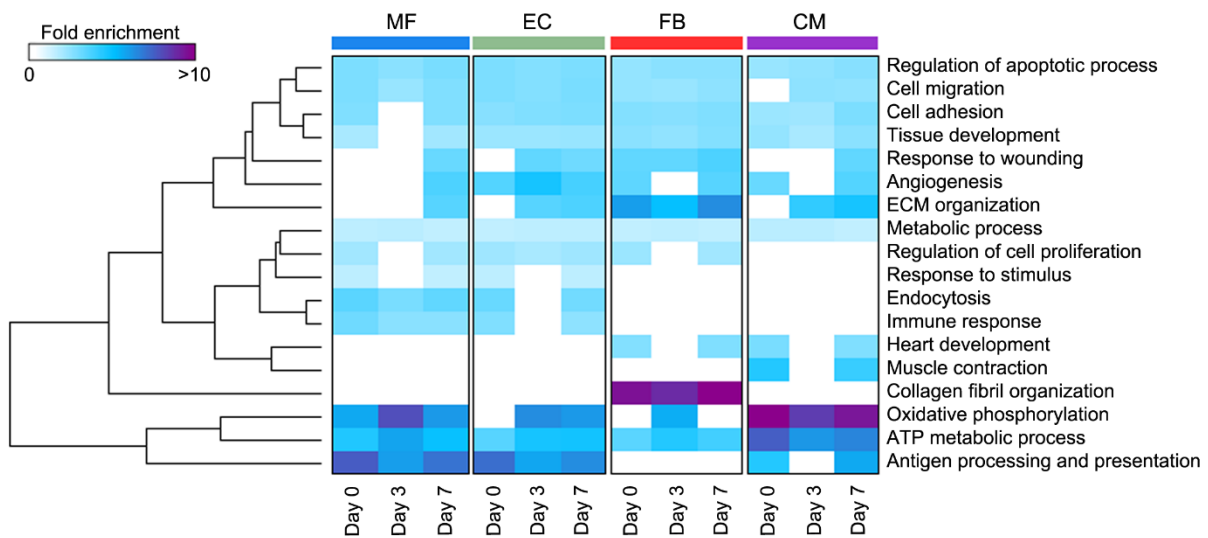
Figure 30: Functional analysis of top expressed genes per time point and cell type. Manually selected list of non-redundant enriched biological processes. Terms with an adjusted p-value < 0.05 were significant. Color corresponds to fold enrichment.

3.3. Cross- talk of cardiac cells orchestrates process such as tissue homeostasis and cardiac repair

The gathered transcriptomic data of the different cell types provides a comprehensive resource for *in silico* creation of cell-cell interaction networks. Cell-cell interactions are mediated by signaling molecules and cell surface proteins which can

be expressed by the signaling cell or by neighboring cells. In order to decipher the signaling network we used the Human Protein Atlas to classify the cellular location and extracellular signaling potential of top expressed genes. The extracellular location of selected MPs and SMs was further verified in the literature and functional analysis of the identified molecules was performed with PANTHER.

Relative frequency of SMs and MPs (Figure 31A) per cell type and time point showed that SMs were more abundant than MPs amongst the genes with the highest intensities. Only slight changes of the relative frequency of expressed MPs could be detected over time and between the different cell types. In contrast to this finding, SM expression exhibited a temporal pattern in all the cell types. It is interesting to note that the expression of SMs (Figure 30B) was less cell type- specific compared to the MP expression (Figure 30C). The high overlap of SMs between the different cell types was also reflected in the similarity of identified overrepresented biological functions associated to the cell type and time point- specific secretomes (Figure 31D).

Mφ were characterized over time by a decrease in SM abundance 3 days post-MI compared to the other time points. Molecules secreted by CRMs were predominantly associated to leukocyte chemotaxis and ECM organization, regulating cell behavior in homeostasis (Wynn et al., 2013). Functional analysis associated the MΦ secretome 3 days post-MI with the regulation of cell migration and immune system process, in accordance with the role of Mφ in inflammatory response (Mantovani et al., 2013). The secretome of Mφ 7 days post-MI was associated with ECM organization, angiogenesis, and regulation of cell proliferation, among others. 7 day post-MI Mφ promote ECM remodeling by inhibiting destructive proteases through the production of endogenous tissue inhibitors of metalloproteinases (e.g. *TIMP1-3*) (Newby, 2008).

Furthermore, we found an increased production of collagen (e.g. *COL1A2*, *COL3A1*, *COL4A1*) together with an enrichment in collagen fibril organization, indicating a pro-fibrotic effect of Mφ through collagen deposition 7 days post-MI. However, it is well known that FBs are the primary collagen-producing cells in the heart (Frangogiannis et al., 2002) and Mφ are more likely to regulate fibrosis through TGF-β1- induced activation of resident and recruited myofibroblasts (Wynn and Barron,

2010).

Figure 31: Secretome and receptome profile of distinct cardiac cells. (A) Relative number of genes encoding for secreted molecules and membrane proteins per cell type and time point. (B) Time-point specific Venn diagrams of secreted molecules. (C) Time-point specific Venn diagrams of membrane proteins. (D) Manually selected list of non-redundant enriched biological processes of genes encoding for secreted molecules. Terms with an adjusted p-value < 0.05 were significant. Color corresponds to fold enrichment.
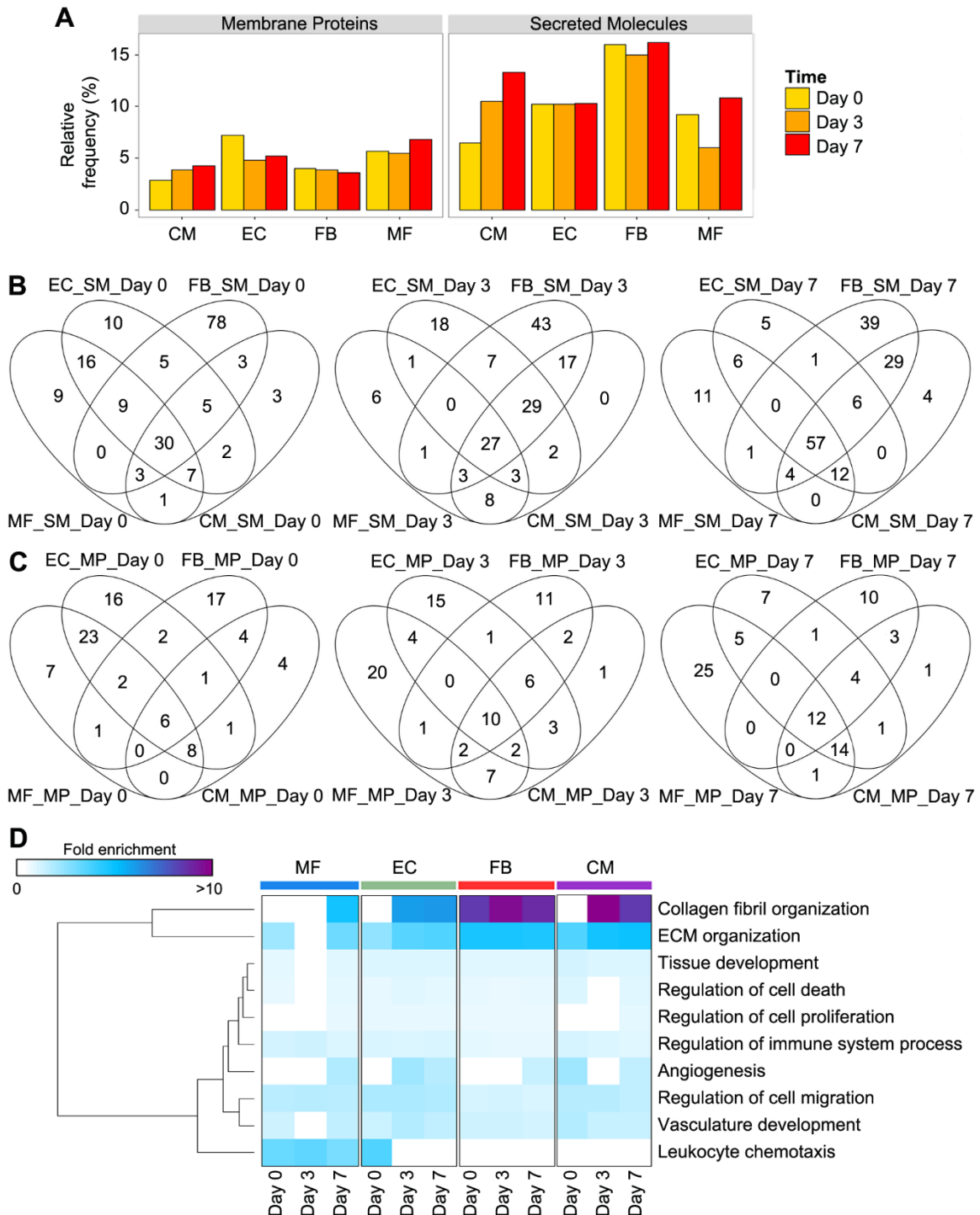
FBs produced the highest levels of SMs at all temporal stages (Figure 31A), which were associated with a variety of processes (Figure 31D). It is interesting to note that FBs shared many SMs with ECs and CMs (Figure 31B) that were mainly linked to ECM organization (e.g. *DCN, LAMC1, LAMB2*). The result indicates that all cell types contribute to changes in ECM composition and organization. In accordance with the described crucial role of FBs during the reparative phase of cardiac repair (Chen and Frangogiannis, 2013), the secretome of post-MI FBs was characterized by increased collagen production (e.g. *COL1A2, COL5A2, COL6A2*). We further found an enrichment of angiogenesis for the secretome of post-MI Mφ, ECs, and FBs. FBs might promote angiogenesis through the recruitment of endothelial progenitor cells (Orimo et al., 2005) which are reportedly increased in peripheral blood after MI (Shintani et al., 2001). Whereas it is well known that Mφ impact angiogenesis on many levels (Rahat et al., 2014) and such MΦ – EC interactions seems to be reciprocal (Baer et al., 2013).

In order to gain a better understanding of possible cell-cell interactions we created a list of all identified SMs and MPs, independent of cell type and temporal pattern of expression, and retrieved experimentally validated interactions between these molecules from Ingenuity. The resulting list of 143 interactions, including 68 SMs and 42 MPs, was imported into cytoscape and the nodes, representing SMs and MPs, arranged according to their cell type (or combination of cell types) expression (Figure 32, legend).

In accordance with the calculated overlap of SMs between cell types (Figure 31B) the SM- MP interaction network showed that only a small set of SMs are uniquely expressed by one cell lineage and that FBs expressed the highest number of cell type specific SMs (Figure 32, outer circle), whereas ECs expressed the highest number of cell type specific MPs (Figure 32, outer circle). SMs (*PGF*, *SEMA3F*) and MPs (*NRP1*, *NRP2, KDR, FLT1*) uniquely expressed by ECs were associated with angiogenesis related processes (Carmeliet et al., 2001), which is in accordance with the known role of ECs as key mediators of angiogenesis (Coultas et al., 2005). FBs were characterized by the secretion of ECM components and fibrotic factors (*TGFB2*, *NOV*, *COL5A3*), in line with the dominant role of FBs in fibrosis (Prabhu and Frangogiannis, 2016).

Interestingly we found that many molecules were co-expressed between specific combinations of two cell lineages: Mφ - EC and FB – CM (Figure 32, second outer circle). The collective expression of different SMs and MPs between Mφ and ECs, together with the high similarity of the expression profiles (Figure 29B) suggests, that ECs and Mφ might share common functionality in the process of cardiac repair. FBs and CMs collectively expressed different SMs, whereas some of these SMs (e.g. *CHID1, FBLN5, COL14A1*) were linked to MPs exclusively expressed by Mφ and ECs (e.g. *ITGA5, APP*), indicating potential crosstalk between the cell type pairs. *MMP9*, which plays a prominent role in ECM remodeling post-MI (Ducharme et al., 2000) was expressed by Mφ and CMs and could potentially be bound by all cell types, supporting the finding that all cell types were involved in ECM organization (Figure 31D). In addition, we found that ADAM9, a molecule that has been shown to be highly expressed during tissue remodeling (Rinchai et al., 2015), was solely expressed by FBs and Mφ and could be bound specifically by FBs through *ITGAV* or by all cell types through *ITGB1*.

SDC2 was the only molecule expressed by all cell types except ECs and was linked to receptors exclusively expressed by Mφ and ECs (*COMT*, *CD40*). The result is in line with the previous finding that *SDC2* plays a fundamental role in angiogenesis by influencing EC adhesion and migration (Noguer et al., 2009). In addition, we found various MPs (e.g. *NRP1*, *CD9*, *CD36*) that were expressed by all cell types but FBs, which are involved in angiogenesis, inflammation, and lipid metabolism (Fantin et al., 2013; Febbraio et al., 2001). SMs co-expressed by all cell types except Mφ could be linked to ECM organization and blood vessel development (Thyboll et al., 2002). In contrast to these findings we couldn't detect a single molecule co-expressed by all cell types except CMs.

All cells expressed various isoforms of the tissue inhibitors of metalloproteinases (*TIMP1-3*), matrixmetalloproteinases (MMP2, MMP14) and thrombospondin (*THBS1*, *THBS2*, *THBS4*) which is in line with the finding that all cell types seem to contribute to ECM organization (Figure 30). Furthermore, all cell types expressed various ECM components (e.g. *DCN*, *BGN*, *B2M*) amongst which *FN1* was linked to the EC- specific MP *STOM* in the created interaction network (Figure 32), suggesting an activation of *STOM* by either a homeotypic or heterotypic paracrine

circuit. The result matches the reported involvement of *STOM* in membrane organization (Salzer et al., 2007).

Collectively, the gathered data indicates a highly connected network of homeotypic and heterotypic paracrine circuits that does not only ensure the maintenance of homeostasis in resting conditions but also governs processes such as immune response, angiogenesis and ECM organization post-MI.
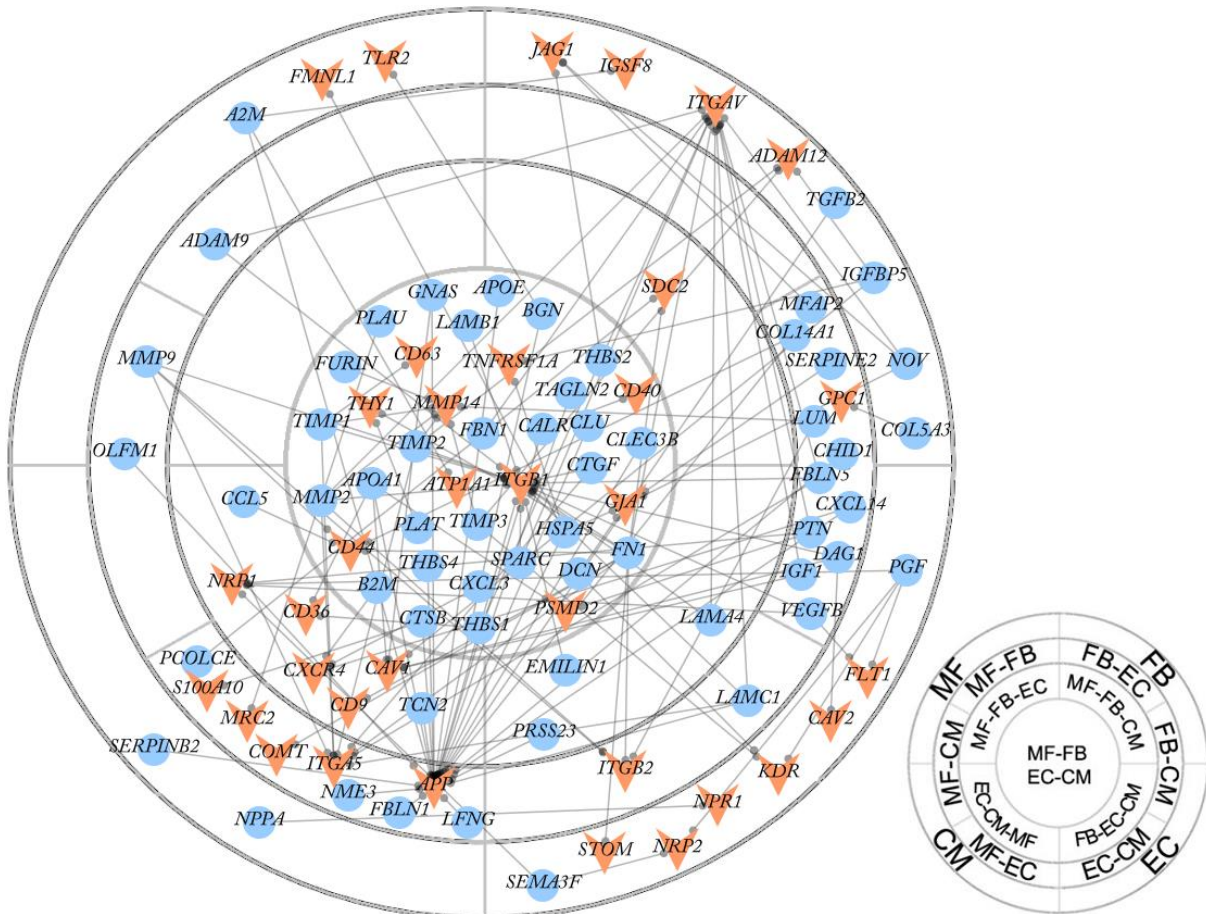
Figure 32: Global SM-MP interaction network. Nodes represent SMs (circles, blue) and MPs (arrow, orange). Nodes are arranged according to the cell type by which they are expressed (legend bottom right).

3.4. Expression profiling identifies cell type specific miRnome and miRNA-mRNA regulatory relationships

miRNAs are able to interfere with a broad variety of BPs and the affected pathways and functions depend on the site accessibility of the miRNA target genes in a specific cell type and given biological context (Sood et al., 2006). It has been shown that miRNAs play a critical role in cardiac repair and circulating miRNAs have been

proposed as diagnostic markers. However, the miRNome of porcine cardiac cells has not been analyzed in depth and knowledge about the miRNA contribution to cell type identity and function is limited. In order to elucidate the cardiac miRNome in pig we analyzed the miRNA expression profile of resting CMs, Mφ, FBs, and ECs and after MI.
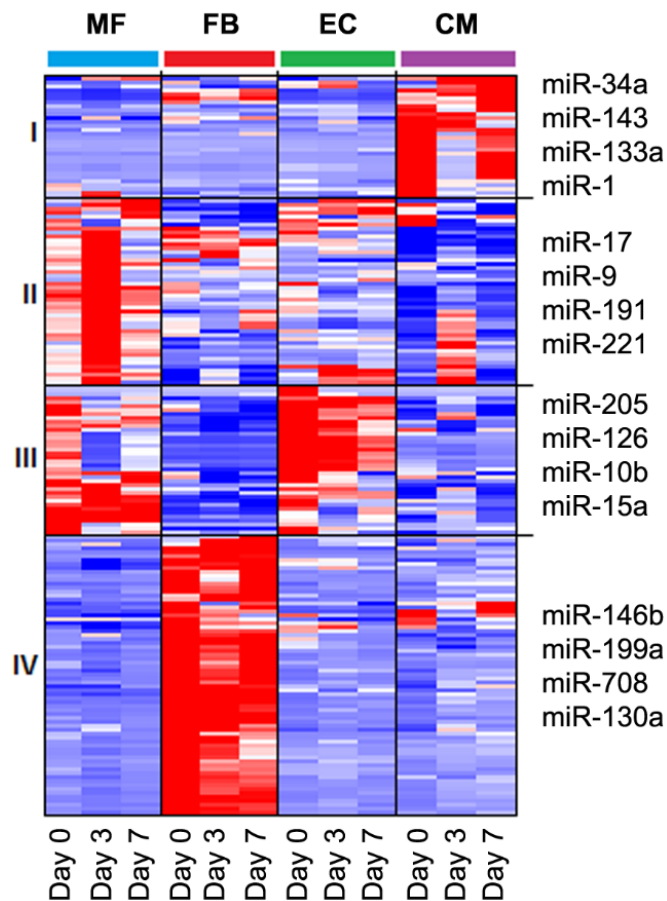
Figure 33: Cell type- specific miRNA expression profile. Highlighted are representative miRNAs based on their implication in relevant biological functions.

The miRNA expression profiles were analyzed with two different objectives in mind: the first analysis aimed at the identification of cell type- specific miRNAs, whereas the second approach tried to improve the understanding of the functional impact of expressed miRNAs through cell type and time point specific miRNA-mRNA interaction networks. The comparison of miRNA expression among cell types led to 187 significantly altered (adj-pval < 0.05) miRNAs that could be grouped into four clusters based on their expression profiles (Figure 33). Three of the four clusters exhibited a cell type- specific expression profile for CM, FB and EC, respectively, whereas the remaining cluster was characterized by elevated expression in MΦ and

EC. Amongst the CM-specific miRNAs (Figure 33, cluster I) we could identify modulators of apoptosis (e.g. miR-34a, miR-193a, miR-1), cytoskeletal dynamics (miR-143, miR-145), cell cycle (e.g. miR-192, miR-215), and cell proliferation (e.g. miR-490, miR-133a). The miRNA profile showed an altered expression in the healthy heart and 7 days post-MI, indicating a relieved miRNA repression 3 days post-MI. Furthermore, the cluster contained the miRNAs miR-1, miR-208b, miR-133a and miR-499 that have been proposed as diagnostic markers in patients with acute myocardial infarction (Widera et al., 2011).

miRNAs with elevated expression in Mφ (Figure 33, cluster II) included four miRNAs of the miR-17/92 cluster, which is highly conserved among vertebrates and implicated in a vast variety of functions such as cell cycle and proliferation (Concepcion et al., 2012; Mogilyansky and Rigoutsos, 2013). Other miRNAs of the cluster were associated to inflammatory response (e.g. miR-9, miR-34c, miR-186), Mφ polarization (e.g. miR-191, miR-363), and cell proliferation (e.g. miR-221, miR-222). Within the cluster we could further identify porcine- specific miRNAs (miR-7139-7142), of which knowledge is limited and further experiments are needed to determine their target genes and functions in Mφ. The third cluster included miRNAs expressed in two cell types, Mφ and EC. Within this cluster three miRNAs (miR-196a, miR-205, miR-429) were specifically expressed in ECs and are implicated in cell proliferation and mesenchymal-to-epithelial transition (Chen et al., 2011b; Gregory et al., 2008; Kim et al., 2009). The cluster further included miR-126 that mediates angiogenesis (Fish et al., 2008) and was reported to be EC-specific in mouse (Wang et al., 2008). Our data from pig indicated a strong expression in ECs and an additional expression in Mφ in the healthy heart. Other miRNAs from the cluster were primarily associated with cell proliferation (e.g. miR-10b, miR-139, miR-182) and apoptosis (e.g. miR-15a, miR-16, miR-30). miRNAs specifically expressed in fibroblasts (Figure 33, cluster IV) included modulators of TGF-β signaling (e.g. miR-146b, members of let-7 miRNA family, miR-487b), cell differentiation (e.g. miR-199a, miR-214, miR-335), apoptosis (e.g. miR-708, miR-149), and angiogenesis (e.g. miR-130a, miR-320, miR-424).

Next, we identified the highest expressed miRNAs at each time point for any given cell type (Figure 34A). Interestingly, 10 miRNAs were amongst the top expressed miRNAs in all cell types but their expression profile differed according to the cell type.

Despite the presence of these miRNAs in all cell types the affected functions might differ, depending on the site accessibility and expression of their target genes in the different cell types. Hence, the top expressed miRNAs were subsequently used to create cell type specific miRNA-mRNA interaction networks (Figure 34B-E, *Material & Methods*). Based on network topology and expression different subnetworks emerged per cell type. In the case of Mφ two subnetworks could be identified (Figure 34B), as already indicated by the expression profile of the top expressed miRNAs (Figure 34A). Accordingly, the first subnetwork included miRNAs with elevated expression in the healthy heart and 7 days post-MI. The network was primarily enriched for response related processes such as immune response and response to stress, indicating a role for miRNAs in the inhibition of aberrant inflammatory reactions. mRNAs regulated by miRNAs with elevated expression in Mφ 3 days post-MI were significantly enriched for developmental and homeostatic processes. The up-regulation of miRNAs that down-regulate homeostatic processes together with the relief of miRNA-mediated repression of immune response genes at day 3 suggest a role for miRNAs in Mφ activation in response to stress.

It was interesting to note that the miRNA-mRNA interactions identified for FBs built a single connected network (Figure 34C). The network could not be divided into further subnetworks on topology alone but the mapped expression values revealed a temporal pattern of activation for different parts of the network. As indicated by the expression profile of the top expressed miRNAs (Figure 34A), the majority of miRNAs were expressed in resting FBs. The target genes of these miRNAs were enriched for developmental processes and the regulation of cell death. Only one miRNA, ssc-let-7g, was up-regulated at day 3 and the target genes include, *ANGPTL2*, *LRP6*, *COL11A1*, and *MMP2*, suggesting an interference with fibrogenic signaling pathways and an inhibitory effect on inflammation (Ren et al., 2013; Santulli, 2014).

The assumption is supported by a recent study in mice heart, which described a similar functional impact of let-7i, a miRNA that shares the seed region with let-7g (Wang et al., 2015). At 7 days post-MI the miRNA –mediated repression of tissue development related genes was relieved, which matches the detected enrichment of heart development in FBs at this temporal stage (Figure 30).
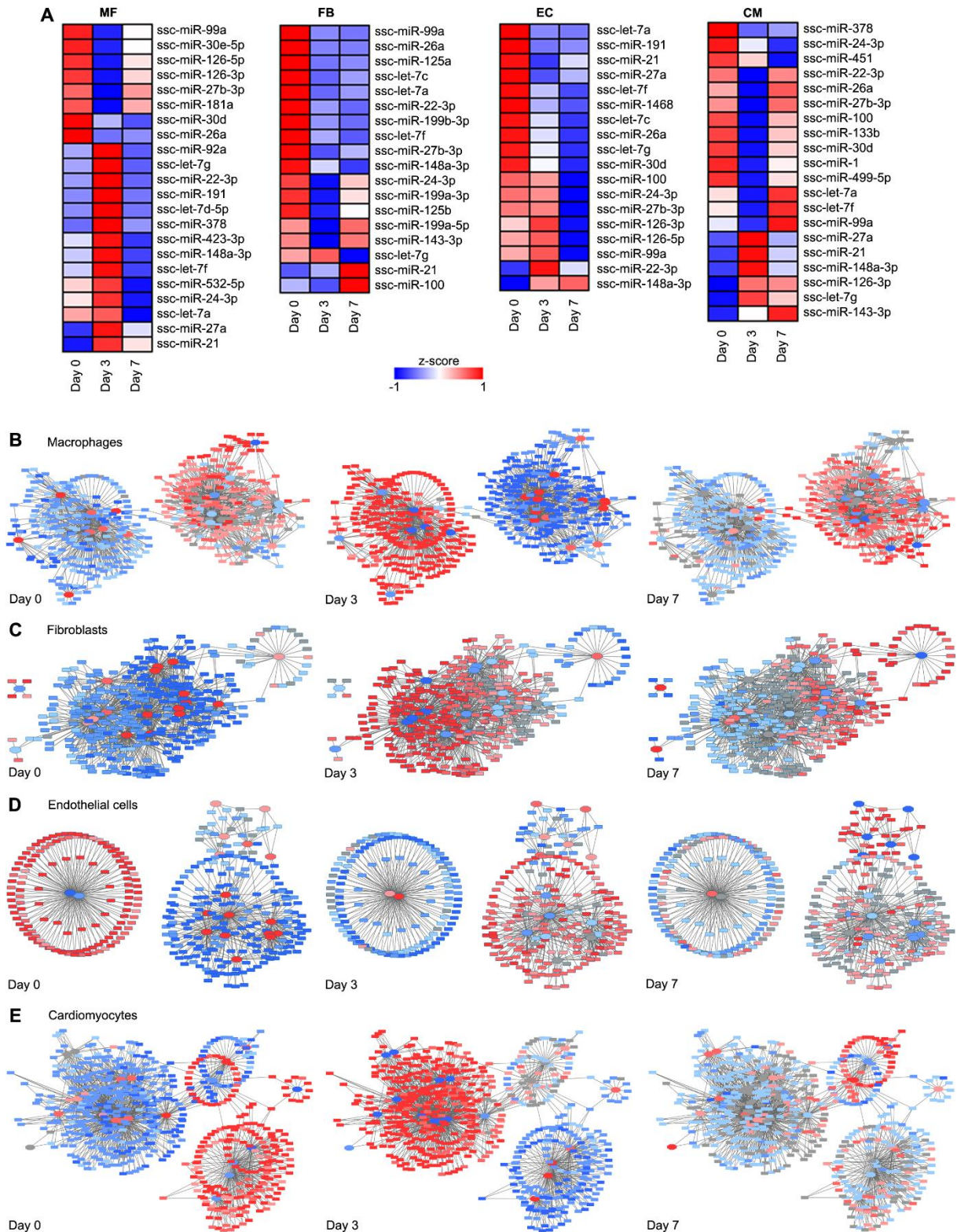
Figure 34: Top expressed miRNAs per cell type. (A) Heatmap of top 5% expressed miRNAs per cell type. (B - E) miRNA – mRNA interaction network of the different cell types. Node fill is mapped to z-score of mRNA and miRNA expression. (B) miRNA – mRNA interaction networks for Mφ. (C) miRNA – mRNA interaction network for FB. Node fill is mapped to z-score of mRNA/miRNA expression. (D) miRNA – mRNA interaction network for EC. Node fill is mapped

to z-score of mRNA/miRNA expression. (E) miRNA – mRNA interaction network for CM. Node fill is mapped to z-score of mRNA/miRNA expression.

Based on network topology and expression the miRNA-mRNA interaction network of ECs could be divided into two subnetworks (Figure 34C). The larger network (218 nodes) was mainly characterized by miRNA activity in resting conditions, which was associated with the repression of cell migration, tissue development and apoptosis related genes. Nevertheless, the expression profile of this subnetwork was rather heterogeneous and 7 days post-MI a small subset of six miRNAs (ssc-miR-126, ssc-miR-99a, ssc-miR-27b, ssc-miR-24, ssc-miR-100, ssc-miR-126) was strongly down-regulated.

Although functional analysis did not result in any enriched processes, the associated genes were linked to ATP-binding (e.g. *DDX3Y, ITM2C, CSNK1E*), mitochondria (e.g. *ODC1, RANBP2*), and included the nuclear receptor *NR4A3* (*NOR1*), which regulates the survival response of ECs to hypoxia (Martorell et al., 2009) and is involved in EC growth (Rius et al., 2006). The smaller network, composed of two miRNAs and 133 mRNAs, was characterized by an elevated miRNA expression 3 and 7 days post-MI and associated with the regulation of the mitogen-activated protein kinase (MAPK) cascade, which might be linked to cell proliferation processes (Zhang and Liu, 2002).

With 622 nodes the miRNA – mRNA interaction network of CMs was the largest network amongst the investigated cell types. Based on topology and expression the network could be roughly divided into two subnetworks, with some straying nodes. Functional analysis of the genes potentially down-regulated by miRNA activity at day 0 did not reveal much but the miRNAs involved in this subnetwork included, amongst others, the cardiac/skeletal muscle specific miRNAs miR-1 and miR-133b, which are known to regulate CM proliferation (Tang et al., 2009; Townley-Tilson et al., 2010). Both miRNAs are dysregulated after MI in humans (Boštjančič et al., 2009), which is supported by our data that shows a down-regulation of these miRNAs post-MI. The CM-enriched miRNA miR-378 was also up-regulated in the healthy heart and has been associated with postnatal remodeling and cell survival (Knezevic et al., 2012). miRNAs up-regulated 3 days post-MI (e.g. miR-148a, miR-21, let-7g) potentially regulated genes associated with myofibril assembly and heart and blood vessel development.

This finding is in line with the described cardiac protective function of miR-21 and miR-148a (Bao and Lin, 2014; Cheng et al., 2010). Furthermore, we found an up-regulation of miR-27a that regulates myosin heavy chain gene expression in neonatal rat (Nishi et al., 2011) and might affect myofibril assembly. It was interesting to note that the expression levels of involved miRNAs and mRNAs were remarkably lower 7 days post-MI compared to the other temporal stages. The expression profile further indicated a restoration of miRNA activity to resting conditions with functional impact on CM proliferation related processes.

Taken together the data showed that the different cell types, except from ECs, expressed distinct sets of miRNAs, and cell type specific miRNA – mRNA interaction networks associated miRNA activity to a broad spectrum of BP that differed in a cell type and time point dependent manner. The data further supported the general notion that the different cell types contribute distinctively to complex processes such as homeostasis and cardiac repair.

DISCUSSION

DISCUSSION

The biological world is driven by data and due to the continuous improvement in technology the rate of generation of genomics, transcriptomics, proteomics, and metabolomics data is exploding. The challenge now is no longer obtaining the data but putting the data to effective use and to infer knowledge from large volumes of collected "omics"- data. Analyzing these massive amounts of data is a computationally intensive task and also requires different statistical techniques compared to smaller sets of data, adding additional layers of complexity. Although the need for new methods to deal with big data is far from being fulfilled, effective solutions have been created that reduce the impact of systematic non-biological differences and permit the identification of biologically meaningful expression patterns.

Due to the high-dimensional nature of "omics"- data, exploratory data analysis techniques are used to get a first glance at the most characteristic features of the generated data and to guide downstream analysis. Statistical analyses are then applied to identify subsets of elements, which have the potential to provide valuable insight into underlying structures of the investigated BPs or disease. In order to establish functional connections between the identified elements enrichment analysis can be applied to determine potentially activated pathways and BPs. Depending on the annotation of the investigated organism, the resulting list of enriched processes can be rather long, which makes it more difficult to uncover underlying pattern of functional activity. The visualization of this data is an integral and challenging part of the data analysis process, because making data more accessible has the potential to change the quality of the information itself.

Although many visualization methods, tools and packages exist that focus on the visualization of enrichment data (Supek et al., 2011; Yin et al., 2012; Zhang et al., 2013a), none of them enables the user to combine expression data with the results of functional analysis in a way that preserves the information value of both analyses. We addressed this need by developing the R package GOplot (Walter et al., 2015) that provides the user with easy to use plotting functions that create original and informative charts to explore the obtained enrichment data. The importance and need for such a visualization tool is supported by the approximately 17 000 downloads within 20 months of its release. The package allows the user to create publication-quality

graphics with only a few lines of code and the high quality and originality of the created plots is demonstrated by their appearance in prestigious scientific journals such as *Nature Cell Biology*, *Circulation Research* and *BMC Genomics* (D'Amato et al., 2016; Gifford and Srivastava, 2016; MacGrogan et al., 2016; Paolinelli-Alfonso et al., 2016; Strikoudis et al., 2016). The package is implemented within the R environment, a powerful and flexible language that is widely used to analyze "omics" data, making it easy accessible for many data analysts. Although other packages have been developed for similar purposes (Kolde and Vilo, 2015; Waardenberg et al., 2015; Yin et al., 2012; Young et al., 2005; Zhang et al., 2013a), GOplot is set apart by its capability to generate plots at different levels of detail: from a general overview to identify the most enriched categories to a more detailed view displaying different types of information for molecules in a given set of categories. Hence, the plots cover all phases of the data analysis processes and are very powerful in the practice of data-driven decision making.

The need to combine and integrate data from multiple sources goes far beyond functional analysis and has led to the emergence of systems biology for a more precise modeling and improved understanding of complex processes and diseases. It is now widely recognized and accepted that multiple levels of regulation have to be considered simultaneously to gain a comprehensive understanding of intricate BPs (Ghasemi et al., 2014; Sperling, 2011). We used a systems biology approach to elucidate the transcriptional landscape in murine Mφ in the health heart and after MI and to decipher the regulatory network of distinct cardiac cells post-MI in pig.

We found that the different cardiac cell types in pig could be distinguished based on their gene expression profiles and that the transcriptional programs were stable enough to ensure cell type identity even in the case of disturbed homeostasis. The result suggested that the different cell types carry out distinct functions during homeostasis and the process of cardiac repair post-MI, which was supported by the result of the performed functional analysis. We found that Mφ were associated with processes such as endocytosis, immune response, and antigen presentation, consistent with their phagocytic nature and known function in innate immune response (Gordon, 2007). Our analysis further confirmed the key role of ECs in angiogenesis

DISCUSSION

(Coultas et al., 2005; Plate et al., 1992) and suggested VEGF-independent regulation of angiogenesis during the reparative phase of cardiac repair potentially mediated by all of the investigated cell types. Although ECs are the predominant mediators of angiogenesis our finding implies a regulatory interaction network of multiple cell types, which is supported by the failure of EC-based proangiogenic therapies that indicate that a single cell type does not sufficiently support angiogenesis to promote cardiac repair (Cochain et al., 2013). In agreement with the described role of FBs in reparative fibrosis (Weber and Brilla, 1992) we found an enrichment in ECM organization and collagen fibril organization for genes highly abundant in cardiac FBs. FBs also contribute to the maintenance of ECM homeostasis and play a critical role in myocardial architecture in the healthy heart (Camelliti et al., 2005; Goldsmith et al., 2014). CMs form interlacing bundles that are the building blocks of cardiac muscle (Bursac et al., 2002) and in line with their contractile function (Zimmermann et al., 2002) resting CMs were characterized by ATP metabolic process, muscle contraction, and oxidative phosphorylation. The processes decreased after MI, consistent with the described necrotic death of CMs after ischemic heart injury (Uemura et al., 2006).

The results imply that the distinct cardiac cell types possess divers regulatory elements that influence functional activity through specific modulations in gene expression. Moreover, the activated transcriptional programs are stable enough to ensure cell type identity post-MI, suggesting a stronger impact of cell type specific imprinting compared to changes in the microenvironment. Nevertheless, when we compared different murine tissue Mφ we found that the tissue of origin and the ontogeny of the Mφ population were additional driving factors that shaped the transcriptional landscape, resulting in tissue heterogeneity of Mφ populations, as previously described (Davies et al., 2013; Ginhoux and Guilliams, 2016; Gordon et al., 2014). Although it has been shown that these transcriptional programs are less stable and can be reprogrammed if Mφ are transplanted from one tissue into another (Lavine et al., 2014).

Recent studies explored the heterogeneity of murine Mφ populations on a transcriptional and epigentic level and identified tissue-dependent programs (Gosselin et al., 2014; Lavine et al., 2014). Our inter-experimental comparison of different murine

DISCUSSION

tissue resident Mφ extended these findings with the identification of a yet unknown cardiac specific gene signature. Among these genes we found three novel surface markers (*Lifr, Egfr, Osmr*) that were tested by qPCR and had not been identified in CRMs before. The membrane expression of LIFR ensures biological activity of leukemia inhibitory factor (LIF) signaling (Ware et al., 1995) and the engagement of LIFR with its ligand is implicated in the onset of inflammation (Sugiura et al., 2000), indicating a potential role for LIFR as immune surveillance receptor. Moreover, it has been shown that the expression of EGFR on Mφ mediates Mφ proliferation (Lamb et al., 2004), suggesting a potential role for EGFR in cell survival of CRMs. Genetic inactivation of OSMR has been reported to be organ-specific (Poling et al., 2014), supporting its appeal as a candidate for tissue-specific therapeutic interventions. The identified surface marker might be used for CRM ablation strategies to further determine the functions of cardiac macrophages in in the healthy heart or for targeted cell-type and tissue-specific treatments.

Previously a set of 35 heart-specific genes had been identified comparing the transcriptional profile of CRMs to spleen and brain (Pinto et al., 2012). Our integrated analysis of murine tissue resident Mφ showed that several genes of this signature were indeed specifically expressed in the heart, but around 20% were expressed in heart and intestine. Indeed, we found a high similarity between the transcriptional profile of murine CRMs and Mφ from the intestine. Both Mφ populations have been described to possess anti-inflammatory properties resembling an M2-like phenotype (Bain and Mowat, 2014; Pinto et al., 2012). Intestinal Mφ reside in a microbiota-exposed environment and are characterized by antigen-presenting processes (Bain and Mowat, 2014; Lavine et al., 2014), whereas CRMs are less exposed to microorganisms and our analysis showed that specific CRM genes were enriched in myofibril assembly and heart development. Thus, environmental cues and resulting functions differ in a tissue-dependent manner and are unlikely the underlying cause for the high similarity between Mφ from heart and gut. However, circulating monocytes contribute to both resident pools of Mφ (Ginhoux and Guilliams, 2016), but whereas the intestinal Mφ pool requires continual renewal from circulating blood monocytes (Bain and Mowat, 2014), CRMs have been found to self-maintain locally with age dependent increase in monocyte contribution (Hashimoto et al., 2013; Molawi et al., 2014). The high similarity

between intestine and heart might suggest a high percentage of mature but monocyte-derived CRMs in the healthy heart.

Mφ do not only exhibit high tissue heterogeneity, but are also very plastic cells that continuously shift their functional phenotype to adapt to changes in their surroundings. Mφ activation has been mostly studied *in vitro*, leading to an oversimplified bipolar M1/M2 classification system (Martinez and Gordon, 2014) which only possess limited capacity to explain the plethora of observed *in vivo* phenotypes (Novak et al., 2014; Varga et al., 2016). We found that although murine post-MI Mφ could be matched on the described M1/M2 polarization system, a more detailed analysis revealed that Mφ populations involved in cardiac repair are mixtures of described *in vitro* phenotypes that are characterized by the expression of M1/M2 markers, consistent with observed *in vivo* phenotypes in the context of skeletal muscle injury (Novak et al., 2014; Varga et al., 2016).

Although the plasticity of Mφ has been widely studied, detailed knowledge about the transcriptional regulation of Mφ in the context of complex disease environments is limited. We identified a global network of 40 TFs that were associated with the temporal regulation of gene expression in murine cardiac Mφ. Among these regulators we identified several TFs that potentially coordinate the transcriptional profile of CRMs, including angiogenesis-related genes, which support the proposed pro-angiogenic function of CRMs (Pinto et al., 2012) and regulators of developmental processes, which might further imply CM – Mφ interactions to maintain cardiac homeostasis (Fujiu et al., 2014). In addition, our analysis revealed IFNγ signaling via *Stat1* as one of the main drivers that cause the observed changes in gene expression 3 days post-MI. These Mφ were characterized by a pro-inflammatory phenotype and the inflammation-induced gene transcription was regulated by multiple TFs, including also regulators of metabolic processes, negative regulators of cell proliferation and regulators of programmed cell death. With the onset of the reparative phase the identified TFs were associated with cell cycle and cell proliferation related processes, supporting recent studies that proposed an increase in proliferative capacity of Mφ at later temporal stages post-injury (Heidt et al., 2014; Lavine et al., 2014; Varga et al., 2016). The multitude of activated TFs and the spectrum of associated processes implied that Mφ

present at the site of inflammation encounter a myriad of signals and that many different factors and interactions shape the transcriptional response. Thus, it seems likely that the classical view, which derived from *in vitro* experiments, of one signal being linked to only one or a few TFs is overly simplistic and does not hold *in vivo* (Schultze, 2015).

In silico deconvolution of the transcriptional profiles of murine post-MI Mφ did not only reveal a mixed phenotype but also implied a dynamically shift in the functional phenotype to orchestrate cardiac repair, as previously proposed (Novak and Koh, 2013). The transition from one phenotype to another is key to restrict the inflammatory phase which directly impacts the infarct size and ventricle remodeling (Nahrendorf et al., 2007). The partial deconvolution approach revealed the activation of anti-inflammatory programs 3 days post-MI and we detected elevated *Il10* expression at the same temporal stage, as it has been described previously in the context of skeletal muscle injury (Novak et al., 2014). *Il10* is the dominant mediator of the anti-inflammatory program in Mφ and network analysis of the regulatory core of post-MI Mφ in mouse disclosed a negative feedback-loop that limits initial inflammation by hypoxia-mediated up-regulation of *Il10*. The result was confirmed by the up-regulation of *Il10* in murine peritoneal Mφ cultured under hypoxic conditions, indicating hypoxia-mediated induction of *Il10* (Cai et al., 2013; Dace et al., 2008; Murata et al., 2002) or stabilization of *Il10* mRNA (Németh et al., 2005; Powell et al., 2000) which is most likely followed by IL10-mediated auto-regulation (Sarkar et al., 2008). However, we cannot exclude the possibility that released molecules of other cells trigger macrophage *Il10* transcription (Saraiva and O'Garra, 2010).

In vitro experiments have shown that the anti-inflammatory effect of IL10 also includes the onset of apoptotic programs in M1-like Mφ (Wan et al., 2014). 3 day post-MI Mφ in mouse, which exhibited a M1-like phenotype, were enriched for apoptotic and cell death related processes and 7 days post-MI Mφ were most similar to *in vitro* Mφ treated with dexamethasone, a synthetic glucocorticoid that induces apoptosis (Haim et al., 2014). The result suggests that apoptotic Mφ might contribute to the phenotype shift, which is supported by the finding that timed treatment of infarcted mice with apoptotic-mimicking particles promotes resolution of inflammation (Harel-Adar et al.,

DISCUSSION

2011).

The phenotype transition of Mφ is a key event in cardiac repair, which makes it an attractive target for therapeutic intervention. A detailed understanding of the phenotype transition is fundamental to develop timed strategies that shift the M1/M2 balance to improve cardiac healing. We found that in addition to microenvironmental factors and an intricate network of activated TFs the deactivation of Mφ is also regulated on a post-transcriptional level. It has been recently shown that RNA-binding proteins such as TTP influence Mφ polarization through the degradation of inflammation-induced mRNAs (Kratochvill et al., 2011; Sedlyarov et al., 2016). Our mRNA stability analysis supports these findings and indicates that pro-inflammatory mRNAs are more prone for degradation due to longer 3'UTRs and an enrichment for AREs, the binding element of TTP. Whereas during the reparative phase mRNAs that were mainly associated with structural proteins were more stable, as previously reported (Sharova et al., 2009). 3'UTRs do not only contain binding sites for RNA-binding proteins but can also contain sequences that allow miRNA targeting (Preusse et al., 2016). We found that miRNAs potentially controlled immune response related genes, but whereas TTP-driven mRNA decay occurs in response to induced inflammation, the data indicates that miRNA activity might also contribute to the suppression of inflammation in the healthy heart. We further found that during the inflammatory phase miRNAs potentially down-regulated cell proliferation, whereas with the resolution of inflammation Mφ regained proliferative capacity, as previously described (Heidt et al., 2014; Varga et al., 2016).

Identified lincRNAs and their association with the closest protein coding genes upstream and downstream of each lincRNA revealed potential functions for lincRNAs in cardiac Mφ in innate immunity. LincRNAs are believed to play significant roles in GRNs (Ounzain 2015) and the identification of altered lincRNA expression in diseases (Cheetham et al., 2013; Garzon et al., 2014; Liu et al., 2014) and their association with important BPs such as cell cycle (Hung et al., 2011), adaptive and innate immunity (Fitzgerald and Caffrey, 2014) and metabolism (Kornfeld and Brüning, 2015) support this assumption. The ceRNA hypothesis, which assumes that the various RNA types are linked via MRE, provides another promising approach for the functional

DISCUSSION

characterization of lincRNAs (Salmena et al., 2011). Based on this hypothesis we identified potential mRNA-lincRNA-miRNA motifs, of which the most abundant type of mRNA - lincRNA - miRNA interactions was characterized by positively correlated expression of all RNAs. Among these interactions we found *Neat1*, which was positively correlated with miR-30b and various mRNAs associated with immune response related processes. The ceRNA hypothesis proposes that lincRNAs function, among others, as miRNA sponges, titrating miRNAs away from their mRNA targets and hence, interfering with miRNA mediated mRNA repression. Our data suggests that the described pro-inflammatory effect of *Neat1* (Imamura et al., 2014) might be an example of such an indirect regulation, where *Neat1* competes with pro-inflammatory protein coding genes for the binding of immune suppressive regulators like miR-30b. The competition between the different RNAs would lead to a depletion of the shared miRNA pool and an attenuation of the repressive effect of miR-30b. However, recent *in silico* modeling of RNA crosstalk (Noorbakhsh et al., 2013) and quantitative measurements of miRNA and target abundance (Denzler et al., 2014) indicate that miRNA activity is only minimally influenced by ceRNAs (Broderick and Zamore, 2014). Despite the mentioned limitations, the identified lincRNAs in cardiac Mφ open up new avenues for therapeutic intervention to positively influence the outcome of cardiac repair.

The analysis of the porcine miRNome revealed that the miRNA expression profiles captured cell type- specific effects, reflecting the fact that miRNA target and pathway genes are not uniformly expressed across all cell lineages (Xie et al., 2014). The cell type- specific miRNA expression profiles might also be influenced by possible ceRNA effects (Xie et al., 2014). In accordance with the literature we found CM-specific miRNAs that have been proposed as diagnostic markers in patients with acute MI (Widera et al., 2011). Furthermore, we identified CM-specific miRNAs that were associated with modulators of apoptosis, cytoskeletal dynamics, cell cycle and cell proliferation. The approach included the global miRNA expression profiles, capturing temporal changes in CM function and activity. miRNAs of the miR-17/92 cluster were highly expressed in porcine Mφ, indicating increased post-transcriptional regulation of cell cycle and cell proliferation related processes. Moreover, we found Mφ – specific miRNAs with known functions in inflammatory response and Mφ polarization (Zhang

et al., 2013c), supporting the key role of miRNAs in Mφ phenotype transition that we had detected in murine Mφ. According to the reparative function of FBs (Porter and Turner, 2009) and their known differentiation into myofibroblasts (Hinz, 2007), miRNAs specifically expressed in FBs were primarily associated with TGF-β signaling and cell differentiation. In contrast to the findings for the other cell types, we did not find a EC - specific miRNA cluster but identified miRNAs involved in mesenchymal-to-epithelial transition (Chen et al., 2011b; Gregory et al., 2008; Kim et al., 2009) that were comparably higher expressed in EC than in any other of the investigated cell types. miRNAs associated with cell proliferation and apoptosis exhibited similar expression profiles in EC and Mφ, suggesting common post-transcriptional regulation of these processes in both cell types. Already on the mRNA level EC and Mφ were very similar and the common miRNA cluster supported this result. The reconstructed cell type and time point specific miRNA – mRNA interaction networks and their associate functional impact mirrored the results of the enrichment analysis of the most abundant mRNAs, influenced by the availability and expression of the target mRNAs (Preusse et al., 2016).

Due to the high plasticity of macrophages it remains challenging to identify population specific surface markers. However, the identification of specific surface markers is an essential requirement for the development of efficient target treatments. We found that a subpopulation of murine CRMs highly expressed the pro-angiogenic factor *LYVE1* (Cho et al., 2007), which indicates the presence of a subpopulation of specialized Mφ that might support cardiac angiogenesis in the healthy heart. 3 days post-MI Mφ in mouse were characterized by *CD40* expression, indicating receptivity of these cells for contact-dependent T-cell activation via CD40:CD154 interactions (Suttles and Stout, 2009) to further amplify the inflammatory response. 7 days post-MI we detected an elevated expression of *Trem2*, which might also contribute to the resolution of inflammation by suppressing the production of pro-inflammatory cytokines (Neumann and Takahashi, 2007) and might especially be used to distinguish between CRMs and anti-inflammatory Mφ in tissue repair. *MRC1*, a widely adopted marker for M2-like macrophages (Stein et al., 1992), was highly expressed in the healthy heart and 30 days post-MI and might also be used as a marker to detect the restoration level of post-MI Mφ.

DISCUSSION

Cell-to-cell communication is essential to orchestrate complex processes such as cardiac repair that involve distinct functional contributions of different cell lineages. We found that the dynamical shift of the functional phenotype of murine cardiac Mφ was coupled with differences in SM and receptor expression, that led to a strong extracellular signaling potential of Mφ at 3 and 7 days post-MI as opposed to a more receptive role of Mφ in the healthy heart and 30 days post-MI. These Mφ expressed high numbers of genes encoding for receptor proteins but comparably low numbers of SMs. By connecting the identified macrocrine and receptome we found a low number of potential homeotypic paracrine signaling pairs, which suggests that the receptome of both populations primarily serves for immune surveillance, a widely proposed function of tissue resident Mφ (Davies et al., 2013). In contrast to this receptive state we found that 3 days post-MI Mφ in mouse expressed equal numbers of SM and MPs that had a high homeotypic paracrine signaling potential. The existence of such positive feedback loop might indicate an important control mechanism in Mφ activation to adequately respond to changes in the microenvironment (Junger, 2011). 7 days post-MI Mφ on the other hand were characterized by an extensive macrocrine that seemed to signal in a heterotypic paracrine fashion. The macrocrine 7 days post-MI was mainly composed of ECM components such as diverse types of collagen and *Lox*, an important enzyme that cross-links collagen fibers and gives collagen its strength and stability (Hornstra et al., 2003). Although we found an increase in collagen production on 7 days post-MI Mφ, it is well known that FBs are the dominant source of collagen production (Chen and Frangogiannis, 2013) and it is more likely that Mφ support the reparative function of FBs (Porter and Turner, 2009) through the secretion of ECM components that contribute to ECM reconstruction and tissue remodeling. The increased cell-to-cell communication potential of 7 days post-MI Mφ might further imply an intensive crosstalk with different cardiac cells in addition to FBs.

The analysis of the secretome and receptome of the distinct cardiac cells in pig showed that SMs were more abundant than MPs among the genes with the highest intensity. Moreover, the different cell lineages expressed similar SMs but differed in their MP expression. The results might imply, that all cell types contribute to change the molecular composition of the microenvironment but only specific cell types are able to detect these changes and respond accordingly. The selective receptor expression

DISCUSSION

emanates from cell type specific transcriptional programs and might also regulate the gene expression through signal input dependent activation of transcriptional regulators, finally resulting in cell type specific functional activity. Our analysis suggests further that FBs produced the highest number of cell type specific SMs which were predominantly associated with processes related to the turnover of the ECM (Díaz-Araya et al., 2015), in accordance with the described crucial role of FBs during the reparative phase of cardiac repair (Chen and Frangogiannis, 2013). A different pattern emerged when calculating the MP overlap between the cell lineages. Whereas ECs and FBs expressed the highest number of cell type specific MPs in the healthy heart, indicating an alert and receptive state of these cell types, Mφ continuously increased the cell type specific expression of MPs over time. Taken together with the comparably low number of cell type specific molecules secreted by Mφ, the result indicated that post-MI Mφ possessed enhanced receptivity for the over-all produced SMs.

The *in silico* constructed global SM - MP interaction network revealed an intricate interplay between homeotypic and heterotypic paracrine circuits that together orchestrate all phases of cardiac repair. Here it was interesting to note that many molecules were commonly expressed in Mφ and ECs or in CMs and FBs, indicating special communication among these cell types and potentially common functions post-MI. The importance of Mφ – EC interactions has been shown for vascular network formation in developing organs (Sunderkötter et al., 1994) and in disease (Ahmad et al., 2002), implying Mφ – EC interactions in angiogenesis related processes during cardiac repair. Interactions between FBs and CMs occur not only during CM hypertrophy and FB proliferation (Fredj et al., 2005) but also during development (Ieda et al., 2009). The actual outcome of FB - CM interactions is age-dependent and while paracrine factors derived by embryonic cardiac FBs increase CM proliferation, molecules secreted by adult cardiac FBs induce CM hypertrophy (Kakkar and Lee, 2010). Moreover, it has been proposed that FBs impair CM regeneration following tissue injury through repression of CM proliferation (Palatinus et al., 2010). Hence, the computationally identified FB – CM interactions might be involved in fibrotic processes, which potentially result in CM hypertrophy.

Taken together, the unique data gathered in this study provide a fundamental

DISCUSSION

resource for the investigation of the functional contribution of distinct cardiac cells to the process of cardiac repair, their cell type-specific transcriptional programs and regulatory mechanisms and the complex network of intercellular communication. Furthermore, the systems biology approach that was taken to analyze and integrate the different molecular and regulatory layers of the presented data provides a comprehensive understanding of the intrinsic and multifaceted regulatory network that governs cardiac repair. Following appropriate quantification of the reads into gene expression levels for mRNA, miRNA, and lncRNA, and subsequent data normalization, artificial intelligence techniques such as PCA and k-means clustering did not only allow a thorough examination of the ad-hoc generated transcriptomic data but also enabled the comparison with publicly available datasets. The development of new visualizations (GOplot) provided a valuable tool that combines functional annotation data with gene expression data and guided the exploratory data analysis towards data-driven decision making. Mathematical modeling of the regulatory core of cardiac Mφ provided valuable insight into Mφ phenotype transition during the process of cardiac repair and partial deconvolution allowed the estimation of the phenotype contribution of M1/M2 to *in vivo* Mφ. Moreover, thanks to these tools, we could extract detailed knowledge about the transcriptional and post-transcriptional regulation of CRMs and Mφ activation in the context of MI at different regulatory levels. Despite their importance only few studies of cardiac Mφ exist, which makes our data a valuable resource to further investigate the role of cardiac Mφ. Our identification of specific surface markers might facilitate future studies that aim to develop efficient target treatment. The markers might also be used to investigate further the behavior of cardiac Mφ *in vivo* through live- cell imaging techniques and cell ablation strategies. These strategies would provide valuable functional information that might support and validate our findings. As it has been shown previously that shifting the M1/M2 balance of the Mφ population at the site of inflammation greatly benefits tissue repair (Harel-Adar et al., 2011). Our data might additionally serve as an important resource to identify additional targets to positively influence the pro-inflammatory to anti-inflammatory phenotype transition to promote cardiac repair. Taking into consideration not only transcriptional regulators but also post-transcriptional mechanisms. miRNAs possess tremendous therapeutic potential in heart disease (Caroli et al., 2013) and our gathered data might be used to select novel candidates for miRNA-based therapies; not only for Mφ

polarization but also to influence EC-mediated angiogenesis, the pro-fibrotic effect of FBs, and, possibly, CM proliferation.

CONCLUSIONS

CONCLUSIONS

1. The R package GOplot enables the user to combine expression data with the results of functional analysis in a unique way that guarantees the preservation of the power of both analyses. In particular, the package helped to improve the understanding of immunological high-throughput data and guides exploratory data analysis towards data-driven decision making.

2. Murine CRMs can be distinguished from other tissue resident Mφ based on their gene expression profile and the expression of specific surface markers.

3. During the process of cardiac repair, Mφ sequentially shift their functional phenotype to contribute to both the inflammatory phase and the proliferative and regenerative phase. The functional complexity is the result of a continuous adaptation to molecular changes in the microenvironment, which is mirrored in the mixed expression of M1/M2 associated programs in post-MI Mφ. Partial deconvolution allowed us to quantify the contribution of pro-inflammatory and anti-inflammatory programs in Mφ.

4. A Boolean network model allowed the identification of an experimentally verifiable negative feedback mechanism, that could be validated *in vitro*. This feedback loop has the potential to limit the initial inflammatory response of murine Mφ through hypoxia-mediated up-regulation of Il10.

5. Post-transcriptional regulators contribute to the phenotype transition of Mφ during cardiac repair. Inflammation-induced mRNAs are more prone for rapid degradation due to longer 3'UTRs and an enrichment for ARE in their 3'UTRs. Hence, identified miRNAs and lincRNAs provide potential targets for the development of efficient targeted treatment.

6. Murine cardiac Mφ change their cell signaling behavior during the process of cardiac repair. Mφ at 3 and 7 days post-MI possess strong extracellular

signaling potential as opposed to a more receptive role of Mφ in the healthy heart and 30 days post-MI to fulfill time point specific functions.

7. The distinct cardiac cells in the porcine heart exhibit cell type- specific gene signatures which result in divergent sets of functions. The transcriptional programs are stable enough to ensure cell type identity even in the case of disturbed homeostasis.

8. The cardiac cells in the porcine heart can be distinguished based on their miRNA expression profiles. Biological processes altered by miRNA activity differ in a cell type and time point dependent manner, capturing cell type specific effects detected on the mRNA level.

9. The different porcine cardiac cells communicate through a highly connected network of autocrine and paracrine circuits that govern processes such as immune response, angiogenesis and ECM organization.

10. Exhaustive bioinformatics analysis and the application of particular mathematical methods to transcriptomics data is necessary to access the overall information content of high-dimensional data provided by omics technology.

Conclusiones

1. El paquete de R GOplot implementado en esta tesis permite al usuario combinar datos de expresión con los resultados de un análisis funcional de una forma novedosa, garantizando que la información de ambas fuentes no se pierda y aumentando su potencial de manera sinérgica. En particular, el paquete ha demostrado ser útil para la mejora del entendimiento de datos de alta dimensionalidad en el contexto de la respuesta inmune y ha guiado el proceso de análisis exploratorio.

2. Los macrófagos cardíacos de ratón son distinguibles a nivel transcripcional de los macrófagos residentes en otros tejidos y expresan marcadores celulares de manera específica.

3. Durante el proceso de reparación del daño cardiaco, los Mφ cambian su fenotipo funcional secuencialmente para contribuir tanto a la fase inflamatoria como a las etapas proliferativa y regenerativa. La complejidad funcional observada es el resultado de una adaptación continua a los cambios moleculares que suceden en el micro-ambiente. Esto se ve reflejado en la expresión mixta, después del infarto, de los marcadores específicos de los programas M1/M2. El uso de deconvolución parcial *in silico* permitió cuantificar la contribución de los programas pro y anti-inflamatorios en Mφ cardiacos tras el infarto.

4. El modelado de la red génica fundamental durante el proceso de reparación cardiaca, utilizando un modelo booleano, permitió identificar que la respuesta inicial a la inflamación en este contexto viene limitada por una sobreexpresión de Il10 en respuesta a las señales de hipoxia, resultado que fue validado experimentalmente.

5. La regulación post-transcripcional juega también un papel esencial en la transición entre estados funcionales de Mφ durante la reparación cardiaca. Los mRNAs inducidos por la inflamación son más propensos a sufrir una degradación rápida debido a que tienen 3'UTRs más largos y a un enriquecimiento en motivos ARE en dichas regiones. Es por ello que los miRNAs y lncRNAs identificados podrían ser utilizados como dianas en terapias personalizados.

6. Los Mφ cardiacos del corazón señalizan de diferentes maneras en las distintas fases del proceso reparativo. Mientras que a 3 y 7 días después del infarto poseen un gran potencial de señalización extracelular, en el corazón sano y 30 días después del infarto tienen un papel mucho más pasivo/receptivo.

7. En cerdo, los diferentes tipos celulares presentan perfiles transcriptómicos específicos y con distintas funciones. Sin embargo, los programas transcripcionales son suficientemente estables para garantizar la identidad celular incluso en situaciones de perturbación de la homeostasis.

8. Las células cardiacas en el corazón porcino también pueden ser distinguidas en base a la expresión de sus miRNAs. Los procesos biológicos alterados por la actividad de los miRNAs son distintos entre los diferentes tiempos y tipos celulares, en paralelo a los cambios acontecidos a nivel de expresión de mRNA.

9. Las células porcinas se comunican a través de una red altamente conectada de circuitos de señales autocrinas y paracrinas que controlan procesos como respuesta inmune, angiogenesis y organización de la matriz extracelular. Además, es interesante remarcar que la comunicación sucede mayoritariamente entre macrófagos y células endoteliales por una parte, y por otra entre cardiomiocitos y fibroblastos.

10. El análisis bioinformático exhaustivo de los datos en la fase exploratoria combinado con la aplicación de modelos matemáticos para la inferencia de mecanismos más detallados en una fase posterior es esencial para extraer toda la información contenida en los datos multidimensionales generados a partir de las tecnologías ómicas.

Bibliography

BIBLIOGRAPHY

Adachi, T., Nakanishi, M., Otsuka, Y., Nishimura, K., Hirokawa, G., Goto, Y., Nonogi, H., and Iwai, N. (2010). Plasma microRNA 499 as a biomarker of acute myocardial infarction. Clinical chemistry *56*, 1183-1185.

Agarwal, V., Bell, G.W., Nam, J.-W., and Bartel, D.P. (2015). Predicting effective microRNA target sites in mammalian mRNAs. Elife *4*, e05005.

Ahmad, S.A., Jung, Y.D., Liu, W., Reinmuth, N., Parikh, A., Stoeltzing, O., Fan, F., and Ellis, L.M. (2002). The role of the microenvironment and intercellular cross-talk in tumor angiogenesis. In Seminars in cancer biology (Elsevier), pp. 105-112.

Ahn, A.C., Tewari, M., Poon, C.-S., and Phillips, R.S. (2006). The limits of reductionism in medicine: could systems biology offer an alternative? PLoS Med *3*, e208.

Ai, J., Zhang, R., Li, Y., Pu, J., Lu, Y., Jiao, J., Li, K., Yu, B., Li, Z., Wang, R.*, et al.* (2010). Circulating microRNA-1 as a potential novel biomarker for acute myocardial infarction. Biochem Biophys Res Commun *391*, 73-77.

Albert, R. (2007). Network inference, analysis, and modeling in systems biology. The Plant Cell *19*, 3327-3338.

Alexander, R.P., Fang, G., Rozowsky, J., Snyder, M., and Gerstein, M.B. (2010). Annotating non-coding regions of the genome. Nature Reviews Genetics *11*, 559-571.

Anders, S., and Huber, W. (2012). Differential expression of RNA-Seq data at the gene level–the DESeq package. Heidelberg, Germany: European Molecular Biology Laboratory (EMBL).

Ando, M., Uehara, I., Kogure, K., Asano, Y., Nakajima, W., Abe, Y., Kawauchi, K., and Tanaka, N. (2010). Interleukin 6 enhances glycolysis through expression of the glycolytic enzymes hexokinase 2 and 6-phosphofructo-2-kinase/fructose-2, 6-bisphosphatase-3. Journal of Nippon Medical School *77*, 97-105.

Baer, C., Squadrito, M.L., Iruela-Arispe, M.L., and De Palma, M. (2013). Reciprocal interactions between endothelial cells and macrophages in angiogenic vascular niches. Experimental cell research *319*, 1626-1634.

Bain, C.C., and Mowat, A.M. (2014). The monocyte-macrophage axis in the intestine. Cellular immunology *291*, 41-48.

Bao, J., and Lin, L. (2014). MiR-155 and miR-148a reduce cardiac injury by inhibiting NF-κB pathway during acute viral myocarditis. Eur Rev Med Pharmacol Sci *18*, 2349-2356.

Barreau, C., Paillard, L., and Osborne, H.B. (2005). AU-rich elements and associated factors: are there unifying principles? Nucleic acids research *33*, 7138-7150.

Bartel, D.P. (2004). MicroRNAs: genomics, biogenesis, mechanism, and function. cell *116*, 281-297.

Baum, J., and Duffy, H.S. (2011). Fibroblasts and myofibroblasts: what are we talking

about? Journal of cardiovascular pharmacology *57*, 376.

Bergmann, O., Zdunek, S., Felker, A., Salehpour, M., Alkass, K., Bernard, S., Sjostrom, S.L., Szewczykowska, M., Jackowska, T., Dos Remedios, C*., et al.* (2015). Dynamics of Cell Generation and Turnover in the Human Heart. Cell *161*, 1566-1575.

Bindea, G., Mlecnik, B., Hackl, H., Charoentong, P., Tosolini, M., Kirilovsky, A., Fridman, W.H., Pages, F., Trajanoski, Z., and Galon, J. (2009). ClueGO: a Cytoscape plug-in to decipher functionally grouped gene ontology and pathway annotation networks. Bioinformatics *25*, 1091-1093.

Bolstad, B.M., Irizarry, R.A., Åstrand, M., and Speed, T.P. (2003). A comparison of normalization methods for high density oligonucleotide array data based on variance and bias. Bioinformatics *19*, 185-193.

Bordbar, A., Mo, M.L., Nakayasu, E.S., Schrimpe-Rutledge, A.C., Kim, Y.M., Metz, T.O., Jones, M.B., Frank, B.C., Smith, R.D., Peterson, S.N*., et al.* (2012). Model-driven multi-omic data analysis elucidates metabolic immunomodulators of macrophage activation. Mol Syst Biol *8*, 558.

Boštjančič, E., Zidar, N., Štajer, D., and Glavač, D. (2009). MicroRNAs miR-1, miR-133a, miR-133b and miR-208 are dysregulated in human myocardial infarction. Cardiology *115*, 163-169.

Boudoulas, K.D., and Hatzopoulos, A.K. (2009). Cardiac repair and regeneration: the Rubik's cube of cell therapy for heart disease. Disease Models and Mechanisms *2*, 344-358.

Braun, D.A., Fribourg, M., and Sealfon, S.C. (2013). Cytokine response is determined by duration of receptor and signal transducers and activators of transcription 3 (STAT3) activation. Journal of Biological Chemistry *288*, 2986-2993.

Bray, I., Tivnan, A., Bryan, K., Foley, N.H., Watters, K.M., Tracey, L., Davidoff, A.M., and Stallings, R.L. (2011). MicroRNA-542-5p as a novel tumor suppressor in neuroblastoma. Cancer letters *303*, 56-64.

Bray, N.L., Pimentel, H., Melsted, P., and Pachter, L. (2016). Near-optimal probabilistic RNA-seq quantification. Nature biotechnology *34*, 525-527.

Brock, G., Pihur, V., Datta, S., and Datta, S. (2011). clValid, an R package for cluster validation. Journal of Statistical Software (Brock et al., March 2008).

Broderick, J.A., and Zamore, P.D. (2014). Competitive endogenous RNAs cannot alter microRNA function in vivo. Molecular cell *54*, 711-713.

Brutsaert, D.L. (2003). Cardiac endothelial-myocardial signaling: its role in cardiac growth, contractile performance, and rhythmicity. Physiological reviews *83*, 59-115.

Bujak, M., and Frangogiannis, N.G. (2007). The role of TGF-β signaling in myocardial infarction and cardiac remodeling. Cardiovascular research *74*, 184-195.

Bursac, N., Parker, K., Iravanian, S., and Tung, L. (2002). Cardiomyocyte cultures with controlled macroscopic anisotropy a model for functional electrophysiological studies of cardiac muscle. Circulation research *91*, e45-e54.

Cai, X., and Cullen, B.R. (2007). The imprinted H19 noncoding RNA is a primary microRNA precursor. Rna *13*, 313-316.

Cai, Z., Luo, W., Zhan, H., and Semenza, G.L. (2013). Hypoxia-inducible factor 1 is required for remote ischemic preconditioning of the heart. Proceedings of the National Academy of Sciences *110*, 17462-17467.

Camelliti, P., Borg, T.K., and Kohl, P. (2005). Structural and functional characterisation of cardiac fibroblasts. Cardiovascular research *65*, 40-51.

Capurro, A., Bodea, L.-G., Schaefer, P., Luthi-Carter, R., and Perreau, V.M. (2015). Computational deconvolution of genome wide expression data from Parkinson's and Huntington's disease brain tissues using population-specific expression analysis. Frontiers in neuroscience *8*, 441.

Carmeliet, P., Moons, L., Luttun, A., Vincenti, V., Compernolle, V., De Mol, M., Wu, Y., Bono, F., Devy, L., Beck, H.*, et al.* (2001). Synergism between vascular endothelial growth factor and placental growth factor contributes to angiogenesis and plasma extravasation in pathological conditions. Nat Med *7*, 575-583.

Caroli, A., Cardillo, M.T., Galea, R., and Biasucci, L.M. (2013). Potential therapeutic role of microRNAs in ischemic heart disease. Journal of cardiology *61*, 315-320.

Cesana, M., Cacchiarelli, D., Legnini, I., Santini, T., Sthandier, O., Chinappi, M., Tramontano, A., and Bozzoni, I. (2011). A long noncoding RNA controls muscle differentiation by functioning as a competing endogenous RNA. Cell *147*, 358-369.

Chalancon, G., Ravarani, C.N., Balaji, S., Martinez-Arias, A., Aravind, L., Jothi, R., and Babu, M.M. (2012). Interplay between gene expression noise and regulatory network architecture. Trends in genetics *28*, 221-232.

Chareonthaitawee, P., Christian, T.F., Hirose, K., Gibbons, R.J., and Rumberger, J.A. (1995). Relation of initial infarct size to extent of left ventricular remodeling in the year after acute myocardial infarction. Journal of the American College of Cardiology *25*, 567-573.

Cheetham, S., Gruhl, F., Mattick, J., and Dinger, M. (2013). Long noncoding RNAs and the genetics of cancer. British journal of cancer *108*, 2419-2425.

Chen, C., Grennan, K., Badner, J., Zhang, D., Gershon, E., Jin, L., and Liu, C. (2011a). Removing batch effects in analysis of expression microarray data: an evaluation of six batch adjustment methods. PloS one *6*, e17238.

Chen, G.Y., and Nuñez, G. (2010). Sterile inflammation: sensing and reacting to damage. Nature Reviews Immunology *10*, 826-837.

Chen, J., Wang, L., Matyunina, L.V., Hill, C.G., and McDonald, J.F. (2011b). Overexpression of miR-429 induces mesenchymal-to-epithelial transition (MET) in metastatic ovarian cancer cells. Gynecologic oncology *121*, 200-205.

Chen, W., and Frangogiannis, N.G. (2013). Fibroblasts in post-infarction inflammation and cardiac repair. Biochimica et Biophysica Acta (BBA)-Molecular Cell Research *1833*, 945-953.

Cheng, Y., Zhu, P., Yang, J., Liu, X., Dong, S., Wang, X., Chun, B., Zhuang, J., and Zhang, C. (2010). Ischaemic preconditioning-regulated miR-21 protects heart against ischaemia/reperfusion injury via anti-apoptosis through its target PDCD4. Cardiovascular research *87*, 431-439.

Cho, C.H., Koh, Y.J., Han, J., Sung, H.K., Jong Lee, H., Morisada, T., Schwendener, R.A., Brekken, R.A., Kang, G., Oike, Y.*, et al.* (2007). Angiogenic role of LYVE-1-positive macrophages in adipose tissue. Circ Res *100*, e47-57.

Clambey, E., Westrich, J., and Eltzschig, H. (2013). Hypoxia inducible factor-1 alpha links reduced oxygen availability to the generation of anti-inflammatory IL-10 expressing T cells (P1328). The Journal of Immunology *190*, 208.208-208.208.

Clark, M.B., Johnston, R.L., Inostroza-Ponta, M., Fox, A.H., Fortini, E., Moscato, P., Dinger, M.E., and Mattick, J.S. (2012). Genome-wide analysis of long noncoding RNA stability. Genome research *22*, 885-898.

Cochain, C., Channon, K.M., and Silvestre, J.-S. (2013). Angiogenesis in the infarcted myocardium. Antioxidants & redox signaling *18*, 1100-1113.

Colombo, T., Farina, L., Macino, G., and Paci, P. (2015). PVT1: a rising star among oncogenic long noncoding RNAs. BioMed research international *2015*.

Concepcion, C.P., Bonetti, C., and Ventura, A. (2012). The miR-17-92 family of microRNA clusters in development and disease. Cancer journal (Sudbury, Mass.) *18*, 262.

Cordes, K.R., and Srivastava, D. (2009). MicroRNA regulation of cardiovascular development. Circulation research *104*, 724-732.

Coultas, L., Chawengsaksophak, K., and Rossant, J. (2005). Endothelial cells and VEGF in vascular development. Nature *438*, 937-945.

D'Amato, G., Luxan, G., del Monte-Nieto, G., Martinez-Poveda, B., Torroja, C., Walter, W., Bochter, M.S., Benedito, R., Cole, S., Martinez, F.*, et al.* (2016). Sequential Notch activation regulates ventricular chamber development. Nat Cell Biol *18*, 7-20.

Dace, D.S., Khan, A.A., Kelly, J., and Apte, R.S. (2008). Interleukin-10 promotes pathological angiogenesis by regulating macrophage response to hypoxia during development. PLoS One *3*, e3381.

Daley, J.M., Brancato, S.K., Thomay, A.A., Reichner, J.S., and Albina, J.E. (2010). The

phenotype of murine wound macrophages. Journal of leukocyte biology *87*, 59-67.

Darwich, L., Coma, G., Pena, R., Bellido, R., Blanco, E.J., Este, J.A., Borras, F.E., Clotet, B., Ruiz, L., Rosell, A.*, et al.* (2009). Secretion of interferon-gamma by human macrophages demonstrated at the single-cell level after costimulation with interleukin (IL)-12 plus IL-18. Immunology *126*, 386-393.

Davies, L.C., Jenkins, S.J., Allen, J.E., and Taylor, P.R. (2013). Tissue-resident macrophages. Nature immunology *14*, 986-995.

Denzler, R., Agarwal, V., Stefano, J., Bartel, D.P., and Stoffel, M. (2014). Assessing the ceRNA hypothesis with quantitative measurements of miRNA and target abundance. Molecular cell *54*, 766-776.

Derrien, T., Johnson, R., Bussotti, G., Tanzer, A., Djebali, S., Tilgner, H., Guernec, G., Martin, D., Merkel, A., Knowles, D.G.*, et al.* (2012). The GENCODE v7 catalog of human long noncoding RNAs: analysis of their gene structure, evolution, and expression. Genome Res *22*, 1775-1789.

Desmouliere, A., Redard, M., Darby, I., and Gabbiani, G. (1995). Apoptosis mediates the decrease in cellularity during the transition between granulation tissue and scar. The American journal of pathology *146*, 56.

Díaz-Araya, G., Vivar, R., Humeres, C., Boza, P., Bolivar, S., and Muñoz, C. (2015). Cardiac fibroblasts as sentinel cells in cardiac tissue: receptors, signaling pathways and cellular functions. Pharmacological research *101*, 30-40.

Diegelmann, R.F., and Evans, M.C. (2004). Wound healing: an overview of acute, fibrotic and delayed healing. Front Biosci *9*, 283-289.

Dimmeler, S., Zeiher, A.M., and Schneider, M.D. (2005). Unchain my heart: the scientific foundations of cardiac repair. The Journal of clinical investigation *115*, 572-583.

DiPietro, L.A. (1995). Wound healing: the role of the macrophage and other immune cells. Shock *4*, 233-240.

Dobaczewski, M., Bujak, M., Li, N., Gonzalez-Quesada, C., Mendoza, L.H., Wang, X.-F., and Frangogiannis, N.G. (2010). Smad3 signaling critically regulates fibroblast phenotype and function in healing myocardial infarction. Circulation research *107*, 418-428.

Dong, S., Cheng, Y., Yang, J., Li, J., Liu, X., Wang, X., Wang, D., Krall, T.J., Delphin, E.S., and Zhang, C. (2009). MicroRNA expression signature and the role of microRNA-21 in the early phase of acute myocardial infarction. Journal of Biological Chemistry *284*, 29514-29525.

Ducharme, A., Frantz, S., Aikawa, M., Rabkin, E., Lindsey, M., Rohde, L.E., Schoen, F.J., Kelly, R.A., Werb, Z., Libby, P., and Lee, R.T. (2000). Targeted deletion of matrix metalloproteinase-9 attenuates left ventricular enlargement and collagen accumulation

after experimental myocardial infarction. J Clin Invest *106*, 55-62.

Durinck, S., Moreau, Y., Kasprzyk, A., Davis, S., De Moor, B., Brazma, A., and Huber, W. (2005). BioMart and Bioconductor: a powerful link between biological databases and microarray data analysis. Bioinformatics *21*, 3439-3440.

Dweep, H., and Gretz, N. (2015). miRWalk2. 0: a comprehensive atlas of microRNA-target interactions. Nature methods *12*, 697-697.

Dweep, H., Sticht, C., Pandey, P., and Gretz, N. (2011). miRWalk–database: prediction of possible miRNA binding sites by "walking" the genes of three genomes. Journal of biomedical informatics *44*, 839-847.

Eltzschig, H.K., and Eckle, T. (2011). Ischemia and reperfusion [mdash] from mechanism to translation. Nature medicine *17*, 1391-1401.

Essandoh, K., Li, Y., Huo, J., and Fan, G.-C. (2016). Mirna-Mediated Macrophage Polarization and its Potential Role in the Regulation of Inflammatory Response. Shock (Augusta, Ga.).

Euler, G. (2015). Good and bad sides of TGFβ-signaling in myocardial infarction. Frontiers in physiology *6*, 66.

Fantin, A., Vieira, J.M., Plein, A., Denti, L., Fruttiger, M., Pollard, J.W., and Ruhrberg, C. (2013). NRP1 acts cell autonomously in endothelium to promote tip cell function during sprouting angiogenesis. Blood *121*, 2352-2362.

Febbraio, M., Hajjar, D.P., and Silverstein, R.L. (2001). CD36: a class B scavenger receptor involved in angiogenesis, atherosclerosis, inflammation, and lipid metabolism. The Journal of clinical investigation *108*, 785-791.

Ferrara, N. (2010). Pathways mediating VEGF-independent tumor angiogenesis. Cytokine & growth factor reviews *21*, 21-26.

Fish, J.E., Santoro, M.M., Morton, S.U., Yu, S., Yeh, R.-F., Wythe, J.D., Ivey, K.N., Bruneau, B.G., Stainier, D.Y., and Srivastava, D. (2008). miR-126 regulates angiogenic signaling and vascular integrity. Developmental cell *15*, 272-284.

Fitzgerald, K.A., and Caffrey, D.R. (2014). Long noncoding RNAs in innate and adaptive immunity. Current opinion in immunology *26*, 140-146.

Flynn, J.L., Chan, J., Triebold, K.J., Dalton, D.K., Stewart, T.A., and Bloom, B.R. (1993). An essential role for interferon gamma in resistance to Mycobacterium tuberculosis infection. The Journal of experimental medicine *178*, 2249-2254.

Fortino, V., Alenius, H., and Greco, D. (2015). BACA: bubble chArt to compare annotations. BMC bioinformatics *16*, 1.

Frangogiannis, N.G., Smith, C.W., and Entman, M.L. (2002). The inflammatory response in myocardial infarction. Cardiovascular research *53*, 31-47.

Frantz, S., and Nahrendorf, M. (2014). Cardiac macrophages and their role in ischemic heart disease. Cardiovascular research, cvu025.

Fredj, S., Bescond, J., Louault, C., Delwail, A., Lecron, J.c., and Potreau, D. (2005). Role of interleukin‐6 in cardiomyocyte/cardiac fibroblast interactions during myocyte hypertrophy and fibroblast proliferation. Journal of cellular physiology *204*, 428-436.

Freemerman, A.J., Johnson, A.R., Sacks, G.N., Milner, J.J., Kirk, E.L., Troester, M.A., Macintyre, A.N., Goraksha-Hicks, P., Rathmell, J.C., and Makowski, L. (2014). Metabolic reprogramming of macrophages: glucose transporter 1 (GLUT1)-mediated glucose metabolism drives a proinflammatory phenotype. The Journal of biological chemistry *289*, 7884-7896.

Friedländer, M.R., Mackowiak, S.D., Li, N., Chen, W., and Rajewsky, N. (2012). miRDeep2 accurately identifies known and hundreds of novel microRNA genes in seven animal clades. Nucleic acids research *40*, 37-52.

Friedman, R.C., Farh, K.K.-H., Burge, C.B., and Bartel, D.P. (2009). Most mammalian mRNAs are conserved targets of microRNAs. Genome research *19*, 92-105.

Fritah, S., Niclou, S.P., and Azuaje, F. (2014). Databases for lncRNAs: a comparative evaluation of emerging tools. Rna *20*, 1655-1665.

Fujiu, K., Wang, J., and Nagai, R. (2014). Cardioprotective function of cardiac macrophages. Cardiovascular research *102*, 232-239.

Garcia-Prieto, J., Garcia-Ruiz, J.M., Sanz-Rosa, D., Pun, A., Garcia-Alvarez, A., Davidson, S.M., Fernandez-Friera, L., Nuno-Ayala, M., Fernandez-Jimenez, R., Bernal, J.A.*, et al.* (2014). beta3 adrenergic receptor selective stimulation during ischemia/reperfusion improves cardiac function in translational models through inhibition of mPTP opening in cardiomyocytes. Basic research in cardiology *109*, 422.

Garg, A., Di Cara, A., Xenarios, I., Mendoza, L., and De Micheli, G. (2008). Synchronous versus asynchronous modeling of gene regulatory networks. Bioinformatics *24*, 1917-1925.

Garg, A., Mohanram, K., Di Cara, A., De Micheli, G., and Xenarios, I. (2009). Modeling stochasticity and robustness in gene regulatory networks. Bioinformatics *25*, i101-i109.

Garg, A., Xenarios, I., Mendoza, L., and DeMicheli, G. (2007). An efficient method for dynamic analysis of gene regulatory networks and in silico gene perturbation experiments. In Annual International Conference on Research in Computational Molecular Biology (Springer), pp. 62-76.

Garzon, R., Volinia, S., Papaioannou, D., Nicolet, D., Kohlschmidt, J., Yan, P.S., Mrozek, K., Bucci, D., Carroll, A.J., Baer, M.R.*, et al.* (2014). Expression and prognostic impact of lncRNAs in acute myeloid leukemia. Proc Natl Acad Sci U S A *111*, 18679-18684.

Gaujoux, R., and Seoighe, C. (2013). CellMix: a comprehensive toolbox for gene

expression deconvolution. Bioinformatics *29*, 2211-2212.

Gautier, E.L., Shay, T., Miller, J., Greter, M., Jakubzick, C., Ivanov, S., Helft, J., Chow, A., Elpek, K.G., Gordonov, S.*, et al.* (2012). Gene-expression profiles and transcriptional regulatory pathways that underlie the identity and diversity of mouse tissue macrophages. Nat Immunol *13*, 1118-1128.

Gaziel-Sovran, A., Segura, M.F., Di Micco, R., Collins, M.K., Hanniford, D., Vega-Saenz de Miera, E., Rakus, J.F., Dankert, J.F., Shang, S., Kerbel, R.S.*, et al.* (2011). miR-30b/30d regulation of GalNAc transferases enhances invasion and immunosuppression during metastasis. Cancer Cell *20*, 104-118.

Ghasemi, O., Ma, Y., Lindsey, M.L., and Jin, Y.F. (2014). Using systems biology approaches to understand cardiac inflammation and extracellular matrix remodeling in the setting of myocardial infarction. Wiley Interdisciplinary Reviews: Systems Biology and Medicine *6*, 77-91.

Gifford, C.A., and Srivastava, D. (2016). Heart disease modelling adds a Notch to its belt. Nature cell biology *18*, 3-5.

Ginhoux, F., and Guilliams, M. (2016). Tissue-resident macrophage ontogeny and homeostasis. Immunity *44*, 439-449.

Goldsmith, E.C., Bradshaw, A.D., Zile, M.R., and Spinale, F.G. (2014). Myocardial fibroblast–matrix interactions and potential therapeutic targets. Journal of molecular and cellular cardiology *70*, 92-99.

Gong, T., Hartmann, N., Kohane, I.S., Brinkmann, V., Staedtler, F., Letzkus, M., Bongiovanni, S., and Szustakowski, J.D. (2011). Optimal deconvolution of transcriptional profiling data using quadratic programming with application to complex clinical blood samples. PloS one *6*, e27156.

Gordon, S. (2007). The macrophage: past, present and future. European journal of immunology *37*, S9-S17.

Gordon, S., Plüddemann, A., and Martinez Estrada, F. (2014). Macrophage heterogeneity in tissues: phenotypic diversity and functions. Immunological reviews *262*, 36-55.

Gordon, S., and Taylor, P.R. (2005). Monocyte and macrophage heterogeneity. Nature Reviews Immunology *5*, 953-964.

Gosselin, D., Link, V.M., Romanoski, C.E., Fonseca, G.J., Eichenfield, D.Z., Spann, N.J., Stender, J.D., Chun, H.B., Garner, H., Geissmann, F., and Glass, C.K. (2014). Environment drives selection and function of enhancers controlling tissue-specific macrophage identities. Cell *159*, 1327-1340.

Graff, J.W., Dickson, A.M., Clay, G., McCaffrey, A.P., and Wilson, M.E. (2012). Identifying functional microRNAs in macrophages with polarized phenotypes. Journal of Biological Chemistry *287*, 21816-21825.

BIBLIOGRAPHY

Gregory, P.A., Bert, A.G., Paterson, E.L., Barry, S.C., Tsykin, A., Farshid, G., Vadas, M.A., Khew-Goodall, Y., and Goodall, G.J. (2008). The miR-200 family and miR-205 regulate epithelial to mesenchymal transition by targeting ZEB1 and SIP1. Nature cell biology *10*, 593-601.

Grimson, A., Farh, K.K.-H., Johnston, W.K., Garrett-Engele, P., Lim, L.P., and Bartel, D.P. (2007). MicroRNA targeting specificity in mammals: determinants beyond seed pairing. Molecular cell *27*, 91-105.

Guttman, M., and Rinn, J.L. (2012). Modular regulatory principles of large non-coding RNAs. Nature *482*, 339-346.

Haim, Y.O., Unger, N.D., Souroujon, M.C., Mittelman, M., and Neumann, D. (2014). Resistance of LPS-activated bone marrow derived macrophages to apoptosis mediated by dexamethasone. Scientific reports *4*, 4323.

Hansson, G.K., Robertson, A.-K.L., and Söderberg-Nauclér, C. (2006). Inflammation and atherosclerosis. Annu. Rev. Pathol. Mech. Dis. *1*, 297-329.

Harada, M., Qin, Y., Takano, H., Minamino, T., Zou, Y., Toko, H., Ohtsuka, M., Matsuura, K., Sano, M., Nishi, J.*, et al.* (2005). G-CSF prevents cardiac remodeling after myocardial infarction by activating the Jak-Stat pathway in cardiomyocytes. Nat Med *11*, 305-311.

Harel-Adar, T., Mordechai, T.B., Amsalem, Y., Feinberg, M.S., Leor, J., and Cohen, S. (2011). Modulation of cardiac macrophages by phosphatidylserine-presenting liposomes improves infarct repair. Proceedings of the National Academy of Sciences *108*, 1827-1832.

Hashimoto, D., Chow, A., Noizat, C., Teo, P., Beasley, M.B., Leboeuf, M., Becker, C.D., See, P., Price, J., Lucas, D.*, et al.* (2013). Tissue-resident macrophages self-maintain locally throughout adult life with minimal contribution from circulating monocytes. Immunity *38*, 792-804.

Heidt, T., Courties, G., Dutta, P., Sager, H.B., Sebas, M., Iwamoto, Y., Sun, Y., Da Silva, N., Panizzi, P., van der Laan, A.M.*, et al.* (2014). Differential contribution of monocytes to heart macrophages in steady-state and after myocardial infarction. Circ Res *115*, 284-295.

Hinz, B. (2007). Formation and function of the myofibroblast during tissue repair. Journal of Investigative Dermatology *127*, 526-537.

Horckmans, M., Ring, L., Duchene, J., Santovito, D., Schloss, M.J., Drechsler, M., Weber, C., Soehnlein, O., and Steffens, S. (2016). Neutrophils orchestrate post-myocardial infarction healing by polarizing macrophages towards a reparative phenotype. European heart journal, ehw002.

Hornstra, I.K., Birge, S., Starcher, B., Bailey, A.J., Mecham, R.P., and Shapiro, S.D. (2003). Lysyl oxidase is required for vascular and diaphragmatic development in mice. The Journal of biological chemistry *278*, 14387-14393.

Hsieh, P.C., Davis, M.E., Lisowski, L.K., and Lee, R.T. (2006). Endothelial-cardiomyocyte interactions in cardiac development and repair. Annual review of physiology *68*, 51.

Hu, X., Paik, P.K., Chen, J., Yarilina, A., Kockeritz, L., Lu, T.T., Woodgett, J.R., and Ivashkiv, L.B. (2006). IFN-γ suppresses IL-10 production and synergizes with TLR2 by regulating GSK3 and CREB/AP-1 proteins. Immunity *24*, 563-574.

Huang, S., Eichler, G., Bar-Yam, Y., and Ingber, D.E. (2005). Cell fates as high-dimensional attractor states of a complex gene regulatory network. Physical review letters *94*, 128701.

Hung, T., Wang, Y., Lin, M.F., Koegel, A.K., Kotake, Y., Grant, G.D., Horlings, H.M., Shah, N., Umbricht, C., Wang, P.*, et al.* (2011). Extensive and coordinated transcription of noncoding RNAs within cell-cycle promoters. Nat Genet *43*, 621-629.

Ideker, T., Ozier, O., Schwikowski, B., and Siegel, A.F. (2002). Discovering regulatory and signalling circuits in molecular interaction networks. Bioinformatics *18*, S233-S240.

Ideker, T., Thorsson, V., Siegel, A.F., and Hood, L.E. (2000). Testing for differentially-expressed genes by maximum-likelihood analysis of microarray data. Journal of Computational Biology *7*, 805-817.

Ieda, M., Tsuchihashi, T., Ivey, K.N., Ross, R.S., Hong, T.-T., Shaw, R.M., and Srivastava, D. (2009). Cardiac fibroblasts regulate myocardial proliferation through β1 integrin signaling. Developmental cell *16*, 233-244.

Imamura, K., Imamachi, N., Akizuki, G., Kumakura, M., Kawaguchi, A., Nagata, K., Kato, A., Kawaguchi, Y., Sato, H., Yoneda, M.*, et al.* (2014). Long noncoding RNA NEAT1-dependent SFPQ relocation from promoter region to paraspeckle mediates IL8 expression upon immune stimuli. Mol Cell *53*, 393-406.

Irizarry, R.A., Hobbs, B., Collin, F., Beazer‐Barclay, Y.D., Antonellis, K.J., Scherf, U., and Speed, T.P. (2003). Exploration, normalization, and summaries of high density oligonucleotide array probe level data. Biostatistics *4*, 249-264.

Janky, R., Verfaillie, A., Imrichova, H., Van de Sande, B., Standaert, L., Christiaens, V., Hulselmans, G., Herten, K., Naval Sanchez, M., Potier, D.*, et al.* (2014). iRegulon: from a gene list to a gene regulatory network using large motif and track collections. PLoS Comput Biol *10*, e1003731.

Jing, Q., Huang, S., Guth, S., Zarubin, T., Motoyama, A., Chen, J., Di Padova, F., Lin, S.C., Gram, H., and Han, J. (2005). Involvement of microRNA in AU-rich element-mediated mRNA instability. Cell *120*, 623-634.

Johnson, W.E., Li, C., and Rabinovic, A. (2007). Adjusting batch effects in microarray expression data using empirical Bayes methods. Biostatistics *8*, 118-127.

Jojic, V., Shay, T., Sylvia, K., Zuk, O., Sun, X., Kang, J., Regev, A., Koller, D., Best, A.J., Knell, J.*, et al.* (2013). Identification of transcriptional regulators in the mouse

immune system. Nat Immunol *14*, 633-643.

Jung, S., Aliberti, J., Graemmel, P., Sunshine, M.J., Kreutzberg, G.W., Sher, A., and Littman, D.R. (2000). Analysis of fractalkine receptor CX3CR1 function by targeted deletion and green fluorescent protein reporter gene insertion. Molecular and cellular biology *20*, 4106-4114.

Junger, W.G. (2011). Immune cell regulation by autocrine purinergic signalling. Nature Reviews Immunology *11*, 201-212.

Kaelin, W.G., and Ratcliffe, P.J. (2008). Oxygen sensing by metazoans: the central role of the HIF hydroxylase pathway. Molecular cell *30*, 393-402.

Kakkar, R., and Lee, R.T. (2010). Intramyocardial fibroblast myocyte communication. Circulation research *106*, 47-57.

Kelder, T., van Iersel, M.P., Hanspers, K., Kutmon, M., Conklin, B.R., Evelo, C.T., and Pico, A.R. (2012). WikiPathways: building research communities on biological pathways. Nucleic acids research *40*, D1301-D1307.

Kim, Y.J., Bae, S.W., Yu, S.S., Bae, Y.C., and Jung, J.S. (2009). miR‑196a regulates proliferation and osteogenic differentiation in mesenchymal stem cells derived from human adipose tissue. Journal of bone and mineral research *24*, 816-825.

Knezevic, I., Patel, A., Sundaresan, N.R., Gupta, M.P., Solaro, R.J., Nagalingam, R.S., and Gupta, M. (2012). A novel cardiomyocyte-enriched MicroRNA, miR-378, targets insulin-like growth factor 1 receptor implications in postnatal cardiac remodeling and cell survival. Journal of Biological Chemistry *287*, 12913-12926.

Kobourov, S.G. (2012). Spring embedders and force directed graph drawing algorithms. arXiv preprint arXiv:1201.3011.

Kocher, A., Schuster, M., Szabolcs, M., Takuma, S., Burkhoff, D., Wang, J., Homma, S., Edwards, N., and Itescu, S. (2001). Neovascularization of ischemic myocardium by human bone-marrow–derived angioblasts prevents cardiomyocyte apoptosis, reduces remodeling and improves cardiac function. Nature medicine 7, 430-436.

Kolde, R., and Vilo, J. (2015). GOsummaries: an R package for visual functional annotation of experimental data. F1000Research *4*.

Kornfeld, J.-W., and Brüning, J.C. (2015). Regulation of metabolism by long, non-coding RNAs. Emerging Roles of Long Noncoding RNAs in Neurological Diseases and Metabolic Disorders, 59.

Kratochvill, F., Machacek, C., Vogl, C., Ebner, F., Sedlyarov, V., Gruber, A.R., Hartweger, H., Vielnascher, R., Karaghiosoff, M., Rulicke, T.*, et al.* (2011). Tristetraprolin-driven regulatory circuit controls quality and timing of mRNA decay in inflammation. Mol Syst Biol *7*, 560.

Krishnamurthy, P., Rajasingh, J., Lambers, E., Qin, G., Losordo, D.W., and Kishore, R.

(2009). IL-10 inhibits inflammation and attenuates left ventricular remodeling after myocardial infarction via activation of STAT3 and suppression of HuR. Circulation research *104*, e9-e18.

Krzywinski, M., Schein, J., Birol, I., Connors, J., Gascoyne, R., Horsman, D., Jones, S.J., and Marra, M.A. (2009). Circos: an information aesthetic for comparative genomics. Genome research *19*, 1639-1645.

Kuhn, A., Kumar, A., Beilina, A., Dillman, A., Cookson, M.R., and Singleton, A.B. (2012). Cell population-specific expression analysis of human cerebellum. BMC genomics *13*, 1.

Kumar, M., and Nerurkar, V.R. (2014). Integrated analysis of microRNAs and their disease related targets in the brain of mice infected with West Nile virus. Virology *452*, 143-151.

Kutmon, M., Lotia, S., Evelo, C.T., and Pico, A.R. (2014). WikiPathways App for Cytoscape: making biological pathways amenable to network analysis and visualization. F1000Research *3*.

Kutmon, M., van Iersel, M.P., Bohler, A., Kelder, T., Nunes, N., Pico, A.R., and Evelo, C.T. (2015). PathVisio 3: an extendable pathway analysis toolbox. PLoS Comput Biol *11*, e1004085.

Kuziel, W.A., Morgan, S.J., Dawson, T.C., Griffin, S., Smithies, O., Ley, K., and Maeda, N. (1997). Severe reduction in leukocyte adhesion and monocyte extravasation in mice deficient in CC chemokine receptor 2. Proceedings of the National Academy of Sciences *94*, 12053-12058.

Lamb, D.J., Modjtahedi, H., Plant, N.J., and Ferns, G.A. (2004). EGF mediates monocyte chemotaxis and macrophage proliferation and EGF receptor is expressed in atherosclerotic plaques. Atherosclerosis *176*, 21-26.

Lambert, J.M., Lopez, E.F., and Lindsey, M.L. (2008). Macrophage roles following myocardial infarction. International journal of cardiology *130*, 147-158.

Lavine, K.J., Epelman, S., Uchida, K., Weber, K.J., Nichols, C.G., Schilling, J.D., Ornitz, D.M., Randolph, G.J., and Mann, D.L. (2014). Distinct macrophage lineages contribute to disparate patterns of cardiac recovery and remodeling in the neonatal and adult heart. Proceedings of the National Academy of Sciences *111*, 16029-16034.

Leal, J., Luengo-Fernández, R., Gray, A., Petersen, S., and Rayner, M. (2006). Economic burden of cardiovascular diseases in the enlarged European Union. European heart journal *27*, 1610-1619.

Lee, W.-Y., Moriarty, T.J., Wong, C.H., Zhou, H., Strieter, R.M., van Rooijen, N., Chaconas, G., and Kubes, P. (2010). An intravascular immune response to Borrelia burgdorferi involves Kupffer cells and iNKT cells. Nature immunology *11*, 295-302.

Leek, J.T., Johnson, W.E., Parker, H.S., Jaffe, A.E., and Storey, J.D. (2012). The sva

package for removing batch effects and other unwanted variation in high-throughput experiments. Bioinformatics *28*, 882-883.

Leek, J.T., Scharpf, R.B., Bravo, H.C., Simcha, D., Langmead, B., Johnson, W.E., Geman, D., Baggerly, K., and Irizarry, R.A. (2010). Tackling the widespread and critical impact of batch effects in high-throughput data. Nature Reviews Genetics *11*, 733-739.

Lewis, B.P., Burge, C.B., and Bartel, D.P. (2005). Conserved seed pairing, often flanked by adenosines, indicates that thousands of human genes are microRNA targets. cell *120*, 15-20.

Li, B., and Dewey, C.N. (2011). RSEM: accurate transcript quantification from RNA-Seq data with or without a reference genome. BMC bioinformatics *12*, 1.

Li, J., Witten, D.M., Johnstone, I.M., and Tibshirani, R. (2011). Normalization, testing, and false discovery rate estimation for RNA-sequencing data. Biostatistics, kxr031.

Li, L., Ng, D.S., Mah, W.C., Almeida, F.F., Rahmat, S.A., Rao, V.K., Leow, S.C., Laudisi, F., Peh, M.T., Goh, A.M.*, et al.* (2015). A unique role for p53 in the regulation of M2 macrophage polarization. Cell death and differentiation *22*, 1081-1093.

Liang, J., and Han, J. (2012). Stochastic Boolean networks: an efficient approach to modeling gene regulatory networks. BMC systems biology *6*, 1.

Liang, Y., Ridzon, D., Wong, L., and Chen, C. (2007). Characterization of microRNA expression profiles in normal human tissues. BMC genomics *8*, 1.

Liu, J., Yao, J., Li, X., Song, Y., Wang, X., Li, Y., Yan, B., and Jiang, Q. (2014). Pathogenic role of lncRNA-MALAT1 in endothelial cell dysfunction in diabetes mellitus. Cell death & disease *5*, e1506.

Liu, N., and Olson, E.N. (2010). MicroRNA regulatory networks in cardiovascular development. Developmental cell *18*, 510-525.

Lu, M., Zhang, Q., Deng, M., Miao, J., Guo, Y., Gao, W., and Cui, Q. (2008). An analysis of human microRNA and disease associations. PloS one *3*, e3420.

Lugrin, J., Parapanov, R., Rosenblatt-Velin, N., Rignault-Clerc, S., Feihl, F., Waeber, B., Muller, O., Vergely, C., Zeller, M., Tardivel, A.*, et al.* (2015). Cutting edge: IL-1alpha is a crucial danger signal triggering acute myocardial inflammation during myocardial infarction. Journal of immunology (Baltimore, Md. : 1950) *194*, 499-503.

Ma'ayan, A. (2011). Introduction to network analysis in systems biology. Science signaling *4*, tr5.

Maamar, H., Raj, A., and Dubnau, D. (2007). Noise in gene expression determines cell fate in Bacillus subtilis. Science *317*, 526-529.

MacGrogan, D., D'Amato, G., Travisano, S., Martinez-Poveda, B., Luxan, G., Del Monte-Nieto, G., Papoutsi, T., Sbroggio, M., Bou, V., Gomez-Del Arco, P.*, et al.* (2016). Sequential Ligand-Dependent Notch Signaling Activation Regulates Valve Primordium

Formation and Morphogenesis. Circ Res *118*, 1480-1497.

Mackaness, G. (1962). Cellular resistance to infection. The Journal of experimental medicine *116*, 381-406.

Mantovani, A., Biswas, S.K., Galdiero, M.R., Sica, A., and Locati, M. (2013). Macrophage plasticity and polarization in tissue repair and remodelling. The Journal of pathology *229*, 176-185.

Mantovani, A., Sica, A., Sozzani, S., Allavena, P., Vecchi, A., and Locati, M. (2004). The chemokine system in diverse forms of macrophage activation and polarization. Trends in immunology *25*, 677-686.

Marcondes, M.C.G., Poling, M., Watry, D.D., Hall, D., and Fox, H.S. (2008). In vivo osteopontin-induced macrophage accumulation is dependent on CD44 expression. Cellular immunology *254*, 56-62.

Martinez, F.O., and Gordon, S. (2014). The M1 and M2 paradigm of macrophage activation: time for reassessment. F1000Prime Rep *6*, 12703.

Martorell, L., Gentile, M., Rius, J., Rodríguez, C., Crespo, J., Badimon, L., and Martínez-González, J. (2009). The hypoxia-inducible factor 1/NOR-1 axis regulates the survival response of endothelial cells to hypoxia. Molecular and cellular biology *29*, 5828-5842.

Masters, M., and Riley, P.R. (2014). The epicardium signals the way towards heart regeneration. Stem cell research *13*, 683-692.

McHugh, C.A., Chen, C.K., Chow, A., Surka, C.F., Tran, C., McDonel, P., Pandya-Jones, A., Blanco, M., Burghard, C., Moradian, A.*, et al.* (2015). The Xist lncRNA interacts directly with SHARP to silence transcription through HDAC3. Nature *521*, 232-236.

Mi, H., Poudel, S., Muruganujan, A., Casagrande, J.T., and Thomas, P.D. (2016). PANTHER version 10: expanded protein families and functions, and analysis tools. Nucleic acids research *44*, D336-D342.

Miller, J.C., Brown, B.D., Shay, T., Gautier, E.L., Jojic, V., Cohain, A., Pandey, G., Leboeuf, M., Elpek, K.G., Helft, J.*, et al.* (2012). Deciphering the transcriptional network of the dendritic cell lineage. Nat Immunol *13*, 888-899.

Mogilyansky, E., and Rigoutsos, I. (2013). The miR-17/92 cluster: a comprehensive update on its genomics, genetics, functions and increasingly important and numerous roles in health and disease. Cell Death & Differentiation *20*, 1603-1614.

Molawi, K., Wolf, Y., Kandalla, P.K., Favret, J., Hagemeyer, N., Frenzel, K., Pinto, A.R., Klapproth, K., Henri, S., Malissen, B.*, et al.* (2014). Progressive replacement of embryo-derived cardiac macrophages with age. J Exp Med *211*, 2151-2158.

Mosser, D.M. (2003). The many faces of macrophage activation. Journal of leukocyte

biology *73*, 209-212.

Mosser, D.M., and Edwards, J.P. (2008). Exploring the full spectrum of macrophage activation. Nature reviews immunology *8*, 958-969.

Murata, Y., Ohteki, T., Koyasu, S., and Hamuro, J. (2002). IFN‐γ and pro‐inflammatory cytokine production by antigen‐presenting cells is dictated by intracellular thiol redox status regulated by oxygen tension. European journal of immunology *32*, 2866-2873.

Murdoch, C., Muthana, M., and Lewis, C.E. (2005). Hypoxia regulates macrophage functions in inflammation. The Journal of Immunology *175*, 6257-6263.

Mutin, M., Canavy, I., Blann, A., Bory, M., Sampol, J., and Dignat-George, F. (1999). Direct evidence of endothelial injury in acute myocardial infarction and unstable angina by demonstration of circulating endothelial cells. Blood *93*, 2951-2958.

Nahrendorf, M., Swirski, F.K., Aikawa, E., Stangenberg, L., Wurdinger, T., Figueiredo, J.-L., Libby, P., Weissleder, R., and Pittet, M.J. (2007). The healing myocardium sequentially mobilizes two monocyte subsets with divergent and complementary functions. The Journal of experimental medicine *204*, 3037-3047.

Narmoneva, D.A., Vukmirovic, R., Davis, M.E., Kamm, R.D., and Lee, R.T. (2004). Endothelial cells promote cardiac myocyte survival and spatial reorganization implications for cardiac regeneration. Circulation *110*, 962-968.

Nathan, C.F., Murray, H.W., Wiebe, M., and Rubin, B.Y. (1983). Identification of interferon-gamma as the lymphokine that activates human macrophage oxidative metabolism and antimicrobial activity. The Journal of experimental medicine *158*, 670-689.

Nelissen-Vrancken, H.M.G., Debets, J.J., Snoeckx, L.H., Daemen, M.J., and Smits, J.F. (1996). Time-related normalization of maximal coronary flow in isolated perfused hearts of rats with myocardial infarction. Circulation *93*, 349-355.

Németh, Z.H., Lutz, C.S., Csóka, B., Deitch, E.A., Leibovich, S.J., Gause, W.C., Tone, M., Pacher, P., Vizi, E.S., and Haskó, G. (2005). Adenosine augments IL-10 production by macrophages through an A2B receptor-mediated posttranscriptional mechanism. The Journal of Immunology *175*, 8260-8270.

Neph, S., Kuehn, M.S., Reynolds, A.P., Haugen, E., Thurman, R.E., Johnson, A.K., Rynes, E., Maurano, M.T., Vierstra, J., Thomas, S*., et al.* (2012). BEDOPS: high-performance genomic feature operations. Bioinformatics *28*, 1919-1920.

Neumann, H., and Takahashi, K. (2007). Essential role of the microglial triggering receptor expressed on myeloid cells-2 (TREM2) for central nervous tissue immune homeostasis. Journal of neuroimmunology *184*, 92-99.

Newby, A.C. (2008). Metalloproteinase expression in monocytes and macrophages and its relationship to atherosclerotic plaque instability. Arteriosclerosis, thrombosis,

and vascular biology *28*, 2108-2114.

Niazi, F., and Valadkhan, S. (2012). Computational analysis of functional long noncoding RNAs reveals lack of peptide-coding capacity and parallels with 3′ UTRs. Rna *18*, 825-843.

Nishi, H., Ono, K., Horie, T., Nagao, K., Kinoshita, M., Kuwabara, Y., Watanabe, S., Takaya, T., Tamaki, Y., Takanabe-Mori, R.*, et al.* (2011). MicroRNA-27a regulates beta cardiac myosin heavy chain gene expression by targeting thyroid hormone receptor beta1 in neonatal rat ventricular myocytes. Mol Cell Biol *31*, 744-755.

Noguer, O., Villena, J., Lorita, J., Vilaro, S., and Reina, M. (2009). Syndecan-2 downregulation impairs angiogenesis in human microvascular endothelial cells. Exp Cell Res *315*, 795-808.

Noorbakhsh, J., Lang, A.H., and Mehta, P. (2013). Intrinsic noise of microRNA-regulated genes and the ceRNA hypothesis. PLoS One *8*, e72676.

Novak, M.L., and Koh, T.J. (2013). Phenotypic transitions of macrophages orchestrate tissue repair. The American journal of pathology *183*, 1352-1363.

Novak, M.L., Weinheimer‐Haus, E.M., and Koh, T.J. (2014). Macrophage activation and skeletal muscle healing following traumatic injury. The Journal of pathology *232*, 344-355.

Oliveros, J. (2013). VENNY. An interactive tool for comparing lists with Venn Diagrams. 2007.

Olson, E.N. (2006). Gene regulatory networks in the evolution and development of the heart. Science *313*, 1922-1927.

Organization, W.H. (2015). World Health Statistics 2014. Geneva: WHO.

Orimo, A., Gupta, P.B., Sgroi, D.C., Arenzana-Seisdedos, F., Delaunay, T., Naeem, R., Carey, V.J., Richardson, A.L., and Weinberg, R.A. (2005). Stromal fibroblasts present in invasive human breast carcinomas promote tumor growth and angiogenesis through elevated SDF-1/CXCL12 secretion. Cell *121*, 335-348.

Ounzain, S., Micheletti, R., Beckmann, T., Schroen, B., Alexanian, M., Pezzuto, I., Crippa, S., Nemir, M., Sarre, A., Johnson, R.*, et al.* (2015). Genome-wide profiling of the cardiac transcriptome after myocardial infarction identifies novel heart-specific long non-coding RNAs. Eur Heart J *36*, 353-368a.

Palatinus, J.A., Rhett, J.M., and Gourdie, R.G. (2010). Translational lessons from scarless healing of cutaneous wounds and regenerative repair of the myocardium. Journal of molecular and cellular cardiology *48*, 550-557.

Pan, Z., Sun, X., Shan, H., Wang, N., Wang, J., Ren, J., Feng, S., Xie, L., Lu, C., Yuan, Y.*, et al.* (2012). MicroRNA-101 inhibited postinfarct cardiac fibrosis and improved left ventricular compliance via the FBJ osteosarcoma oncogene/transforming growth

factor-beta1 pathway. Circulation *126*, 840-850.

Paolinelli-Alfonso, M., Villalobos-Escobedo, J.M., Rolshausen, P., Herrera-Estrella, A., Galindo-Sánchez, C., López-Hernández, J.F., and Hernandez-Martinez, R. (2016). Global transcriptional analysis suggests Lasiodiplodia theobromae pathogenicity factors involved in modulation of grapevine defensive response. BMC genomics *17*, 615.

Paradis, E., Claude, J., and Strimmer, K. (2004). APE: analyses of phylogenetics and evolution in R language. Bioinformatics *20*, 289-290.

Patro, R., Mount, S.M., and Kingsford, C. (2014). Sailfish enables alignment-free isoform quantification from RNA-seq reads using lightweight algorithms. Nature biotechnology *32*, 462-464.

Pavesi, G., Mereghetti, P., Zambelli, F., Stefani, M., Mauri, G., and Pesole, G. (2006). MoD Tools: regulatory motif discovery in nucleotide sequences from co-regulated or homologous genes. Nucleic acids research *34*, W566-W570.

Pearce, E.L., Mullen, A.C., Martins, G.A., Krawczyk, C.M., Hutchins, A.S., Zediak, V.P., Banica, M., DiCioccio, C.B., Gross, D.A., Mao, C.A.*, et al.* (2003). Control of effector CD8+ T cell function by the transcription factor Eomesodermin. Science *302*, 1041-1043.

Pinto, A.R., Godwin, J.W., and Rosenthal, N.A. (2014). Macrophages in cardiac homeostasis, injury responses and progenitor cell mobilisation. Stem cell research *13*, 705-714.

Pinto, A.R., Ilinykh, A., Ivey, M.J., Kuwabara, J.T., D'Antoni, M.L., Debuque, R., Chandran, A., Wang, L., Arora, K., Rosenthal, N.A., and Tallquist, M.D. (2016). Revisiting Cardiac Cellular Composition. Circ Res *118*, 400-409.

Pinto, A.R., Paolicelli, R., Salimova, E., Gospocic, J., Slonimsky, E., Bilbao-Cortes, D., Godwin, J.W., and Rosenthal, N.A. (2012). An abundant tissue macrophage population in the adult murine heart with a distinct alternatively-activated macrophage profile. PloS one *7*, e36814.

Plaisier, C.L., Bare, J.C., and Baliga, N.S. (2011). miRvestigator: web application to identify miRNAs responsible for co-regulated gene expression patterns discovered through transcriptome profiling. Nucleic acids research *39*, W125-W131.

Plate, K.H., Breier, G., Weich, H.A., and Risau, W. (1992). Vascular endothelial growth factor is a potential tumour angiogenesis factor in human gliomas in vivo.

Poling, J., Gajawada, P., Richter, M., Lorchner, H., Polyakova, V., Kostin, S., Shin, J., Boettger, T., Walther, T., Rees, W.*, et al.* (2014). Therapeutic targeting of the oncostatin M receptor-beta prevents inflammatory heart failure. Basic research in cardiology *109*, 396.

Ponting, C.P., Oliver, P.L., and Reik, W. (2009). Evolution and functions of long

noncoding RNAs. Cell *136*, 629-641.

Porter, K.E., and Turner, N.A. (2009). Cardiac fibroblasts: at the heart of myocardial remodeling. Pharmacology & therapeutics *123*, 255-278.

Powell, M.J., Thompson, S.A., Tone, Y., Waldmann, H., and Tone, M. (2000). Posttranscriptional regulation of IL-10 gene expression through sequences in the 3′-untranslated region. The Journal of Immunology *165*, 292-296.

Prabhu, S.D., and Frangogiannis, N.G. (2016). The Biological Basis for Cardiac Repair After Myocardial Infarction From Inflammation to Fibrosis. Circulation Research *119*, 91-112.

Preusse, M., Theis, F.J., and Mueller, N.S. (2016). miTALOS v2: Analyzing Tissue Specific microRNA Function. PloS one *11*, e0151771.

Rahat, M.A., Hemmerlein, B., and Iragavarapu-Charyulu, V. (2014). The regulation of angiogenesis by tissue cell-macrophage interactions. Frontiers in physiology *5*.

Rath, M., Müller, I., Kropf, P., Closs, E.I., and Munder, M. (2015). Metabolism via arginase or nitric oxide synthase: two competing arginine pathways in macrophages. M1/M2 Macrophages: The Arginine Fork in the Road to Health and Disease, 13.

Ren, S., Johnson, B.G., Kida, Y., Ip, C., Davidson, K.C., Lin, S.L., Kobayashi, A., Lang, R.A., Hadjantonakis, A.K., Moon, R.T., and Duffield, J.S. (2013). LRP-6 is a coreceptor for multiple fibrogenic signaling pathways in pericytes and myofibroblasts that are inhibited by DKK-1. Proc Natl Acad Sci U S A *110*, 1440-1445.

Repsilber, D., Kern, S., Telaar, A., Walzl, G., Black, G.F., Selbig, J., Parida, S.K., Kaufmann, S.H., and Jacobsen, M. (2010). Biomarker discovery in heterogeneous tissue samples-taking the in-silico deconfounding approach. BMC bioinformatics *11*, 1.

Rinchai, D., Kewcharoenwong, C., Kessler, B., Lertmemongkolchai, G., and Chaussabel, D. (2015). Abundance of ADAM9 transcripts increases in the blood in response to tissue damage. F1000Research *4*.

Rinn, J.L., and Chang, H.Y. (2012). Genome regulation by long noncoding RNAs. Annual review of biochemistry *81*.

Riquelme, P., Tomiuk, S., Kammler, A., Fändrich, F., Schlitt, H.J., Geissler, E.K., and Hutchinson, J.A. (2013). IFN-γ-induced iNOS expression in mouse regulatory macrophages prolongs allograft survival in fully immunocompetent recipients. Molecular Therapy *21*, 409-422.

Ritchie, M.E., Phipson, B., Wu, D., Hu, Y., Law, C.W., Shi, W., and Smyth, G.K. (2015). limma powers differential expression analyses for RNA-sequencing and microarray studies. Nucleic acids research, gkv007.

Rius, J., Martínez-González, J., Crespo, J., and Badimon, L. (2006). NOR-1 is involved in VEGF-induced endothelial cell growth. Atherosclerosis *184*, 276-282.

Roberts, A., and Pachter, L. (2013). Streaming fragment assignment for real-time analysis of sequencing experiments. Nature methods *10*, 71-73.

Robinette, M.L., Fuchs, A., Cortez, V.S., Lee, J.S., Wang, Y., Durum, S.K., Gilfillan, S., and Colonna, M. (2015). Transcriptional programs define molecular characteristics of innate lymphoid cell classes and subsets. Nat Immunol *16*, 306-317.

Robinson, M.D., McCarthy, D.J., and Smyth, G.K. (2010). edgeR: a Bioconductor package for differential expression analysis of digital gene expression data. Bioinformatics *26*, 139-140.

Robinson, M.D., and Oshlack, A. (2010). A scaling normalization method for differential expression analysis of RNA-seq data. Genome biology *11*, 1.

Roy, S., Schmeier, S., Arner, E., Alam, T., Parihar, S.P., Ozturk, M., Tamgue, O., Kawaji, H., de Hoon, M.J., Itoh, M.*, et al.* (2015). Redefining the transcriptional regulatory dynamics of classically and alternatively activated macrophages by deepCAGE transcriptomics. Nucleic Acids Res *43*, 6969-6982.

Rusinova, I., Forster, S., Yu, S., Kannan, A., Masse, M., Cumming, H., Chapman, R., and Hertzog, P.J. (2013). Interferome v2. 0: an updated database of annotated interferon-regulated genes. Nucleic acids research *41*, D1040-D1046.

Salmena, L., Poliseno, L., Tay, Y., Kats, L., and Pandolfi, P.P. (2011). A ceRNA hypothesis: the Rosetta Stone of a hidden RNA language? Cell *146*, 353-358.

Salzer, U., Mairhofer, M., and Prohaska, R. (2007). Stomatin: A new paradigm of membrane organization emerges. Dynamic Cell Biology *1*, 20-33.

Santulli, G. (2014). Angiopoietin-like proteins: a comprehensive look. Frontiers in endocrinology *5*, 4.

Saraiva, M., and O'Garra, A. (2010). The regulation of IL-10 production by immune cells. Nature Reviews Immunology *10*, 170-181.

Sarkar, S., Sinsimer, K.S., Foster, R.L., Brewer, G., and Pestka, S. (2008). AUF1 isoform-specific regulation of anti-inflammatory IL10 expression in monocytes. Journal of Interferon & Cytokine Research *28*, 679-691.

Schott, J., Reitter, S., Philipp, J., Haneke, K., Schäfer, H., and Stoecklin, G. (2014). Translational regulation of specific mRNAs controls feedback inhibition and survival during macrophage activation. PLoS Genet *10*, e1004368.

Schultze, J.L. (2015). Transcriptional programming of human macrophages: on the way to systems immunology. Journal of Molecular Medicine *93*, 589-597.

Schwerk, C., and Schulze-Osthoff, K. (2003). Non-apoptotic functions of caspases in cellular proliferation and differentiation. Biochemical pharmacology *66*, 1453-1458.

Sedlyarov, V., Fallmann, J., Ebner, F., Huemer, J., Sneezum, L., Ivin, M., Kreiner, K., Tanzer, A., Vogl, C., Hofacker, I., and Kovarik, P. (2016). Tristetraprolin binding site

atlas in the macrophage transcriptome reveals a switch for inflammation resolution. Mol Syst Biol *12*, 868.

Sellke, F.W., Armstrong, M.L., and Harrison, D.G. (1990). Endothelium-dependent vascular relaxation is abnormal in the coronary microcirculation of atherosclerotic primates. Circulation *81*, 1586-1593.

Sharova, L.V., Sharov, A.A., Nedorezov, T., Piao, Y., Shaik, N., and Ko, M.S. (2009). Database for mRNA half-life of 19 977 genes obtained by DNA microarray analysis of pluripotent and differentiating mouse embryonic stem cells. DNA research *16*, 45-58.

Shaulian, E., and Karin, M. (2002). AP-1 as a regulator of cell life and death. Nature cell biology *4*, E131-E136.

Shay, T., and Kang, J. (2013). Immunological Genome Project and systems immunology. Trends in immunology *34*, 602-609.

Shehade, H., Acolty, V., Moser, M., and Oldenhove, G. (2015). Cutting edge: hypoxia-inducible factor 1 negatively regulates Th1 function. The Journal of Immunology *195*, 1372-1376.

Shen-Orr, S.S., Tibshirani, R., Khatri, P., Bodian, D.L., Staedtler, F., Perry, N.M., Hastie, T., Sarwal, M.M., Davis, M.M., and Butte, A.J. (2010). Cell type–specific gene expression differences in complex tissues. Nature methods *7*, 287-289.

Shibuya, M. (2008). Vascular endothelial growth factor-dependent and -independent regulation of angiogenesis. BMB reports *41*, 278-286.

Shintani, S., Murohara, T., Ikeda, H., Ueno, T., Honma, T., Katoh, A., Sasaki, K., Shimada, T., Oike, Y., and Imaizumi, T. (2001). Mobilization of endothelial progenitor cells in patients with acute myocardial infarction. Circulation *103*, 2776-2779.

Silver, J.D., Ritchie, M.E., and Smyth, G.K. (2009). Microarray background correction: maximum likelihood estimation for the normal–exponential convolution. Biostatistics, kxn042.

Skroblin, P., and Mayr, M. (2014). "Going long": long non-coding RNAs as biomarkers. Circulation research *115*, 607-609.

Smyth, G.K. (2005). Limma: linear models for microarray data. In Bioinformatics and computational biology solutions using R and Bioconductor (Springer), pp. 397-420.

Sood, P., Krek, A., Zavolan, M., Macino, G., and Rajewsky, N. (2006). Cell-type-specific signatures of microRNAs on target mRNA expression. Proceedings of the National Academy of Sciences of the United States of America *103*, 2746-2751.

Soos, T., Sims, T., Barisoni, L., Lin, K., Littman, D., Dustin, M., and Nelson, P. (2006). CX3CR1+ interstitial dendritic cells form a contiguous network throughout the entire kidney. Kidney international *70*, 591-596.

Sperling, S.R. (2011). Systems biology approaches to heart development and

congenital heart disease. Cardiovascular research *91*, 269-278.

Stark, A., Brennecke, J., Bushati, N., Russell, R.B., and Cohen, S.M. (2005). Animal MicroRNAs confer robustness to gene expression and have a significant impact on 3 ′ UTR evolution. Cell *123*, 1133-1146.

Stein, M., Keshav, S., Harris, N., and Gordon, S. (1992). Interleukin 4 potently enhances murine macrophage mannose receptor activity: a marker of alternative immunologic macrophage activation. The Journal of experimental medicine *176*, 287-292.

Stout, R.D., and Suttles, J. (1996). The many roles of CD40 in cell-mediated inflammatory responses. Immunology today *17*, 487-492.

Strikoudis, A., Lazaris, C., Trimarchi, T., Galvao Neto, A.L., Yang, Y., Ntziachristos, P., Rothbart, S., Buckley, S., Dolgalev, I., Stadtfeld, M.*, et al.* (2016). Regulation of transcriptional elongation in pluripotency and cell differentiation by the PHD-finger protein Phf5a. Nat Cell Biol *18*, 1127-1138.

Sturn, A., Quackenbush, J., and Trajanoski, Z. (2002). Genesis: cluster analysis of microarray data. Bioinformatics *18*, 207-208.

Subramanian, A., Tamayo, P., Mootha, V.K., Mukherjee, S., Ebert, B.L., Gillette, M.A., Paulovich, A., Pomeroy, S.L., Golub, T.R., and Lander, E.S. (2005). Gene set enrichment analysis: a knowledge-based approach for interpreting genome-wide expression profiles. Proceedings of the National Academy of Sciences *102*, 15545-15550.

Sugiura, S., Lahav, R., Han, J., Kou, S.Y., Banner, L.R., De Pablo, F., and Patterson, P.H. (2000). Leukaemia inhibitory factor is required for normal inflammatory responses to injury in the peripheral and central nervous systems in vivo and is chemotactic for macrophages in vitro. European Journal of Neuroscience *12*, 457-466.

Sun, Y. (2008). Myocardial repair/remodelling following infarction: roles of local factors. Cardiovascular research.

Sunderkötter, C., Steinbrink, K., Goebeler, M., Bhardwaj, R., and Sorg, C. (1994). Macrophages and angiogenesis. Journal of leukocyte biology *55*, 410-422.

Supek, F., Bošnjak, M., Škunca, N., and Šmuc, T. (2011). REVIGO summarizes and visualizes long lists of gene ontology terms. PloS one *6*, e21800.

Sutton, M.G.S.J., and Sharpe, N. (2000). Left ventricular remodeling after myocardial infarction pathophysiology and therapy. Circulation *101*, 2981-2988.

Szklarczyk, D., Franceschini, A., Wyder, S., Forslund, K., Heller, D., Huerta-Cepas, J., Simonovic, M., Roth, A., Santos, A., Tsafou, K.P.*, et al.* (2015). STRING v10: protein-protein interaction networks, integrated over the tree of life. Nucleic Acids Res *43*, D447-452.

Tachibana, C. (2015). Transcriptomics today: Microarrays, RNA-seq, and more. Science *349*, 544-546.

Takeda, N., O'Dea, E.L., Doedens, A., Kim, J.-w., Weidemann, A., Stockmann, C., Asagiri, M., Simon, M.C., Hoffmann, A., and Johnson, R.S. (2010). Differential activation and antagonistic function of HIF-α isoforms in macrophages are essential for NO homeostasis. Genes & development *24*, 491-501.

Tamamori, M., Ito, H., Hiroe, M., Marumo, F., and Hata, R.I. (1997). Stimulation of collagen synthesis in rat cardiac fibroblasts by exposure to hypoxic culture conditions and suppression of the effect by natriuretic peptides. Cell Biol Int *21*, 175-180.

Tang, Y., Zheng, J., Sun, Y., Wu, Z., Liu, Z., and Huang, G. (2009). MicroRNA-1 regulates cardiomyocyte apoptosis by targeting Bcl-2. International heart journal *50*, 377-387.

Tarjan, R.E. (1975). Efficiency of a good but not linear set union algorithm. Journal of the ACM (JACM) *22*, 215-225.

Taylor, G.A., Carballo, E., Lee, D.M., Lai, W.S., Thompson, M.J., Patel, D.D., Schenkman, D.I., Gilkeson, G.S., Broxmeyer, H.E., Haynes, B.F., and Blackshear, P.J. (1996). A pathogenetic role for TNF alpha in the syndrome of cachexia, arthritis, and autoimmunity resulting from tristetraprolin (TTP) deficiency. Immunity *4*, 445-454.

Thomson, D.W., and Dinger, M.E. (2016). Endogenous microRNA sponges: evidence and controversy. Nature Reviews Genetics *17*, 272-283.

Thyboll, J., Kortesmaa, J., Cao, R., Soininen, R., Wang, L., Iivanainen, A., Sorokin, L., Risling, M., Cao, Y., and Tryggvason, K. (2002). Deletion of the laminin α4 chain leads to impaired microvessel maturation. Molecular and Cellular Biology *22*, 1194-1202.

Tooze, R.M., Stephenson, S., and Doody, G.M. (2006). Repression of IFN-γ induction of class II transactivator: a role for PRDM1/Blimp-1 in regulation of cytokine signaling. The Journal of Immunology *177*, 4584-4593.

Townley-Tilson, W.D., Callis, T.E., and Wang, D. (2010). MicroRNAs 1, 133, and 206: critical factors of skeletal and cardiac muscle development, function, and disease. The international journal of biochemistry & cell biology *42*, 1252-1255.

Trapnell, C., Hendrickson, D.G., Sauvageau, M., Goff, L., Rinn, J.L., and Pachter, L. (2013). Differential analysis of gene regulation at transcript resolution with RNA-seq. Nature biotechnology *31*, 46-53.

Trapnell, C., Williams, B.A., Pertea, G., Mortazavi, A., Kwan, G., Van Baren, M.J., Salzberg, S.L., Wold, B.J., and Pachter, L. (2010). Transcript assembly and quantification by RNA-Seq reveals unannotated transcripts and isoform switching during cell differentiation. Nature biotechnology *28*, 511-515.

Uemura, R., Xu, M., Ahmad, N., and Ashraf, M. (2006). Bone marrow stem cells prevent left ventricular remodeling of ischemic heart through paracrine signaling.

Circulation research *98*, 1414-1421.

Uhlen, M., Fagerberg, L., Hallstrom, B.M., Lindskog, C., Oksvold, P., Mardinoglu, A., Sivertsson, A., Kampf, C., Sjostedt, E., Asplund, A*., et al.* (2015). Proteomics. Tissue-based map of the human proteome. Science *347*, 1260419.

Uren, N.G., Crake, T., Lefroy, D.C., de Silva, R., Davies, G.J., and Maseri, A. (1994). Reduced coronary vasodilator function in infarcted and normal myocardium after myocardial infarction. New England Journal of Medicine *331*, 222-227.

Uva, P., and De Rinaldis, E. (2008). CrossHybDetector: detection of cross-hybridization events in DNA microarray experiments. BMC bioinformatics *9*, 1.

van Amerongen, M.J., Harmsen, M.C., Petersen, A.H., Popa, E.R., and van Luyn, M.J. (2008). Cryoinjury: a model of myocardial regeneration. Cardiovasc Pathol *17*, 23-31.

Van Rooij, E., Sutherland, L.B., Thatcher, J.E., DiMaio, J.M., Naseem, R.H., Marshall, W.S., Hill, J.A., and Olson, E.N. (2008). Dysregulation of microRNAs after myocardial infarction reveals a role of miR-29 in cardiac fibrosis. Proceedings of the National Academy of Sciences *105*, 13027-13032.

Varga, T., Mounier, R., Horvath, A., Cuvellier, S., Dumont, F., Poliska, S., Ardjoune, H., Juban, G., Nagy, L., and Chazaud, B. (2016). Highly Dynamic Transcriptional Signature of Distinct Macrophage Subsets during Sterile Inflammation, Resolution, and Tissue Repair. Journal of immunology (Baltimore, Md. : 1950) *196*, 4771-4782.

Vausort, M., Wagner, D.R., and Devaux, Y. (2014). Long noncoding RNAs in patients with acute myocardial infarction. Circulation research *115*, 668-677.

Vivers, S., Dransfield, I., and Hart, S.P. (2002). Role of macrophage CD44 in the disposal of inflammatory cell corpses. Clinical science (London, England : 1979) *103*, 441-449.

Waardenberg, A.J., Bassett, S.D., Bouveret, R., and Harvey, R.P. (2015). CompGO: an R package for comparing and visualizing Gene Ontology enrichment differences between DNA binding experiments. BMC bioinformatics *16*, 1.

Wagner, G.P., and Zhang, J. (2011). The pleiotropic structure of the genotype–phenotype map: the evolvability of complex organisms. Nature Reviews Genetics *12*, 204-213.

Walter, W., Sánchez-Cabo, F., and Ricote, M. (2015). GOplot: an R package for visually combining expression data with functional analysis. Bioinformatics *31*, 2912-2914.

Wan, J., Benkdane, M., Teixeira-Clerc, F., Bonnafous, S., Louvet, A., Lafdil, F., Pecker, F., Tran, A., Gual, P., Mallat, A*., et al.* (2014). M2 Kupffer cells promote M1 Kupffer cell apoptosis: a protective mechanism against alcoholic and nonalcoholic fatty liver disease. Hepatology *59*, 130-142.

Wang, G.-K., Zhu, J.-Q., Zhang, J.-T., Li, Q., Li, Y., He, J., Qin, Y.-W., and Jing, Q.

(2010). Circulating microRNA: a novel potential biomarker for early diagnosis of acute myocardial infarction in humans. European heart journal *31*, 659-666.

Wang, J., Huang, W., Xu, R., Nie, Y., Cao, X., Meng, J., Xu, X., Hu, S., and Zheng, Z. (2012). MicroRNA-24 regulates cardiac fibrosis after myocardial infarction. J Cell Mol Med *16*, 2150-2160.

Wang, S., Aurora, A.B., Johnson, B.A., Qi, X., McAnally, J., Hill, J.A., Richardson, J.A., Bassel-Duby, R., and Olson, E.N. (2008). The endothelial-specific microRNA miR-126 governs vascular integrity and angiogenesis. Developmental cell *15*, 261-271.

Wang, X., Wang, H.-X., Li, Y.-L., Zhang, C.-C., Zhou, C.-Y., Wang, L., Xia, Y.-L., Du, J., and Li, H.-H. (2015). MicroRNA Let-7i negatively regulates cardiac inflammation and fibrosis. Hypertension *66*, 776-785.

Wang, Y., Huang, X., Cang, H., Gao, F., Yamamoto, T., Osaki, T., and Yi, J. (2007). The endogenous reactive oxygen species promote NF-κ B activation by targeting on activation of NF-κ B-inducing kinase in oral squamous carcinoma cells. Free radical research *41*, 963-971.

Wang, Y., Xu, Z., Jiang, J., Xu, C., Kang, J., Xiao, L., Wu, M., Xiong, J., Guo, X., and Liu, H. (2013). Endogenous miRNA sponge lincRNA-RoR regulates Oct4, Nanog, and Sox2 in human embryonic stem cell self-renewal. Dev Cell *25*, 69-80.

Ware, C.B., Horowitz, M.C., Renshaw, B.R., Hunt, J.S., Liggitt, D., Koblar, S.A., Gliniak, B.C., McKenna, H.J., Papayannopoulou, T., and Thoma, B. (1995). Targeted disruption of the low-affinity leukemia inhibitory factor receptor gene causes placental, skeletal, neural and metabolic defects and results in perinatal death. Development *121*, 1283-1299.

Warnes, G.R., Bolker, B., Bonebakker, L., Gentleman, R., Huber, W., Liaw, A., Lumley, T., Maechler, M., Magnusson, A., and Moeller, S. (2013). gplots: Various R programming tools for plotting data. R package version 2.12. 1. (Available online at: h ttp://CRAN. R-project. org/package= gplots).

Weber, K., and Brilla, C. (1992). Factors associated with reactive and reparative fibrosis of the myocardium. In Cellular and Molecular Alterations in the Failing Human Heart (Springer), pp. 291-301.

Widera, C., Gupta, S.K., Lorenzen, J.M., Bang, C., Bauersachs, J., Bethmann, K., Kempf, T., Wollert, K.C., and Thum, T. (2011). Diagnostic and prognostic impact of six circulating microRNAs in acute coronary syndrome. Journal of molecular and cellular cardiology *51*, 872-875.

Woodcock, E.A., and Matkovich, S.J. (2005). Cardiomyocytes structure, function and associated pathologies. The international journal of biochemistry & cell biology *37*, 1746-1751.

Wynn, T.A., and Barron, L. (2010). Macrophages: master regulators of inflammation and fibrosis. In Seminars in liver disease (© Thieme Medical Publishers), pp. 245-257.

Wynn, T.A., Chawla, A., and Pollard, J.W. (2013). Macrophage biology in development, homeostasis and disease. Nature *496*, 445-455.

Xiang, J.F., Yin, Q.F., Chen, T., Zhang, Y., Zhang, X.O., Wu, Z., Zhang, S., Wang, H.B., Ge, J., Lu, X.*, et al.* (2014). Human colorectal cancer-specific CCAT1-L lncRNA regulates long-range chromatin interactions at the MYC locus. Cell Res *24*, 513-531.

Xie, P., Liu, Y., Li, Y., Zhang, M.Q., and Wang, X. (2014). MIROR: a method for cell-type specific microRNA occupancy rate prediction. Molecular BioSystems *10*, 1377-1384.

Xin, M., Olson, E.N., and Bassel-Duby, R. (2013). Mending broken hearts: cardiac development as a basis for adult heart regeneration and repair. Nature reviews Molecular cell biology *14*, 529-541.

Xue, J., Schmidt, S.V., Sander, J., Draffehn, A., Krebs, W., Quester, I., De Nardo, D., Gohel, T.D., Emde, M., Schmidleithner, L.*, et al.* (2014). Transcriptome-based network analysis reveals a spectrum model of human macrophage activation. Immunity *40*, 274-288.

Yang, F., Bi, J., Xue, X., Zheng, L., Zhi, K., Hua, J., and Fang, G. (2012). Up‐regulated long non‐coding RNA H19 contributes to proliferation of gastric cancer cells. FEBS Journal *279*, 3159-3165.

Yin, T., Cook, D., and Lawrence, M. (2012). ggbio: an R package for extending the grammar of graphics for genomic data. Genome biology *13*, 1.

Young, A., Whitehouse, N., Cho, J., and Shaw, C. (2005). OntologyTraverser: an R package for GO analysis. Bioinformatics *21*, 275-276.

Yu, R.Y.-L., Wang, X., Pixley, F.J., Yu, J.J., Dent, A.L., Broxmeyer, H.E., Stanley, E.R., and Ye, B.H. (2005). BCL-6 negatively regulates macrophage proliferation by suppressing autocrine IL-6 production. Blood *105*, 1777-1784.

Yue, D., Liu, H., and Huang, Y. (2009). Survey of computational algorithms for microRNA target prediction. Current genomics *10*, 478-492.

Zangrando, J., Zhang, L., Vausort, M., Maskali, F., Marie, P.-Y., Wagner, D.R., and Devaux, Y. (2014). Identification of candidate long non-coding RNAs in response to myocardial infarction. BMC genomics *15*, 1.

Zhang, H., Meltzer, P., and Davis, S. (2013a). RCircos: an R package for Circos 2D track plots. BMC bioinformatics *14*, 1.

Zhang, M., and Shah, A.M. (2014). ROS signalling between endothelial cells and cardiac cells. Cardiovascular research *102*, 249-257.

Zhang, Q., Chen, C.Y., Yedavalli, V.S., and Jeang, K.T. (2013b). NEAT1 long noncoding RNA and paraspeckle bodies modulate HIV-1 posttranscriptional expression. mBio *4*, e00596-00512.

Zhang, W., and Liu, H.T. (2002). MAPK signal pathways in the regulation of cell proliferation in mammalian cells. Cell research *12*, 9-18.

Zhang, Y., Zhang, M., Zhong, M., Suo, Q., and Lv, K. (2013c). Expression profiles of miRNAs in polarized macrophages. International journal of molecular medicine *31*, 797-802.

Zhang, Y., Zheng, D., Xiong, Y., Xue, C., Chen, G., Yan, B., and Ye, Q. (2014). miR‐202 suppresses cell proliferation in human hepatocellular carcinoma by downregulating LRP6 post‐transcriptionally. FEBS letters *588*, 1913-1920.

Zhao, S., Fung-Leung, W.-P., Bittner, A., Ngo, K., and Liu, X. (2014). Comparison of RNA-Seq and microarray in transcriptome profiling of activated T cells. PloS one *9*, e78644.

Zhao, T., Zhao, W., Chen, Y., Ahokas, R.A., and Sun, Y. (2010). Vascular endothelial growth factor (VEGF)-A: role on cardiac angiogenesis following myocardial infarction. Microvascular research *80*, 188-194.

Zhao, Y., Li, C., Wang, M., Su, L., Qu, Y., Li, J., Yu, B., Yan, M., Yu, Y., Liu, B., and Zhu, Z. (2013). Decrease of miR-202-3p expression, a novel tumor suppressor, in gastric cancer. PLoS One *8*, e69756.

Zhou, P., and Pu, W.T. (2016). Recounting Cardiac Cellular Composition. Circulation research *118*, 368-370.

Zhu, B., Suzuki, K., Goldberg, H.A., Rittling, S.R., Denhardt, D.T., McCulloch, C.A., and Sodek, J. (2004). Osteopontin modulates CD44‐dependent chemotaxis of peritoneal macrophages through G‐protein‐coupled receptors: Evidence of a role for an intracellular form of osteopontin. Journal of cellular physiology *198*, 155-167.

Zimmermann, W.-H., Schneiderbanger, K., Schubert, P., Didie, M., Münzel, F., Heubach, J., Kostin, S., Neuhuber, W., and Eschenhagen, T. (2002). Tissue engineering of a differentiated cardiac muscle construct. Circulation research *90*, 223-230.

Zinovyev, A., Viara, E., Calzone, L., and Barillot, E. (2008). BiNoM: a Cytoscape plugin for manipulating and analyzing biological networks. Bioinformatics *24*, 876-877.

APPENDIX

During the research period, the PhD candidate has contributed to the following publications:

Walter, W., Trappetti, V., Alonso-Herranz, L., Crespo, I., Ibberson, M., Cedenilla, M., Karaszewska, A., N, V., G. Arroyo, A., Xenarios, I., Sánchez-Cabo, F., and Ricote, M. Deciphering the dynamic transcriptional landscape of cardiac macrophages in the healthy heart and after myocardial infarction. *Manuscript in preparation*

A-González, N., Quintana, J.A., García-Silva, S., Mazariegos, M., González de la Aleja, A., Nicolás-Ávila, J.A., **Walter, W.**, Adrover, J.M., Crainiciuc, G., Kuchroo, V., Rothlin, C.V., Peinado, H., Castrillo, A., Ricote, M., and Hidalgo, A. Phagocytosis imprints heterogeneity in tissue-resident macrophages. *Manuscript under review.*

D'Amato, G., Luxán, G., del Monte-Nieto, G., Martínez-Poveda, B., Torroja, C., **Walter, W.**, Bochter, M.S., Benedito, R., Cole, S., Martınez, F., Hadjantonakis, A-K., Uemura, A., Jiménez-Borreguero, L.J., and de la Pompa, J.L. (2015). Sequential Notch activation regulates ventricular chamber development. Nature cell biology *18*, 7-20.

Walter, W., Sánchez-Cabo, F., and Ricote, M. (2015). GOplot: an R package for visually combining expression data with functional analysis. Bioinformatics *31*, 2912-2914.